AN EXPERIMENTAL INVESTIGATION OF A SPHERICAL REFLECTOR ANTENNA FOR OPERATION IN RAIN AT MILLIMETER WAVELENGTHS

by

Timothy William Street

B.Sc. Queen's University, 2003

A THESIS SUBMITTED IN PARTIAL FULFILMENT OF THE REQUIREMENTS FOR THE DEGREE OF

MASTER OF APPLIED SCIENCE

in

THE FACULTY OF GRADUATE STUDIES

Electrical & Computer Engineering

The University of British Columbia

MAY 2005

AN EXPERIMENTAL INVESTIGATION OF A SPHERICAL REFLECTOR ANTENNA FOR OPERATION IN RAIN AT MILLIMETER WAVELENGTHS

ABSTRACT

This thesis is an extensive investigation of an innovative spherical reflector antenna design for operation at millimetre wavelengths in rain. Radiation pattern measurements were performed at three elevation angles (10°, 30°, 50°) and three frequencies (27.5 GHz, 31.5 GHz, 35 GHz). Wet-antenna attenuation measurements were also performed at three reflector angles (20°, 30°, 40°), and at the three frequencies mentioned above. The antenna investigated consists of a 30 cm diameter shallow spherical reflector with a relatively large ratio of focal length to diameter. The reflector is illuminated by a pyramidal feed horn which is fixed in a downward facing position, while the reflector swivels in the vertical plane to accommodate the direction of incident radiation.

The antenna's performance was compared to that of a conventional parabolic reflector antenna under both dry and wet conditions with favourable results. Beamwidth values varied approximately between 1° and 3° and sidelobe levels varied approximately between -12 dB and -20 dB depending on the frequency and elevation angle. Under wet conditions the antenna performed quite well with a maximum observed attenuation level of 1.6 dB at the worst reflector angle used; while conventional reflector antennas experience attenuation levels of up to 10 dB. Cross-polarization discrimination of the dry antenna was also found to be approximately 34 dB.

AN EXPERIMENTAL INVESTIGATION OF A SPHERICAL REFLECTOR ANTENNA FOR OPERATION IN RAIN AT MILLIMETER WAVELENGTHS

TABLE OF CONTENTS

AN EXPERIMENTAL INVESTIGATION OF A SPHERICAL REFLECTOR ANTENNA FOR OPERATION IN RAIN AT MILLIMETER WAVELENGTHS

LIST OF TABLES

AN EXPERIMENTAL INVESTIGATION OF A SPHERICAL REFLECTOR ANTENNA FOR OPERATION IN RAIN AT MILLIMETER WAVELENGTHS

LIST OF FIGURES

AN EXPERIMENTAL INVESTIGATION OF A SPHERICAL REFLECTOR ANTENNA FOR OPERATION IN RAIN AT MILLIMETER WAVELENGTHS

ACKNOWLEDGEMENTS

I would like to thank my supervisor, Dr. M.M.Z. Kharadly, whose support and guidance helped me enormously throughout my research. I would also like to thank Rob Ross for his help with software as well as the university technicians Dave Fletcher, Donald Dawson, and Ken Madore for their much needed help with lab equipment and machining of parts. I am also grateful to the University of British Columbia for providing the facilities needed for me to complete my research. Finally, I would like to thank my family for their support throughout all of my research.

Chapter 1

INTRODUCTION

Satellite communications are commonly used throughout the world. They play an integral role in many aspects of communications. With the ever increasing demand for more channels these communications systems are constantly moving into higher and higher frequency ranges. For this reason system designers are dealing with many new challenges as technology changes with increasing frequency. A frequency range of current interest is the ka-band, 17.3 GHz to 31 GHz.

1.1 BACKGROUND

In 1993 the National Aeronautics and Space Administration (NASA) launched a program known as The Advanced Communications Technology Satellite (ACTS) experiment. The experiment's goal was to determine the feasibility of satellite communications at the Ka-Band in rain through path-attenuation caused by rain from earth to satellite. The ACTS experiment was carried out at seven different locations around North America, one of them being in Vancouver at the University of British Columbia (U.B.C.). The parabolic receiving antennas used in the ACTS propagation

experiment were found to introduce significant amounts of attenuation themselves when used under rainy conditions [1]-[5]. This meant that the collected ACTS attenuation data has become of minimal use in system design, modeling, mitigation processes or any other scientific or regulatory use. This is because any use of the contaminated data would largely amplify the requirements needed for a proper system design.

At U.B.C. it was decided that there was a need to investigate the wet-antenna attenuation problem by performing simulated-rain experiments using the ACTS receiving terminal [6]. These experiments used a system of four raised sprinklers which were adjustable to control the intensity and drop size of the simulated rain, allowing a range of rain types from heavy showers to mist. Figures 4(a) and 4(b) in [6] shown below, are typical of the results of these experiments. Models were then developed to separate and therefore salvage a reasonable estimate of the true path-attenuation data from the overall attenuation data [6]. Later, another study [7] attributed the wet antenna attenuation on the irregularities of the reflector part of the antenna, which in effect contradicts all other previous studies [e.g. 8, 9, and 10].

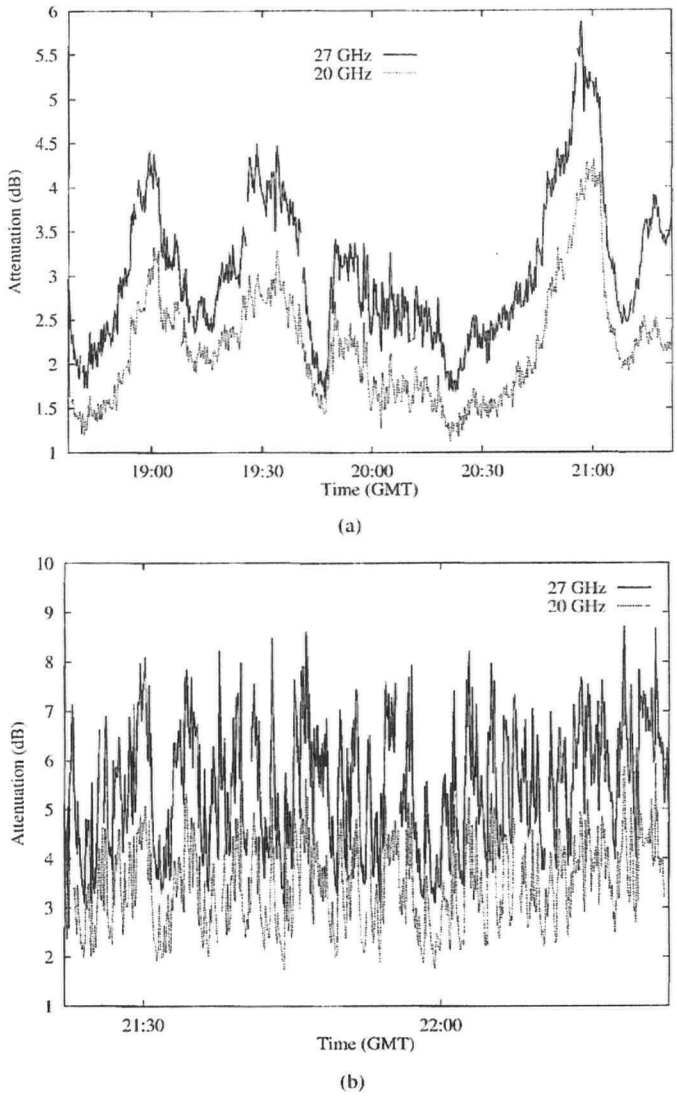

Fig. 4. (a) Simulated-rain experiment 96/08/20 for mist-like precipitation. (b) Simulated-rain experiment 96/08/20 for moderate rain.

Figure 1-1 Simulated Rain Experiment Plots from [6]

The performance of some conventional antennas at the ka-band frequencies under rainy conditions were also investigated [8], [9], using the same experimental set-up as for the ACTS antenna. These investigations [8], [9], provided the opportunity to explore further the possibility of minimizing the problem [8] or correcting for rain attenuation entirely [11]. Through experimentation, a number of key elements in identifying the problem and possible solutions to mitigating the effects of rain on antenna performance were established. The main findings were as follows:

i. Attenuation values of up to 10 dB could be expected in the Ka-band.

ii. Average attenuation on all antennas tested were comparable, however peak values differed greatly.

iii. Smaller aperture antennas had higher attenuation levels. This was due to the increased probability that larger areas of the smaller aperture antennas were covered with rain as compared to the larger aperture antennas.

Through theoretical investigations (e.g. [10]), it was shown there are two sources of loss associated with reflector antennas operating under rainy conditions; reflector loss and radome loss. It was also found [10], that a layer of water on a dielectric radiating surface, e.g. a radome, caused much higher signal attenuation than a layer of water on a smooth metallic reflector, i.e., the majority of the signal attenuation was due to feed loss not reflector loss. As mentioned previously, one of the models developed [7] to salvage the path-attenuation data from the ACTS propagation experiment, however, found that the majority of the attenuation was due to water on the reflector. This finding is contrary to the evidence previously given by Cheah in [10], and Kharadly and Ross in [6].

From these findings it became clear that there was a need to develop ground station antennas whose performance is not degraded in rainy conditions, for use in the ka band. Two approaches evolved. The first being to develop an antenna where its radiating surface faces downwards and therefore does not get wet, however its radiation direction is upwards towards the satellite. Such an antenna was developed by Kharadly and Chan [11], [12]. The second approach was to use an antenna whose only surface exposed to rain is the metallic reflector which, when wet, contributes a relatively small amount of attenuation [9, 10]. In this case, the feed would point downwards to keep it from getting wet since the results as indicated in [10] show only the feed radome being wet causes significant attenuation.

This thesis deals, essentially, with the extensive testing at mm-wavelengths and with the evaluation of a spherical reflector antenna using the second approach. This antenna was earlier conceived and designed by Dr. Kharadly of the Department of E.C.E. at U.B.C.

1.2 Organization of The Thesis

The thesis is divided into six chapters. The essential background of the ACTS propagation experiment is discussed in Chapter 1. This leads to identifying the causes of wet-antenna attenuation and to the investigation of possible solutions. Chapter 2 discusses the general properties and characteristics of spherical reflector antennas. It also discusses the suitability and advantages of spherical reflector antennas in certain applications.

Chapter 3 gives a description of the antenna used in this investigation, along with a discussion on how it operates. In Chapter 4 the experimental setups and procedures are described. These include radiation pattern measurements, wet-antenna attenuation measurements, and cross-polarization discrimination measurements. It also includes a description of the antenna range and all of the equipment used for each of the tests. In Chapter 5 samples of the experimental results are given.

Chapter 6 includes a discussion of the experimental results, conclusions and recommended future work. The seven appendices include the full set of results collected from all of the measurements performed, as well as a copy of the LabVIEW programs written to collect the measurements.

Chapter 2

SPHERICAL REFLECTOR ANTENNA PROPERTIES

Currently there are many types of antennas used in satellite communications systems in the ka-band. Each type of antenna has its own characteristics that cause it to be suitable for certain applications. There are a number of different types of antennas which are used for satellite terminals. These include, but are not limited to, the spherical reflector [13], parabolic reflector [6], and the lens antenna [14]. The spherical reflector has a simple design and much lower cost of manufacturing [15] as compared to the lens antenna or parabolic reflector, which makes it very attractive to use. Spherical reflector antennas also provide a very wide bandwidth. Due to its wide bandwidth the same reflector antenna can usually be used for both the up-link and down-link; reducing the system cost even further.

2.1 GEOMETRY OF A SPHERICAL REFLECTOR

A spherical reflector is made up of a section of a spherical surface, where the entire reflector consists of the same radius of curvature. In Figure 2.1-1 below, the line attached to the exact center of the reflector and also normal to the reflector at this point is called the *principal axis*. The point at which the principal axis meets the reflector is known as the *vertex*, V. The *center of curvature* C is the center of the sphere, and the distance between the vertex and the center of curvature is known as the *radius of curvature*, which is denoted by *R*. Lastly, half way between the vertex and the center of curvature is the *paraxial focal point* F, and the distance from this point to the vertex is the *paraxial focal length* f.

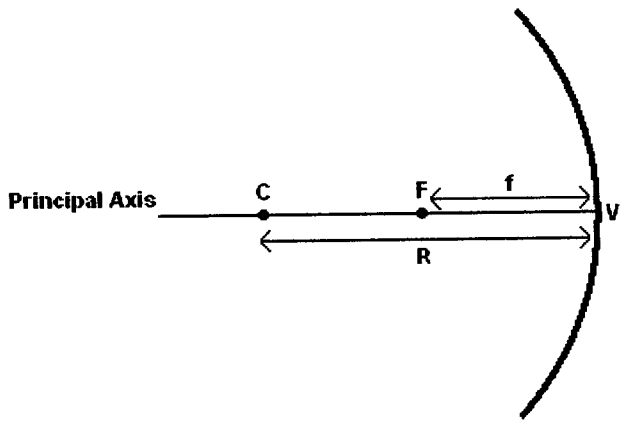

Figure 2.1-1 Geometry of a Spherical Reflector

Spherical reflectors are generally characterized by their *f/D* ratio, where *f* is the paraxial focal point and *D* is the diameter of the reflector. This ratio defines the size and curvature rate of the dish. In off-axis fed spherical reflectors this ratio is generally known as *L/D*, where *L* is the distance between the feed source and the reflector.

Spherical reflectors differ from parabolic reflectors in how the incident and reflected waves come to a focus. For parabolic reflectors, once incident rays are reflected they then travel to focus at one point, known as the focal point. This occurs no matter where on the reflector the incident wave is reflected from and is due to the changing radius of curvature of the parabolic dish. It also follows that when a source is placed at the focus of a parabolic reflector it will radiate waves that reflect off the dish and come out completely parallel; this is known as collimation. Rays that are parallel are known to be collimated. Spherical reflectors do not have this property; this is because they have a constant radius of curvature.

When waves incident on the spherical reflector are reflected, they do not come to a perfect focus, as shown in Figure 2.1-2 below. The path lengths for each part of the incoming wave are not equal. The farther towards the edges of the reflector that incident waves are reflected off of a spherical dish, the farther in front of the focal point the waves will cross the principal axis. This phenomenon is known as *spherical aberration*, and for this reason it is said that spherical reflectors have a *focal length* or *region* not a focal point. It is because of this that the feed for a spherical reflector can be moved over the focal region to scan the main beam without nearly as much loss in gain that a parabolic

reflector would experience. The constant radius of curvature of a spherical reflector allows you to radiate in many different directions with the same radiation pattern by simply moving the feed along an arc with the same curvature as the sphere. This allows for a wide range of beam scanning angles. If one were to move the feed for a parabolic reflector away from the focal point, you would immediately experience a sharp change in the radiation pattern with high losses of gain. This is due to the parabolic reflector not having the constant radius of curvature. To accomplish the same change in direction of radiation, while still maintaining the performance of the antenna you must move the entire dish structure.

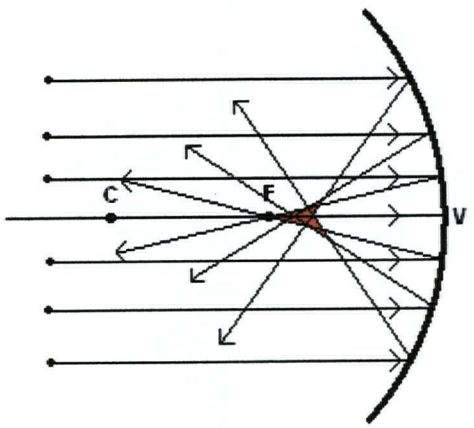

Figure 2.1-2 Larger Focal Region due to Spherical Aberration

2.2 SUITABILITY OF SPHERICAL REFLECTORS

Spherical reflector antennas are an attractive alternative for use in satellite communications systems due to their much lower cost [15]. This lower cost is realizable due to a number of reasons. The spherical geometry allows the main beam to be scanned by only moving the feed source not the entire dish. This allows for a cheaper motor system to be used, as well as a lighter less costly support structure for the reflector. For large reflectors this accounts for a large part of the costs involved. Also contributing to lower costs is the constant radius of curvature, this allows for a much cheaper and easier manufacturing process. There is less difficulty in preserving surface error margins, and for large reflectors where multiple panels make up the reflector this has a large impact on costs. For lens antennas it is more difficult to design a support structure [16]. This is because both the front and the back of the lens need to be clear of obstructions. This leaves only the outer edge of the lens to be used for this purpose.

2.3 PERFORMANCE MEASURES

Performance measures are a set of antenna characteristics which can be measured and compared between multiple antennas. They allow system designers to make informed decisions on which antenna will suit specific applications, without having to completely test the antenna themselves.

2.3.1 RADIATION PATTERN

The radiation pattern is a graphical representation of field strength transmitted or received by the antenna. It is usually shown in either its principal E-plane or H-plane patterns. It displays the directional radiation characteristics of the antenna, as well as its sidelobe levels and beamwidth. For these reasons it allows system designers to assess an antennas performance and suitability for certain applications.

2.3.2 BEAMWIDTH

Beamwidth is another one of the properties which are used to characterize the performance of antennas. Beamwidth describes the width of the main lobe on a two-dimensional radiation pattern. It is defined as the angle between two points on the main lobe which are equal to half of its maximum value (-3 dB). Beamwidth plays a crucial role in determining if the antenna is useful in certain applications. For instance, if the antenna has a very narrow beam and is used for reception, the approximate direction of the transmitter can be found. In the case of an antenna with a very wide beamwidth, it would be useful for broadcasting a signal to a large number of receivers. Beamwidth is also related to directive gain. Generally, the narrower the beamwidth the larger the gain will be [17]. In satellite communications it is advantageous to have a very narrow beamwidth. This is to help minimize the interference of other satellite or terrestrial signals.

2.3.3 GAIN AND DIRECTIVITY

Gain or directive gain which it is sometimes called is a measure of directivity. It describes how much power is radiated in a certain direction and at a given distance relative to that of an isotrope. Also, gain generally refers to the gain in the direction of maximum radiation. Directivity is defined as the maximum radiation intensity to the average radiation intensity averaged over all angles. Directivity can be calculated from the pattern solid angle Ω_p, which describes the width of the main lobe of the three-dimensional antenna pattern [18]:

$$D = 4\pi/\Omega_p. \qquad (2.3\text{-}1)$$

For an antenna with a single main lobe (such as reflector antennas) the pattern solid angle Ω_p, may be approximated as the product of the -3 dB beamwidths in the E-plane and H-plane. As a result directivity can be calculated as [18]:

$$D \approx 4\pi/(BW_{E\text{-}plane}\, BW_{H\text{-}plane}). \qquad (2.3\text{-}2)$$

High directivity and gain is needed in satellite communications in order to transmit and receive signals successfully.

2.3.4 Cross-Polarization Discrimination (XPD)

Antenna polarization refers to the orientation of the electric field vector. The electric field vector can be oriented in a linear, spherical or circular fashion. The polarization in which an antenna is intended to receive and transmit at is called the co-polarization. The antenna's ability to differentiate between vertical and horizontal polarization is called cross-polarization discrimination or XPD. It is a measure of how well the antenna only transmits or receives in the intended polarization. Loss due to power being radiated in a polarization state orthogonal to the intended polarization contributes to lower aperture efficiency. Large XPD is important when you have two antennas whose polarizations are orthogonal to each other operating in close proximity to one another; it helps avoid interference.

2.3.5 Reflector Illumination

Reflector illumination refers to the radiation from the feed. The intensity of the feed horn's radiation varies over the antenna's aperture. The power loss from the main lobe of the feed's radiation pattern, at the point in which the beamwidth of this lobe is equal to the width of the reflector, is known as edge taper. The amount of edge taper given by the feed horn is important in maximizing the performance of the antenna. If there is too sharp a taper, the result is an inefficient use of the reflector causing a loss of gain and widening of the main beam. Too little taper causes excess amounts of radiation spilling over the edges of the reflector, resulting in larger sidelobes and backlobes. In

Figures 2.3-1 and 2.3-2 below, two examples are shown. Typically, the value of edge taper for optimum antenna performance is between 8-10 dB.

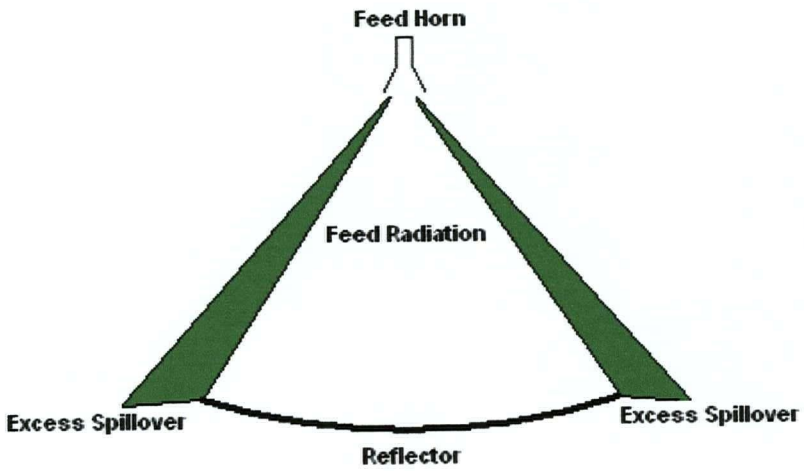

Figure 2.3-1 Reflector Illumination with Low Edge Taper

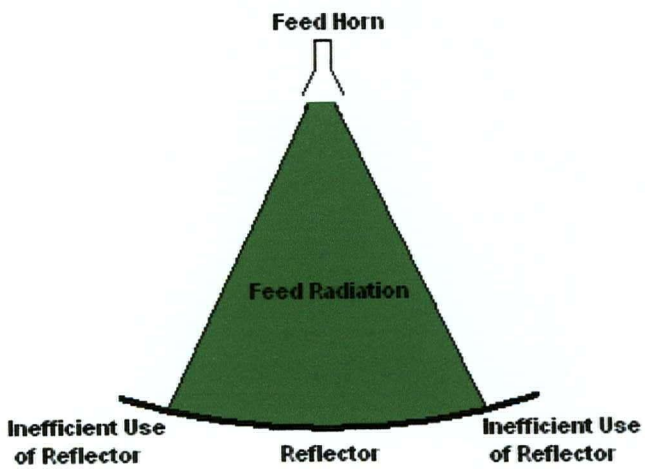

Figure 2.3-2 Reflector Illumination with High Edge Taper

Chapter 3

THE ANTENNA

The antenna used is a spherical reflector antenna with a pyramidal feed horn. This chapter describes the details of the antenna and its specifications.

3.1 ANTENNA DESCRIPTION

As shown in Figure 3.1-1 and Figure 3.1-2 below, the antenna consists of a pyramidal feed horn and a spherical reflector. The structure surrounding these components in Figures 3.1-1 and 3.1-2 is the experimental support structure and antenna turntable. This support structure allows for measurements to be taken in both the E-plane and H-plane. The feed horn is mounted above the reflector at the focal point facing downwards. The spherical reflector itself is a shallow reflector; it has a high ratio of focal length f to diameter D. The reflector is attached to an adjustable bar that allows it to rotate in the vertical plane. This makes it possible to receive radiation at various elevation angles.

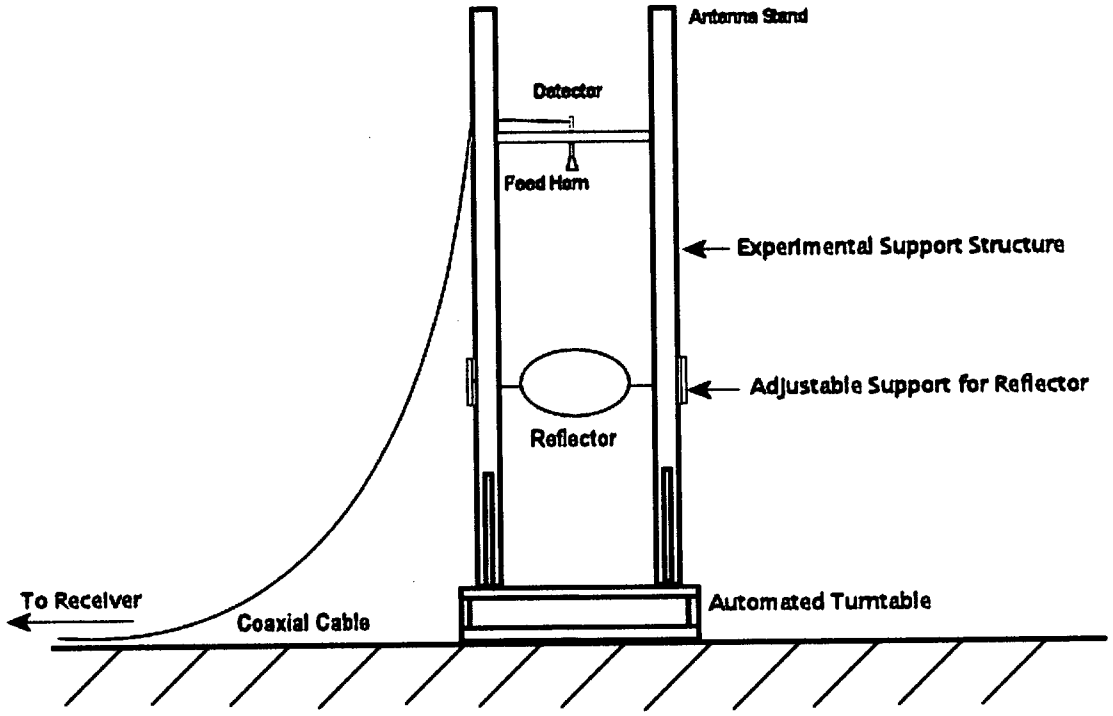

Figure 3.1-1 Front View of Spherical Reflector Antenna

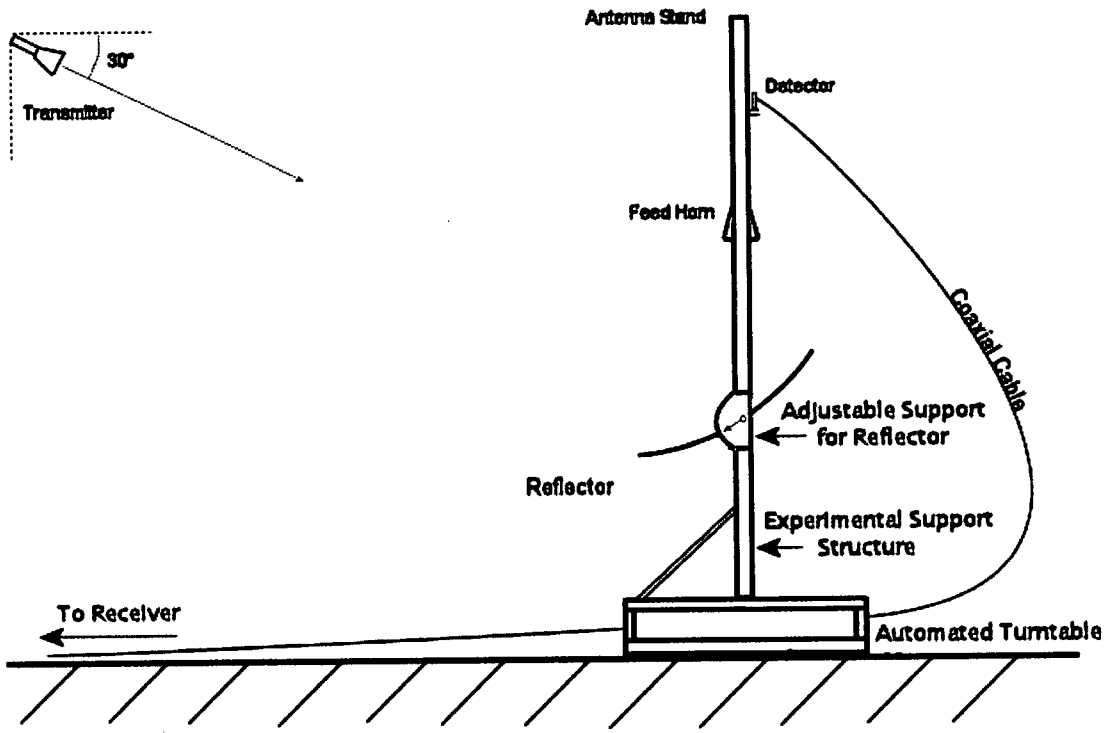

Figure 3.1-2 Side View of Spherical Reflector Antenna

3.2 SPHERICAL REFLECTOR ANTENNA SPECIFICATIONS

The specifications for the reflector and feed horn used are given below in Tables 3.2-1 and 3.2-2, respectively.

PARAMETER	SPECIFICATION
Aperture Size (cm)	30
f/D Ratio (F=75cm)	2.5
Frequencies of Operation (GHz)	27.5, 31.5, 35
Elevation Angles θ	0° - 90°
Polarization	Linear (Vertical)

Table 3.2-1 Reflector Specifications

PARAMETER	SPECIFICATION
Aperture Width (E-plane) (mm)	33
Aperture Length (H-plane) (mm)	40
Flare Angle	12.5°
Polarization	Linear (Vertical)

Table 3.2-2 Feed Horn Specifications

3.3 OPERATING PRINCIPLES

As described above, the spherical reflector is able to rotate in the vertical plane to accommodate for incident radiation at different elevation angles θ. The range of possible elevation angles of incident radiation can vary from 0° (horizontal) to 90° (vertical). Figure 3.3-1 shows a general case, where the angle of the reflector is such that the incident radiation is reflected into the feed horn. Figures 3.3-2 and 3.3-3 show the two elevation angles of 0° and 90° where the reflectors angle is at its most extreme positions. One can see from these figures that the reflector can accommodate receiving or transmitting at satellite elevation angles between 0° and 90° through rotation from the horizontal position (0°) to an inclination of 45°.

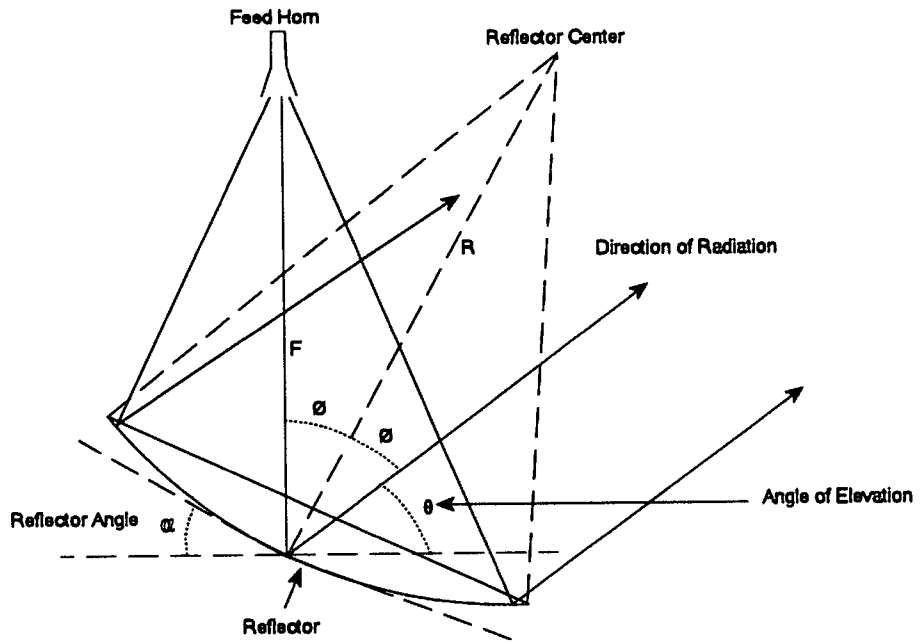

Figure 3.3-1 Ray Diagram Showing Relationship between Elevation Angle and Reflector Angle

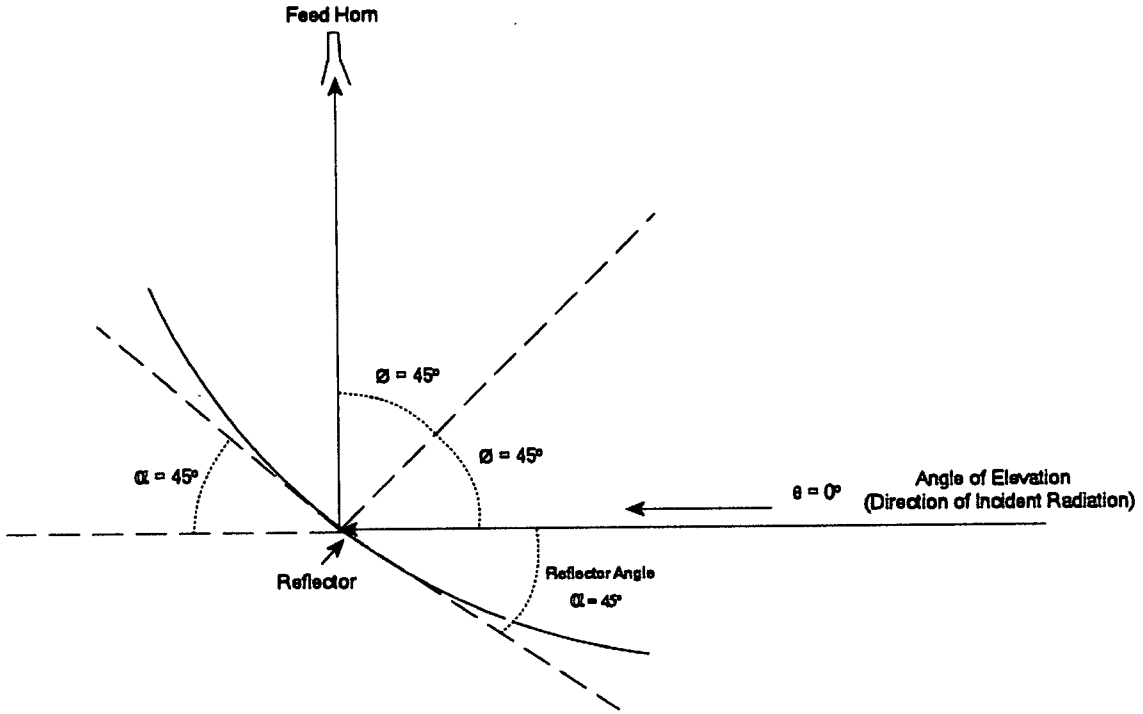

Figure 3.3-2 Ray Diagram with Elevation Angle = 0° and Reflector Angle = 45°

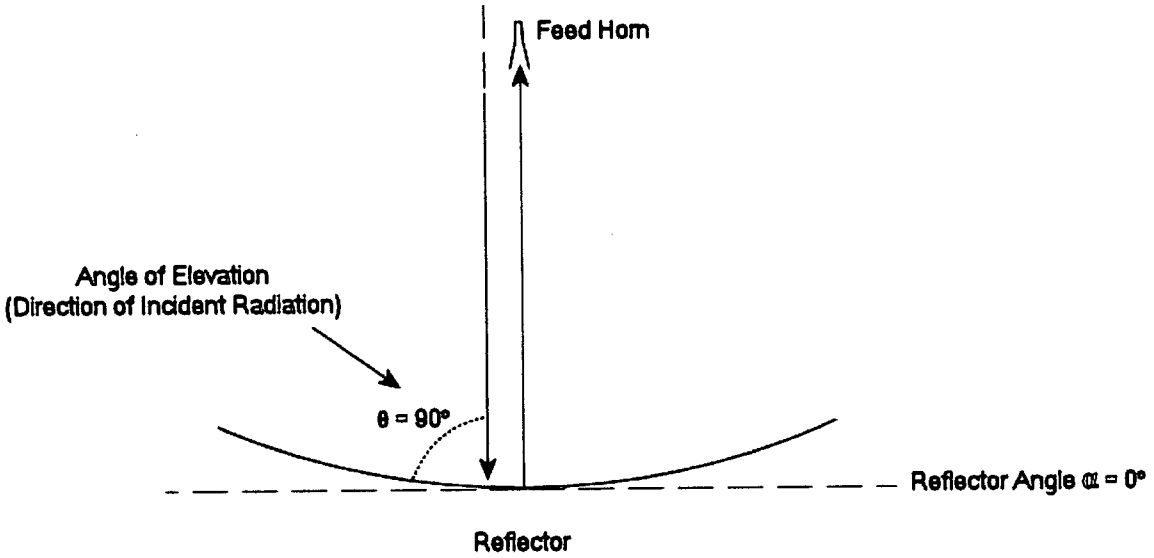

Figure 3.3-3 Ray Diagram with Elevation Angle = 90° and Reflector Angle = 0°

Chapter 4

EXPERIMENTAL SETUP & PROCEDURES

This chapter describes the experimental setup for each of the test procedures as well as the antenna range. This includes the radiation patterns for both the spherical reflector antenna and the feed horn on its own. It also includes the wet-antenna attenuation and the cross-polarization discrimination measurements. It also provides a detailed list of all of the equipment used.

4.1 ANTENNA RANGE

The outdoor range was used to measure the radiation patterns of both the feed horn and antenna, as well as perform the wet-antenna attenuation measurements. It was located on the roof of the MacLeod electrical engineering building. Most antenna ranges allow for far-field measurements which usually require a distance of $2\ d^2/\lambda$, where d is the diameter of the reflector. For the antenna range used the available distance was about 18.3 meters. For the lowest frequency of 27.5 GHz, the far-field equates 16.5 meters. For 31.5 GHz, far-field equates to 18.9 meters and for 35 GHz it is 21 meters. Due to

this slight deficiency in range length there will be a slight increase in sidelobe levels and beamwidth. However, due to the accuracy of the equipment used for the range measurements this effect should be negligible.

The range setup consisted of a frequency source which fed a pyramidal horn to act as the transmitter on one end of the antenna range. The transmitter was mounted on top of a 30 foot pole. On the other end of the antenna range there was the antenna under test which acted as the receiving antenna. This antenna was mounted on a turntable which was controlled from within the lab. The antenna under test was connected to a detector which was in turn connected to a low loss cable which ran to the receiver located inside the lab. The receiver measured the relative amplitude difference between a reference signal, sampled at the output of the frequency source, and the detector located at the antenna under test. The amplitude information was then passed from the receiver to a computer using a data acquisition I/O card. Using a program written in LabVIEW the computer also controlled the motorized turntable and synchronized the timing of recording data to match the angle of which it was received at. The turntable was able to turn in the horizontal plane in order to automate the azimuth (H-plane) pattern measurements. However, automation was not possible for the elevation (E-plane) patterns; these were performed manually. There was a protractor mounted on the side of the antenna structure to enable the elevation patterns to be measured. The accuracy of the manual elevation pattern measurements is estimated to be within $\pm 1°$. The accuracy of the automated azimuth pattern measurements is estimated to be less than $\pm 1°$, and the

amplitude data of the receiver is within ±1 dB. There was also absorbing material placed in front of the antenna under test, in an attempt to minimize ground reflections.

When performing the wet-antenna attenuation measurements a plastic frame holding a system of eight elevated sprinklers (approximately 1.5 meters above the antenna) was erected and used to simulate rain. The sprinkler heads were adjustable in order to model a wide range of rain types. To supply the water to the sprinkler heads a large hose ran from inside the lab to a junction which fed all of the sprinkler heads evenly. The hose was manually turned on and off for each experiment. The signal strength measurements recorded were the peak values of the main lobe, and were plotted versus time. A LabVIEW program was also used in these tests to synchronize the recording of incoming data and time.

The frequency source used was an HP 8690B Sweep Oscillator, the receiver was a Scientific Atlanta 1750, and the data acquisition I/O card was a National Instruments 6025E along with National Instruments LabVIEW software. In Figure 4.1-1 a block diagram of the antenna range setup is shown. In Figure 4.1-2 a photo of the antenna setup is shown, and in Figure 4.1-3 a photo of the transmitter horn is also shown. As seen in the photo, the transmitter was a pyramidal horn. The frame used for holding the sprinkler heads is also shown in the photo.

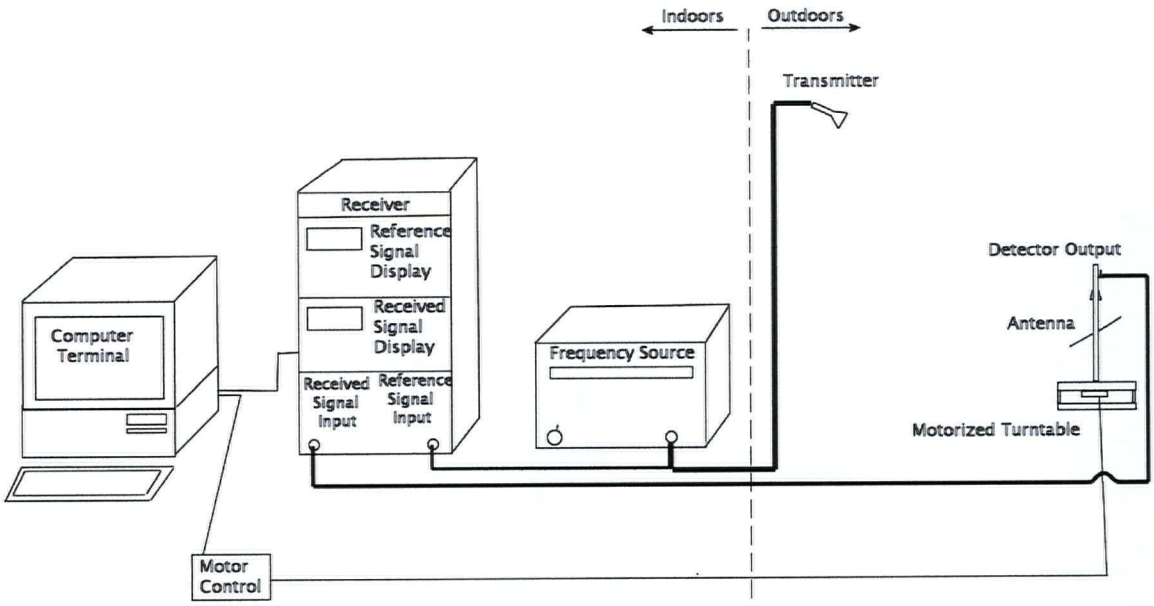

Figure 4.1-1 Antenna Range Diagram

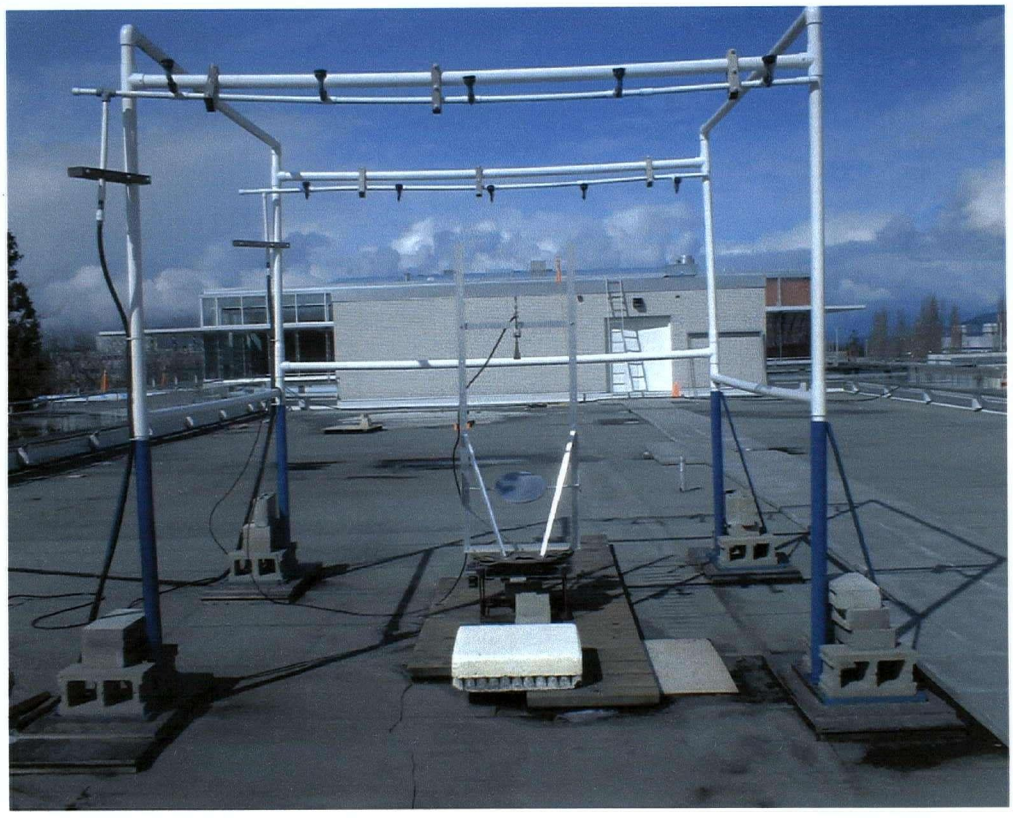

Figure 4.1-2 Antenna Setup Photograph

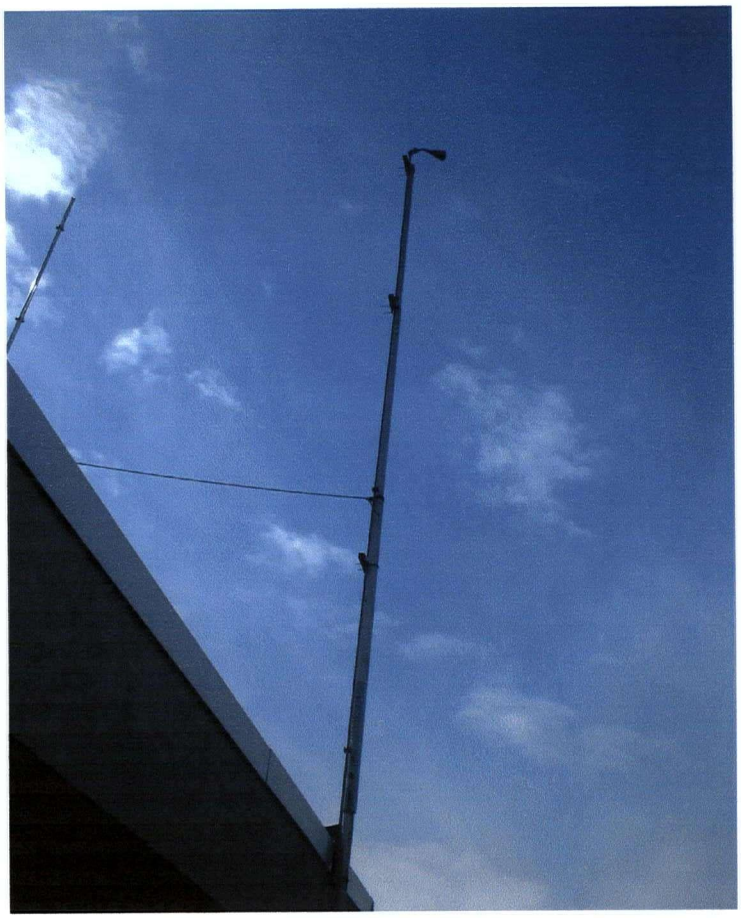

Figure 4.1-3 Transmitter Horn Photograph

4.2 MEASUREMENTS

The experimental investigation consisted of three types of measurements: radiation pattern measurements of the pyramidal feed horn and spherical reflector antenna, wet-antenna attenuation measurements and XPD measurements. Each of the test procedures were based on the equipment described above which was available within the university. The following sections describe the individual procedures in more detail.

4.2.1 RADIATION PATTERN MEASUREMENTS

Radiation pattern measurements were performed for both the pyramidal feed horn, and the spherical reflector antenna. The measurements consisted of two parts: the azimuth plane (H-plane), and the elevation plane (E-plane). Each set of measurements are described in the following sections.

4.2.1.1 RADIATION PATTERN MEASUREMENTS FOR THE PYRAMIDAL FEED HORN

Radiation patterns measurements for the feed horn consisted of both the azimuth and elevation planes and were conducted at 27.5, 31.5, and 35 GHz. As described in section 4.1 above, only the H-plane measurements were able to be automated for more accurate results; the E-plane measurements were done manually.

4.2.1.2 RADIATION PATTERN MEASUREMENTS FOR THE SPHERICAL REFLECTOR ANTENNA

Radiation pattern measurements for the antenna were performed at the same three frequencies as above, four different focal lengths and three different elevation angles. The four focal lengths tested were 70, 75, 80, and 85 cm. This was simply done by moving the feed structure vertically along the antenna support structure.

The three different elevation angles tested were 10°, 30°, and 50°. Adjusting the elevation angle proved to be a little complicated. This was because the transmitting horn was mounted on top of a 30 foot pole fixed at an angle of 30°. Instead of changing the angle in which the transmitter was pointed, and therefore avoiding lowering the pole each time a change was made, the elevation angle was adjusted by tilting the antenna structure towards or away from the angle of transmission. By tilting the antenna structure 20° towards the transmitter it achieved the same effect as if the transmitting horn was angled 50° towards the ground from the horizontal. It follows that by tilting the antenna structure 20° away from the transmitter it was the same as if the transmitting horn was angled 10° towards the ground from the horizontal. This is shown in Figure 4.2-1 and Figure 4.2-2 below. To accomplish this, the reflector angle also had to be adjusted by 10° in opposite directions for each elevation angle in order to still reflect the signal into the horn. The true situation in which the elevation angle would have actually been changed to 10° is shown in Figures 4.2-3. The virtual method used to simulate an elevation angle of 10° is shown in Figure 4.2-4. This made the process of changing the elevation angle much easier and also made it possible to be done by only one person. It also eliminated the need to move the receiving antenna and the entire support structure back and forth each time the elevation angle was changed. For example, if the transmitter horn was shifted by 20° to an elevation angle of 50°, the receiving antenna and support structure would have to be moved 8 meters forward, for the transmitter to be aligned with the receiving antenna.

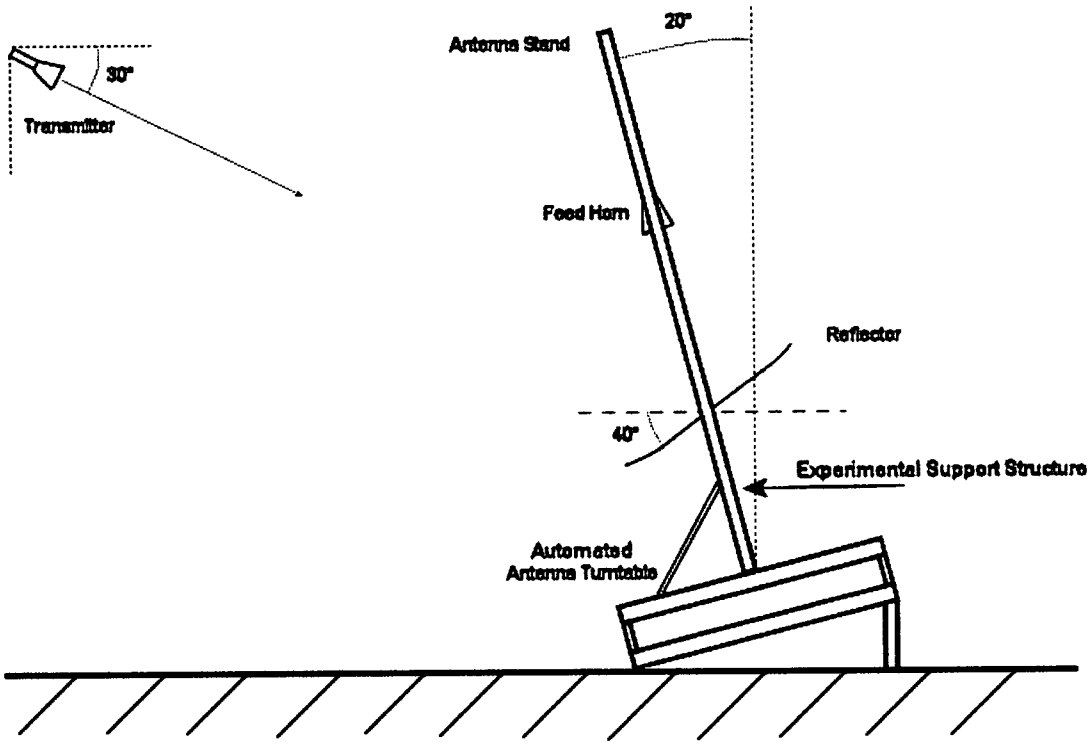

Figure 4.2-1 Side View of Antenna Setup for Elevation Angle of 50°

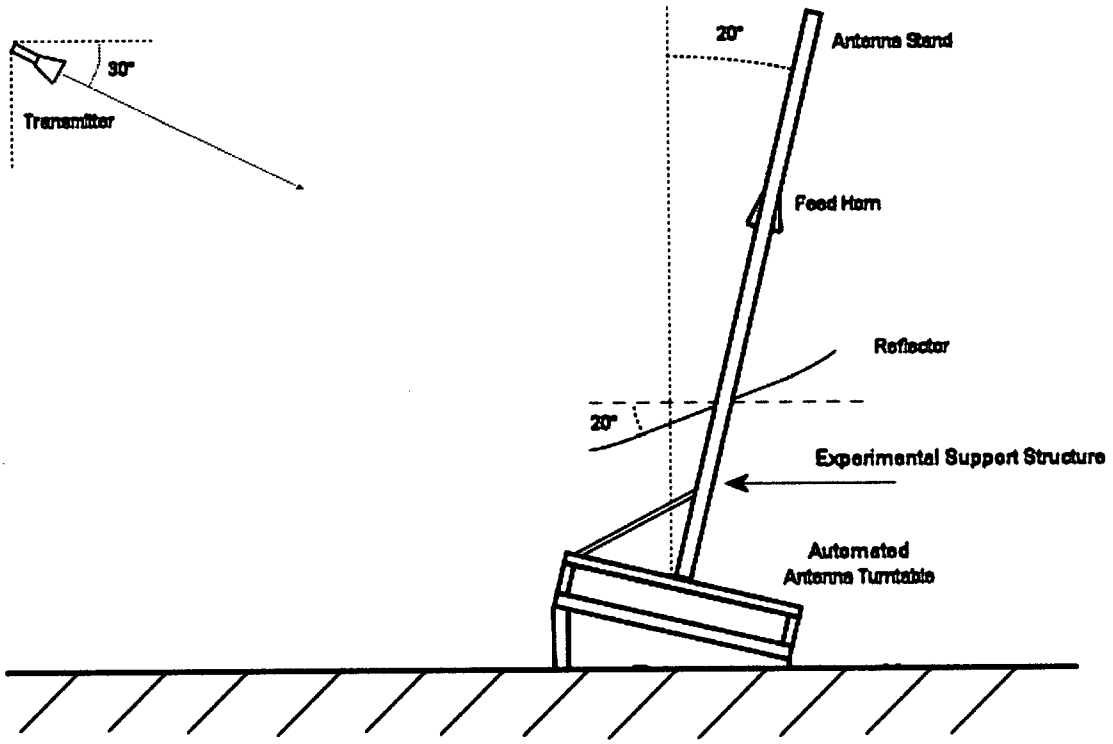

Figure 4.2-2 Side View of Antenna Setup for Elevation Angle of 10°

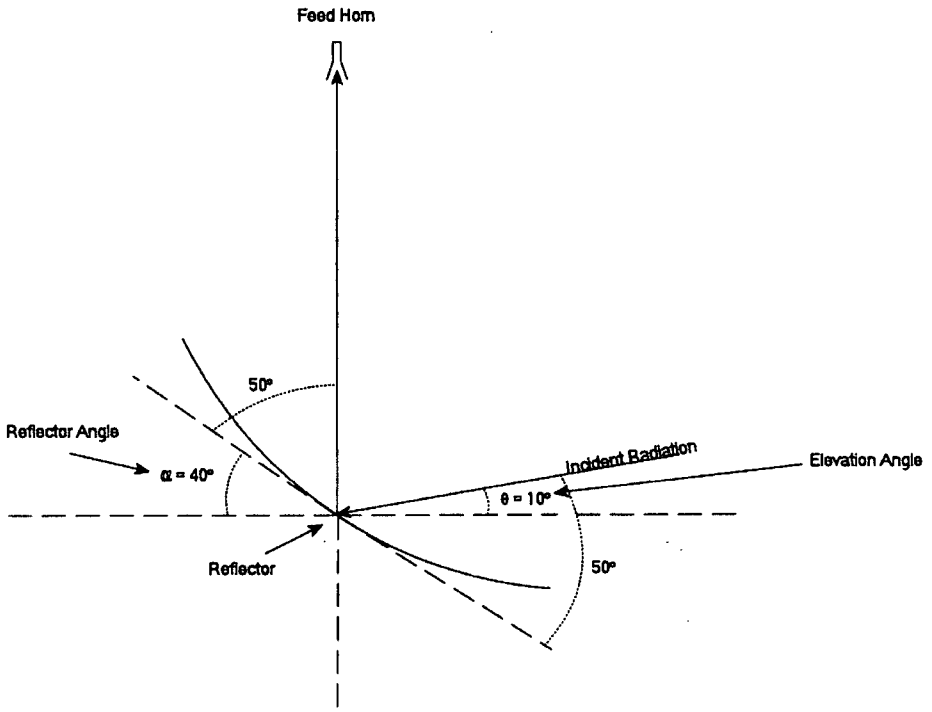

Figure 4.2-3 True Situation, with Elevation Angle = 10° and Reflector Angle = 40°

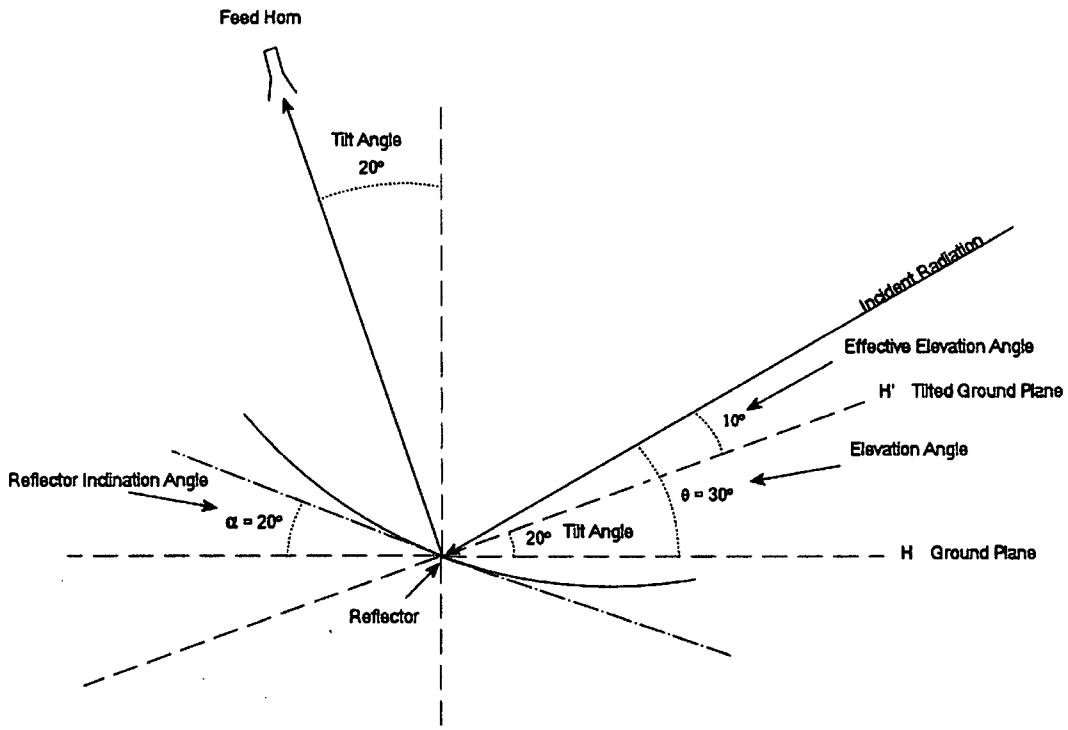

Figure 4.2-4 Simulation Method, with Elevation Angle = 10° and Reflector Angle = 20°

4.2.2 WET-ANTENNA ATTENUATION MEASUREMENTS

The wet-antenna attenuation measurements were performed using the antenna range setup as shown in Figure 4.1-2 with the eight elevated sprinkler heads. Signal strength measurements were taken at each of the three frequencies and simulated elevation angles tested in the radiation pattern measurements in Section 4.2.1, however only one focal length was used. This was because focal length does not affect the relative signal strength level between a dry and wet antenna. The tests were also only completed on clear days when there was no chance of rain activity along the propagation path.

Each measurement was timed to last 180 seconds. For the first 30-50 seconds the antenna is acting as a receive antenna under dry conditions. This provides a reference signal for comparison. After this period, the simulated rain is manually turned on and the remaining time is spent with the water turned on. Wind speed and direction were clearly not controllable and at times caused the spray from the sprinkler heads to drift away from the antenna under test. An effort was made to only perform the measurements on days when there was little or no wind, however even small amounts of wind would effect the direction of spray. With this in mind, it was not found to be a problem as the frame holding the eight sprinkler heads usually produced wide enough sprays to account for light winds.

4.2.3 Cross-Polarization Discrimination (XPD) Measurements

Cross-polarization discrimination (XPD) was measured at all three frequencies being tested. The signal strength was recorded at the co-polar position for each frequency. A 90° waveguide twist was then added above the feed horn to place the horn in the cross-polar position. Signal strengths were then recorded at each frequency. The XPD was then calculated from the pairs of signal strength values at each frequency.

Chapter 5

EXPERIMENTAL RESULTS

For each of the test measurements a sample of the results is included in this section. Radiation patterns of both the antenna and feed horn will be given along with wet-antenna attenuation measurements showing the performance of the antenna under rainy conditions. Cross-polarization discrimination results will also be given.

5.1 RADIATION PATTERN MEASUREMENTS FOR THE PYRAMIDAL FEED HORN

A summary of the results is given below in Tables 5.1-1 and 5.1-2 for the H-plane and E-plane respectively. Included are sidelobe level and beamwidth measurements. The radiation patterns for the H-plane are shown in Figures 5.1-1, 5.1-2, and 5.1-3, the E-plane patterns are shown in Appendix B. For comparison, theoretical calculations for the sidelobe levels and beamwidths of the feed horn are also given in Table 5.1-3.

FREQUENCY	ELEVATION ANGLE	
	30°	
	SLL (dB)	BW (deg)
27.5 GHz	-25.8	22.6
31.5 GHz	-19.9	19.6
35 GHz	-18.7	18.9

Table 5.1-1 Results Chart for H-plane Horn Radiation Pattern Measurements

FREQUENCY	ELEVATION ANGLE	
	30°	
	SLL (dB)	BW (deg)
27.5 GHz	-13	18
31.5 GHz	-11	16
35 GHz	-12	11

Table 5.1-2 Results Chart for E-plane Horn Radiation Pattern Measurements

Theoretical results for the feed horn's beamwidths in both the E and H planes and at all three frequencies were calculated using [19, pg 601]. The results are shown below in Table 5.1-3.

FREQUENCY	PLANE	
	H-Plane	E-Plane
	BW (deg)	
27.5 GHz	21.8	17.5
31.5 GHz	19.1	15.3
35 GHz	17.2	13.7

Table 5.1-3 Calculated H-Plane and E-Plane Beamwidth Results for the Feed Horn

The feed horn's edge taper has the most influence on the resulting radiation pattern and directivity of the reflector [20, pp. 332]. Table 5.1-4 displays the feed horn's edge tapers at each of the three frequencies. The edge taper value accounts for the spherical spreading loss [20, pp. 332] which was approximately 0.074 dB.

FREQUENCY	PLANE	
	H-Plane	E-Plane
	Edge Taper (dB)	
27.5 GHz	2.824	4.074
31.5 GHz	3.824	6.074
35 GHz	4.074	9.574

Table 5.1-4 E-Plane and H-Plane Feed Horn Edge Tapers

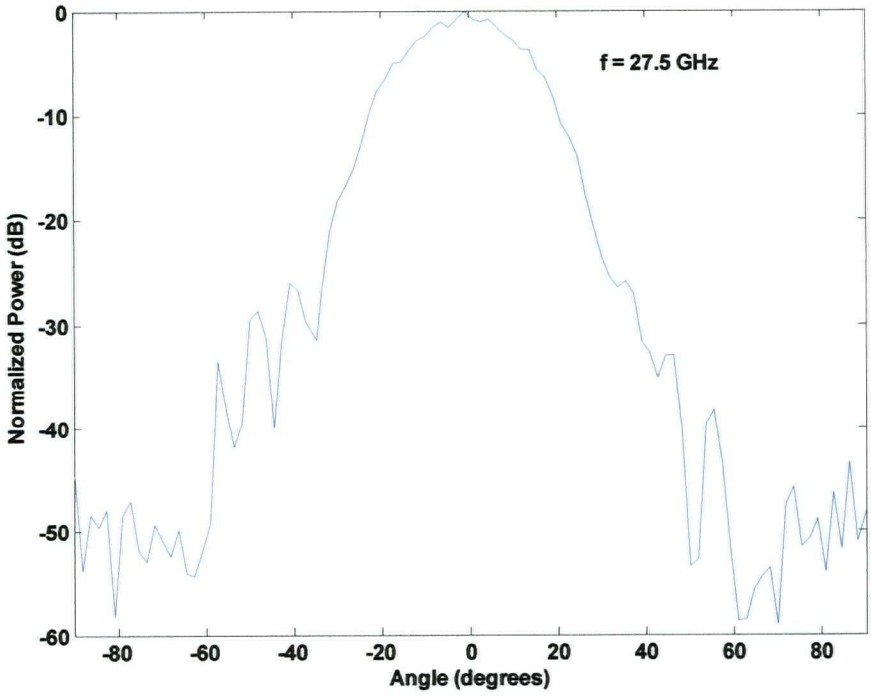

Figure 5.1-1 H-plane Radiation Pattern at f = 27.5 GHz for the Pyramidal Feed Horn

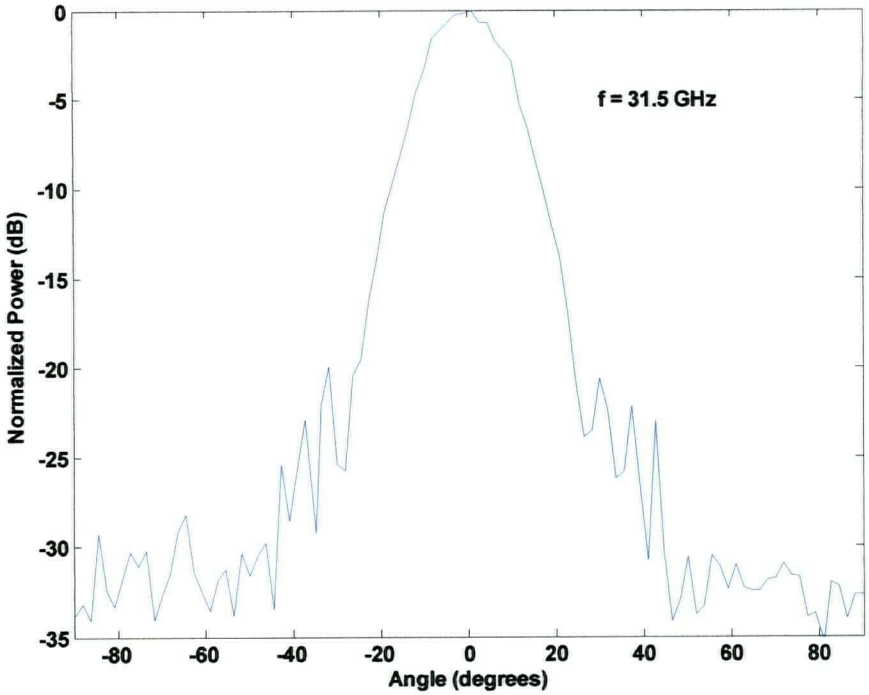

Figure 5.1-2 H-plane Radiation Pattern at f = 31.5 GHz for the Pyramidal Feed Horn

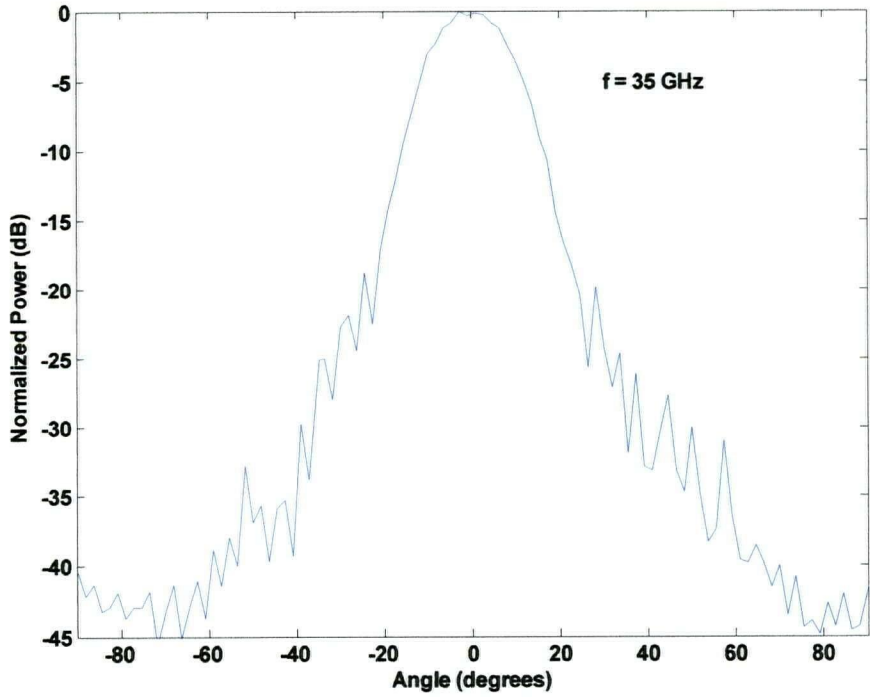

Figure 5.1-3 H-plane Radiation Pattern at f = 35 GHz for the Pyramidal Feed Horn

5.2 Radiation Pattern Measurements for the Spherical Reflector Antenna

A summary of the results, including sidelobe levels and beamwidths for each pattern, is given below in Tables 5.2-1 and 5.2-2. Samples of radiation patterns are also shown, with the remaining patterns in Appendix C and Appendix D. Unfortunately, the accuracy of which the manual elevation plane measurements were taken did not allow for reliable sidelobe levels to be recorded. For this reason the sidelobe levels were not included in Table 5.2-2, showing the results of the E-plane measurements. For comparison, theoretical results for a parabolic reflector of the same size were calculated. Directivities of the calculated and measured results are also given.

Focal Length: 70 cm

FREQUENCY	ELEVATION ANGLE					
	10°		30°		50°	
	SLL (dB)	BW (deg)	SLL (dB)	BW (deg)	SLL (dB)	BW (deg)
27.5 GHz	-9.1	5.9	-8.3	3.4	-8.8	3.3
31.5 GHz	-10.8	3.8	-10.4	3.1	-10.7	3.1
35 GHz	-12.9	3.3	-14.6	2.9	-12.8	2.9

Focal Length: 75 cm

FREQUENCY	ELEVATION ANGLE					
	10°		30°		50°	
	SLL (dB)	BW (deg)	SLL (dB)	BW (deg)	SLL (dB)	BW (deg)
27.5 GHz	-13.0	3.9	-14.6	2.8	-9.5	4.2
31.5 GHz	-16.1	2.6	-16.2	2.5	-15.8	3.5
35 GHz	-19.0	2.3	-18.2	1.7	-18.0	2.6

Focal Length: 80 cm

FREQUENCY	ELEVATION ANGLE					
	10°		30°		50°	
	SLL (dB)	BW (deg)	SLL (dB)	BW (deg)	SLL (dB)	BW (deg)
27.5 GHz	-14.2	3.7	-12	2.4	-16.6	3.4
31.5 GHz	-15.5	2.5	-12.4	2.3	-19.9	2.6
35 GHz	-17	1.9	-16.9	1.5	-20.4	2.2

Focal Length: 85 cm

FREQUENCY	ELEVATION ANGLE					
	10°		30°		50°	
	SLL (dB)	BW (deg)	SLL (dB)	BW (deg)	SLL (dB)	BW (deg)
27.5 GHz	-11.2	2.8	-13.3	2.4	-13.7	5.2
31.5 GHz	-13.2	2.5	-14.6	2.0	-14.4	2.5
35 GHz	-15.6	1.9	-15.3	1.8	-15.8	2.0

Table 5.2-1 Results Chart for H-plane Spherical Reflector Radiation Pattern Measurements

Focal Length: 70 cm

FREQUENCY	ELEVATION ANGLE		
	10°	30°	50°
	BW (deg)	BW (deg)	BW (deg)
27.5 GHz	1.8	1.3	1.4
31.5 GHz	1.6	1.2	1.3
35 GHz	1.5	1.5	1.1

Focal Length: 75 cm

FREQUENCY	ELEVATION ANGLE		
	10°	30°	50°
	BW (deg)	BW (deg)	BW (deg)
27.5 GHz	2.0	1.7	1.3
31.5 GHz	1.9	1.4	1.1
35 GHz	1.6	1.3	1.0

Focal Length: 80 cm

FREQUENCY	ELEVATION ANGLE		
	10°	30°	50°
	BW (deg)	BW (deg)	BW (deg)
27.5 GHz	1.8	2.8	1.4
31.5 GHz	1.6	1.8	1.3
35 GHz	1.5	1.3	1.1

Focal Length: 85 cm

FREQUENCY	ELEVATION ANGLE		
	10°	30°	50°
	BW (deg)	BW (deg)	BW (deg)
27.5 GHz	1.9	1.6	1.4
31.5 GHz	1.8	2.0	1.1
35 GHz	1.6	1.2	1.1

Table 5.2-2 Results Chart for E-plane Spherical Reflector Radiation Pattern Measurements

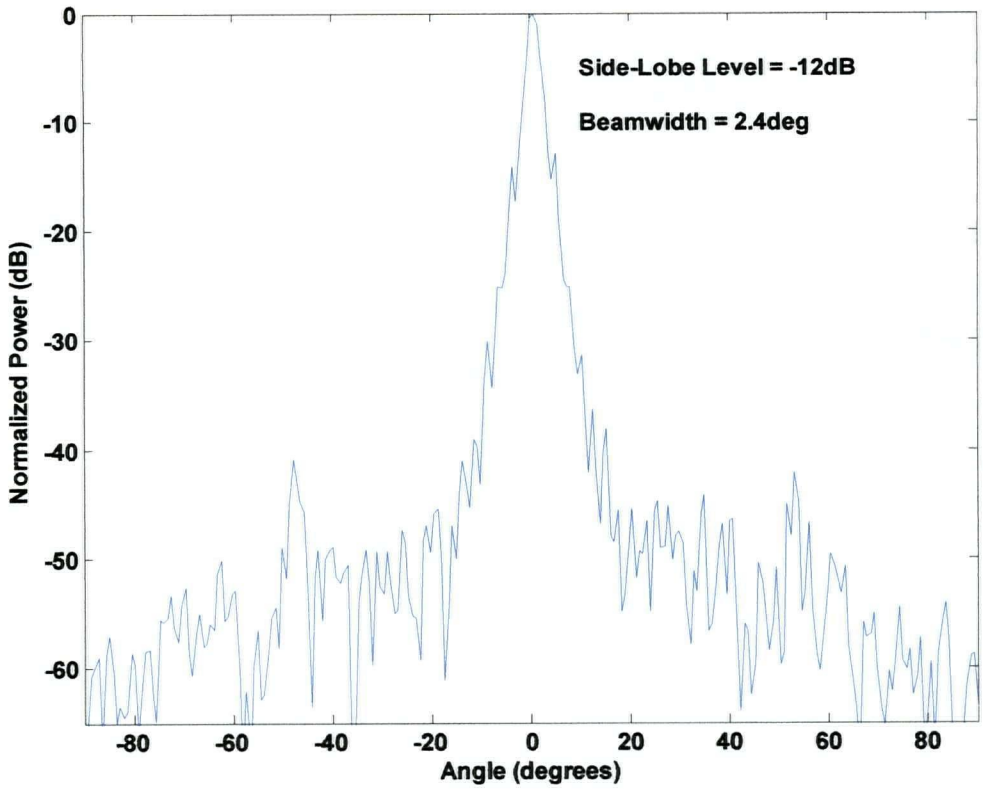

Figure 5.2-1 H-plane Radiation Pattern for the Spherical Reflector Antenna with Focal Length = 80 cm, f = 27.5 GHz, and Elevation Angle ≈ 30°

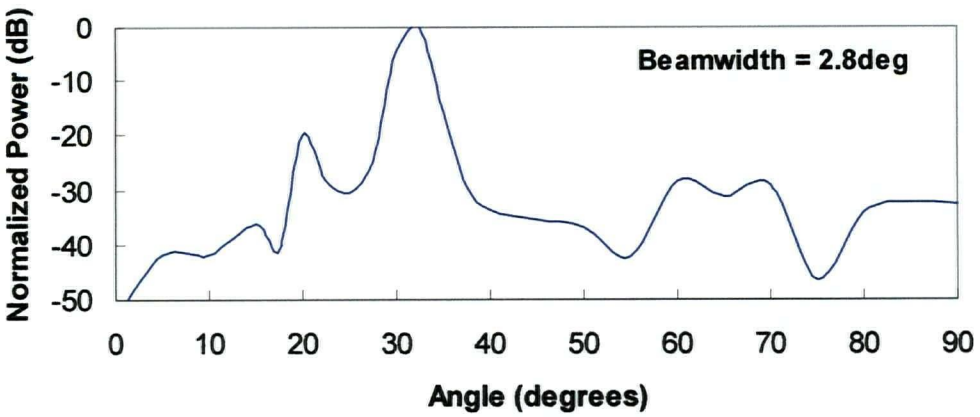

Figure 5.2-2 E-plane Radiation Pattern for the Spherical Reflector Antenna with Focal Length = 80 cm, f = 27.5 GHz, and Elevation Angle ≈ 30°

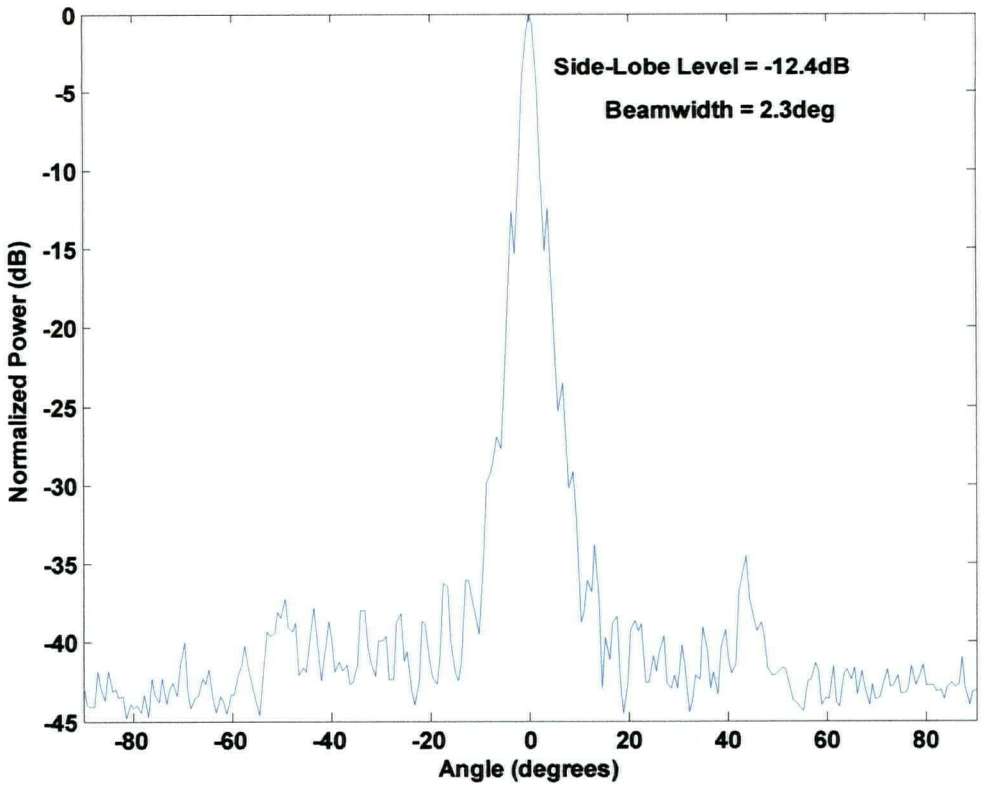

Figure 5.2-3 H-plane Radiation Pattern for the Spherical Reflector Antenna with Focal Length = 80 cm, f = 31.5 GHz, and Elevation Angle ≈ 30°

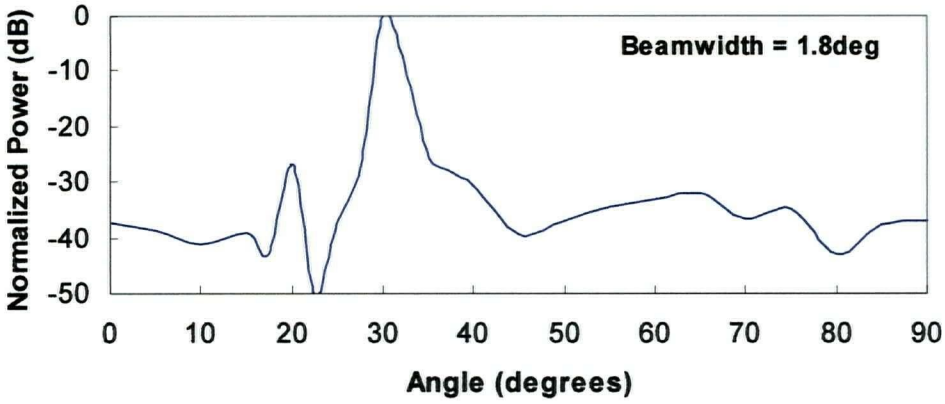

Figure 5.2-4 E-plane Radiation Pattern for the Spherical Reflector Antenna with Focal Length = 80 cm, f = 31.5 GHz, and Elevation Angle ≈ 30°

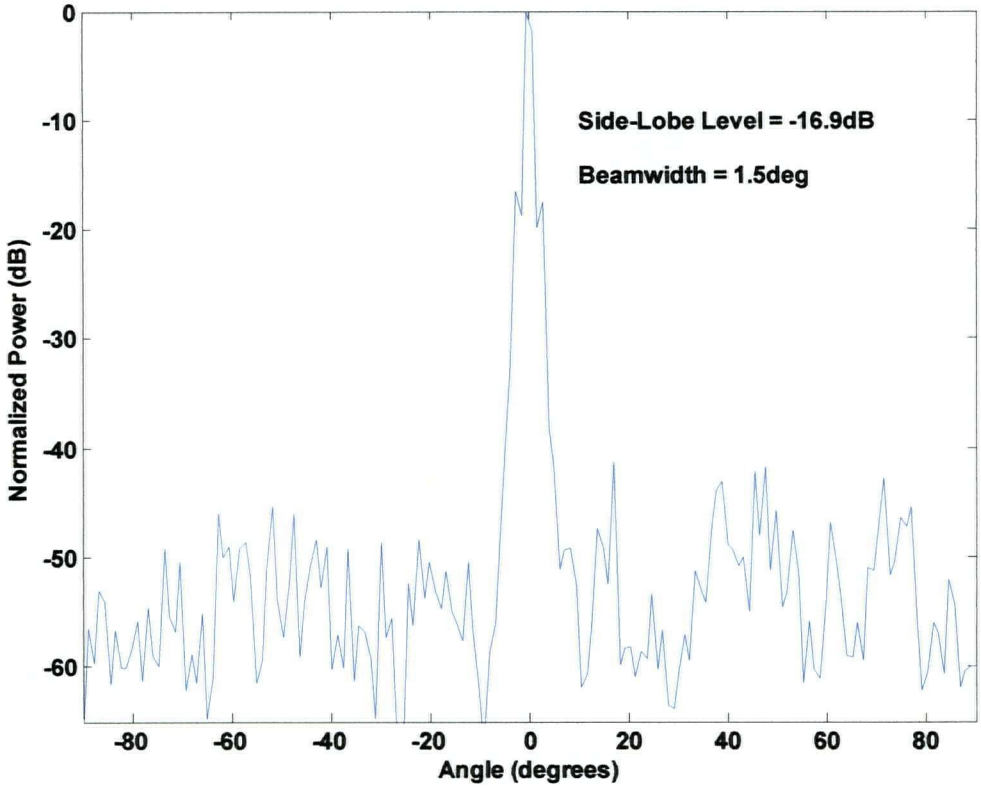

Figure 5.2-5 H-plane Radiation Pattern for the Spherical Reflector Antenna with Focal Length = 80 cm, f = 35 GHz, and Elevation Angle ≈ 30°

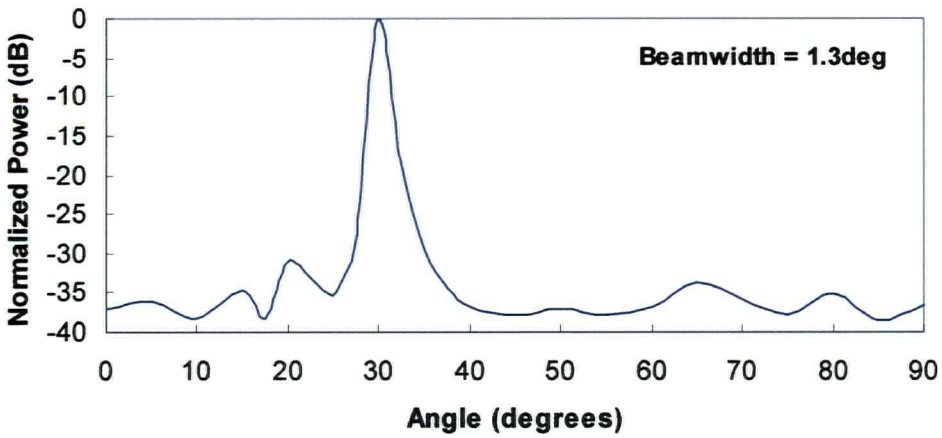

Figure 5.2-6 E-plane Radiation Pattern for the Spherical Reflector Antenna with Focal Length = 80 cm, f = 35 GHz, and Elevation Angle ≈ 30°

Theoretical results for a 30 cm parabolic reflector with a parabolic distribution were calculated using [20, pg 320]. The results include sidelobe levels and beamwidths for both the E-plane and H-plane. They are shown below in Table 5.2-3 for an elevation angle of 30° and a focal length of 80 cm.

FREQUENCY	PLANE			
	H-Plane		E-Plane	
	SLL (dB)	BW (deg)	SLL (dB)	BW (deg)
27.5 GHz	-19.4	2.2	-19.9	2.3
31.5 GHz	-19.8	2.0	-20.7	2.0
35 GHz	-19.9	1.8	-22	1.8

Table 5.2-3 Calculated Results for a Parabolic Reflector Antenna with Focal Length = 80 cm, and Elevation Angle = 30°

Directivity was also calculated from both the measured spherical reflector data and the calculated parabolic reflector data. This was done using the method mentioned in Section 2.3.3 [18] and Equation 2.3-2. The directivities of the two reflectors at all three frequencies are shown below, in Table 5.2-4. Once again this is for an elevation angle of 30° and a focal length of 80 cm.

FREQUENCY	ANTENNA	
	Spherical Reflector (measured)	**Parabolic Reflector (calculated)**
	Directivity (dB)	Directivity (dB)
27.5 GHz	37.8	39.1
31.5 GHz	40	40.1
35 GHz	43.2	41

Table 5.2-4 Calculated Directivities for Spherical and Parabolic Reflector Antennas

5.3 WET-ANTENNA ATTENUATION MEASUREMENTS

A summary of the wet-antenna attenuation results is given in Table 5.3-1. It includes the highest, lowest and average attenuation values. Signal strength plots are also shown below for each frequency at a reflector angle of 30°. The full set of plots, are given in Appendix E.

FREQUENCY	REFLECTOR ANGLE (α)								
	α = 20° *			α = 30° **			α = 40° ***		
	Attenuation (dB)			Attenuation (dB)			Attenuation (dB)		
	High	Low	Average	High	Low	Average	High	Low	Average
27.5 GHz	0.9	0.5	**0.7**	0.5	0.1	**0.3**	0.3	0	**0.1**
31.5 GHz	1.4	0.7	**0.9**	1.1	0.1	**0.5**	1.0	0.1	**0.3**
35 GHz	1.6	1.0	**1.3**	1.5	0.8	**1.1**	1.0	0.6	**0.8**

Table 5.3-1 Results Chart for Wet-Antenna Attenuation Measurements

*Corresponds to a simulated (virtual) elevation angle of 10°
**Corresponds to a TRUE elevation angle of 30°
***Corresponds to a simulated (virtual) elevation angle of 50°

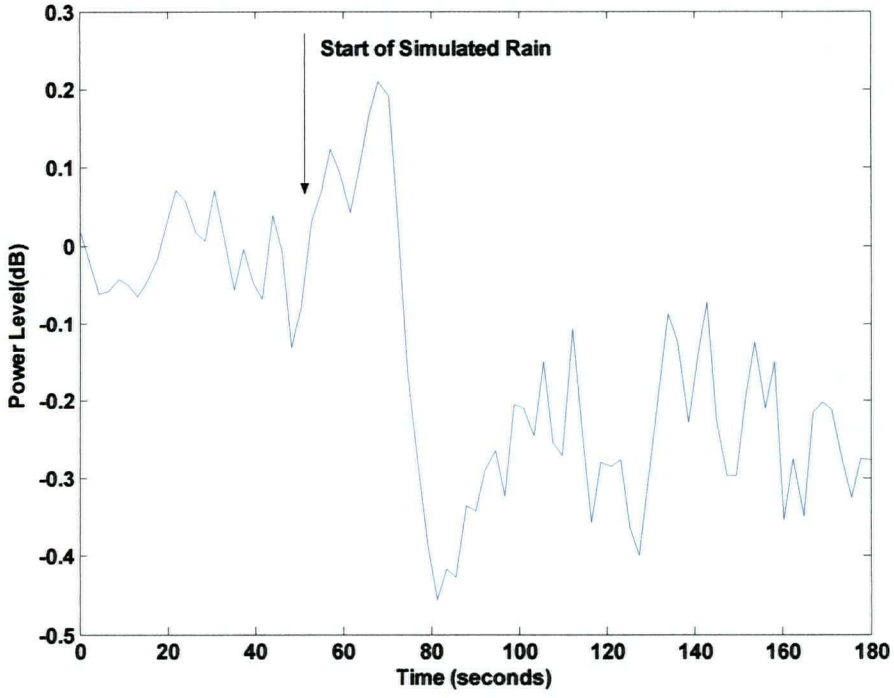

Figure 5.3-1 Rain-Attenuation Plot for Reflector Angle ≈ 30° and f = 27.5 GH

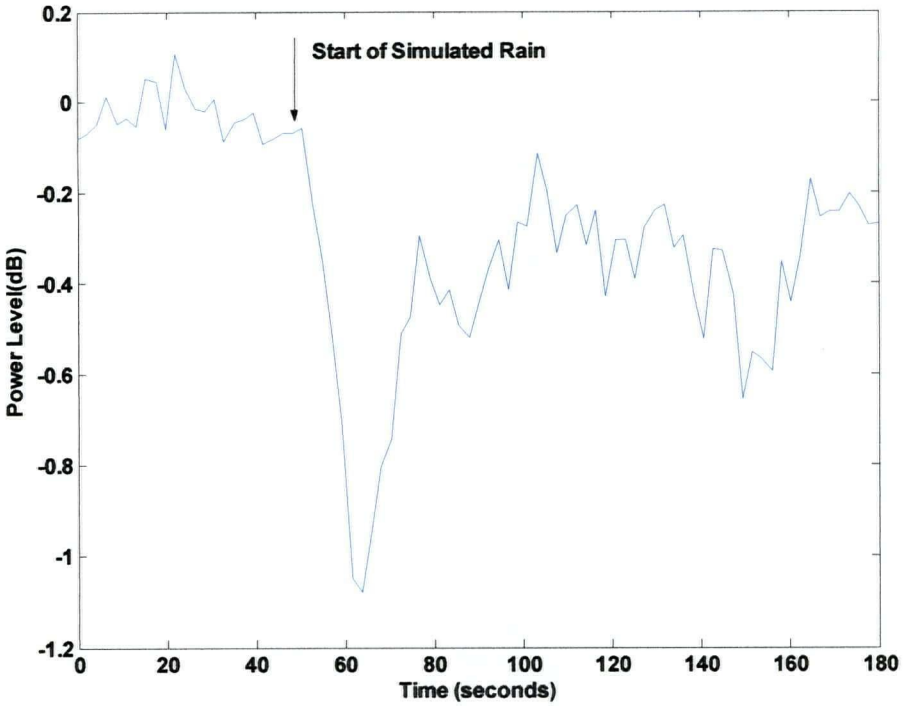

Figure 5.3-2 Rain Attenuation Plot for Reflector Angle ≈ 30 ° and f = 31.5 GHz

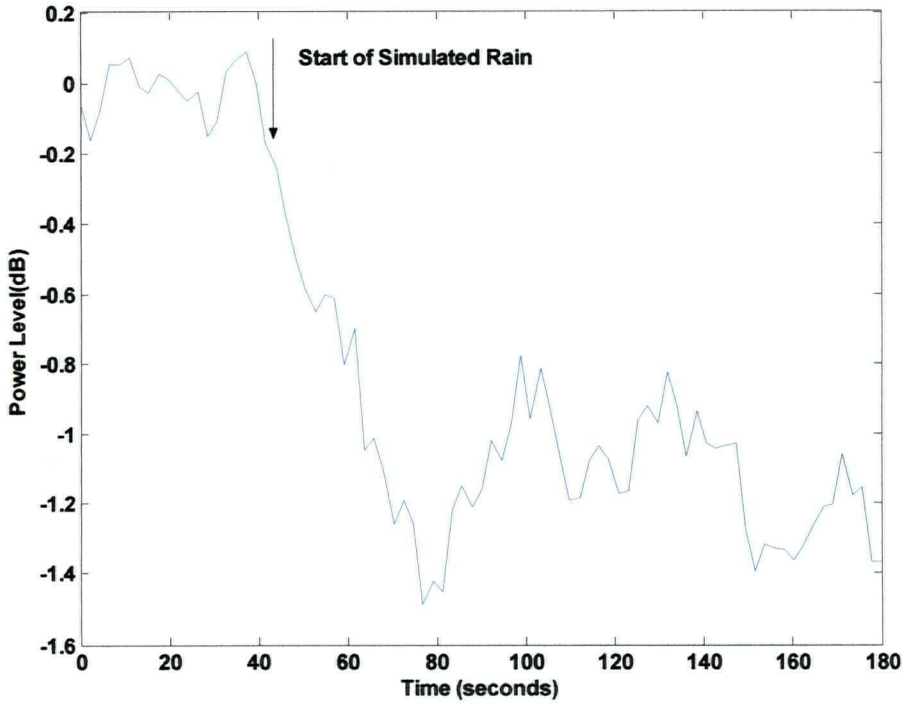

Figure 5.3-3 Rain Attenuation Plot for Reflector Angle ≈ 30° and f = 35 GHz

5.4 Cross-Polarization Discrimination (XPD) Results

Cross-polarization discrimination measurements were taken using a waveguide twist placed in series with the feed horn. It was found the antenna had an XPD value of between approximately 33-34 dB for all three frequencies tested.

Chapter 6

DISCUSSION, CONCLUSIONS AND FURTHER WORK

6.1 PYRAMIDAL FEED HORN

In Figure 6.1-1 below, a plot of both the measured and calculated beamwidths are shown. The calculated beamwidths were found using [19, pg 601]. Comparing the calculated and measured results for the pyramidal feed horn, one can see the beamwidths are quite similar.

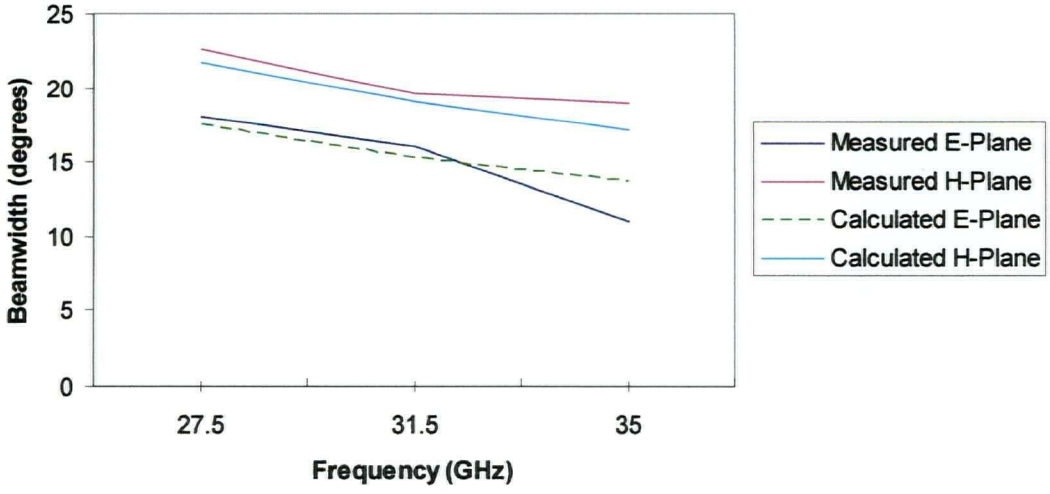

Figure 6.1-1 Measured and Calculated Beamwidths for the Feed Horn

The edge tapers for each frequency are shown in Table 5.1-4 for both the E and H planes. As expected the feed horn's edge taper changed significantly with frequency, as it is dependent on the feed horn's beamwidth. Edge taper is the power loss from the main lobe at the point which the beamwidth is equal to the width of the reflector. Therefore, as the beamwidth of the feed horn decreased with increasing frequency, the feed horn's edge taper would increase. The edge tapers provided by the feed were found to be lower than optimal. Typically, to command the best performance from an antenna the edge taper should be between 8-10 dB. The average edge taper provided by the pyramidal feed horn was approximately 5.1 dB. This meant there were higher amounts of spillover than one would typically want for the best possible performance of the antenna.

6.2 THE ANTENNA UNDER DRY CONDITIONS

As discussed in Chapter 5, radiation pattern measurements for the antenna were performed at four focal lengths (70, 75, 80, and 85 cm), three frequencies (27.5, 31.5, and 35 GHz), and three elevation angles (10, 30, and 50°). As expected, the beamwidths of the antenna decreased with increasing frequency. The focal length of 80 cm had the lowest average beamwidth values; however the sidelobe levels were slightly larger than at focal lengths of 75 cm and 85 cm. The sensitivity of the antenna's focal length on beamwidth can be seen below, in Figure 6.2-1.

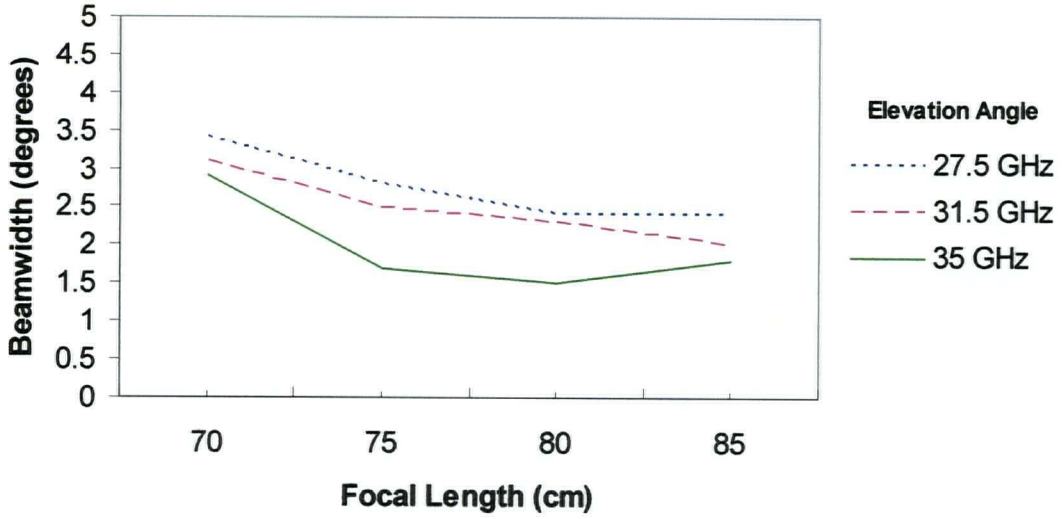

Figure 6.2-1 Beamwidth vs. Focal Length, for Elevation Angle ≈ 30°

From Figure 6.2-1, one can see there is a low sensitivity to a change in focal length on beamwidth, between 75 cm and 85 cm. Between these focal lengths, 80 cm has the lowest beamwidth; however, the difference is quite small. This was also the case for elevation angles of 10° and 50° in both the E-plane and the H-plane. These comparison plots can be seen in Appendix F, Figure F-1 and F-2.

In Figure 6.2-2 below, the sensitivity to a change in focal length on sidelobe levels is shown. One can see that the sidelobe levels do vary with a change in focal length. It is evident that the sidelobe levels are lowest at a focal length of 75 cm while at an elevation angle of 30°. In Appendix F, the plots for elevation angles 10° and 50° are shown in Figures F-3 and F-4. One can see at an elevation angle of 50°, the sidelobe levels at a focal length of 75 cm are slightly higher than at 80 cm. At an elevation angle of 10°, the sidelobe levels are roughly equal at focal lengths of 75 cm and 80 cm. The

small variations between sidelobe levels could be due to the equipment being slightly out of alignment when being put together. For example, the feed horn or its supporting structure could have been slightly crooked after an adjustment in focal length or elevation angle was made. However it is clear the sidelobe levels are consistently quite high at a focal length of 70 cm. This is most likely due to a focal length of 70 cm being too low for the feed horn to capture a lot of the power in the main lobe. Therefore the power difference between the main lobe and first sidelobe is much lower.

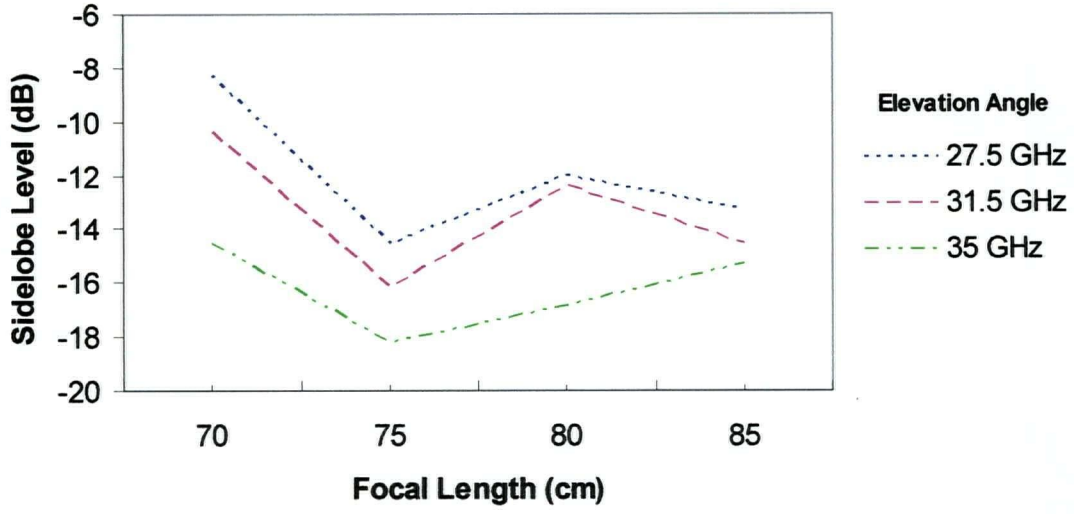

Figure 6.2-2 Sidelobe Level vs. Focal Length, for Elevation Angle ≈ 30°

The average sidelobe level and beamwidth were both found to be the lowest at a focal length of 80 cm. With these findings, it was decided that 80 cm was the overall preferred focal length. However, depending on the application, one may choose a different focal length to be more suitable. For example, one may want to give up a small amount in beamwidth, in order to have the lowest possible sidelobe levels at a certain elevation angle.

The relationships between beamwidth, sidelobe level, frequency, and elevation angle for a focal length of 80 cm are shown below in Figures 6.2-3 and 6.2-4.

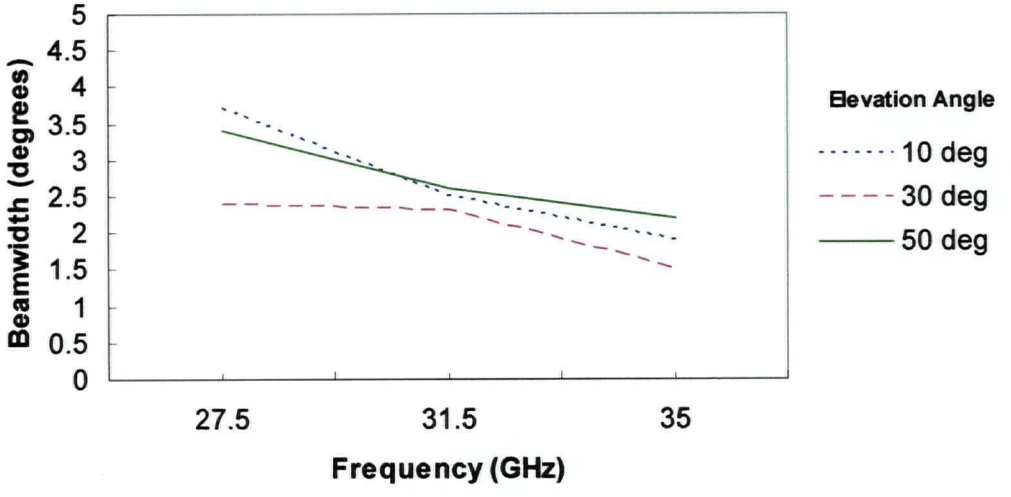

Figure 6.2-3 Beamwidth vs. Frequency, for Focal Length = 80 cm

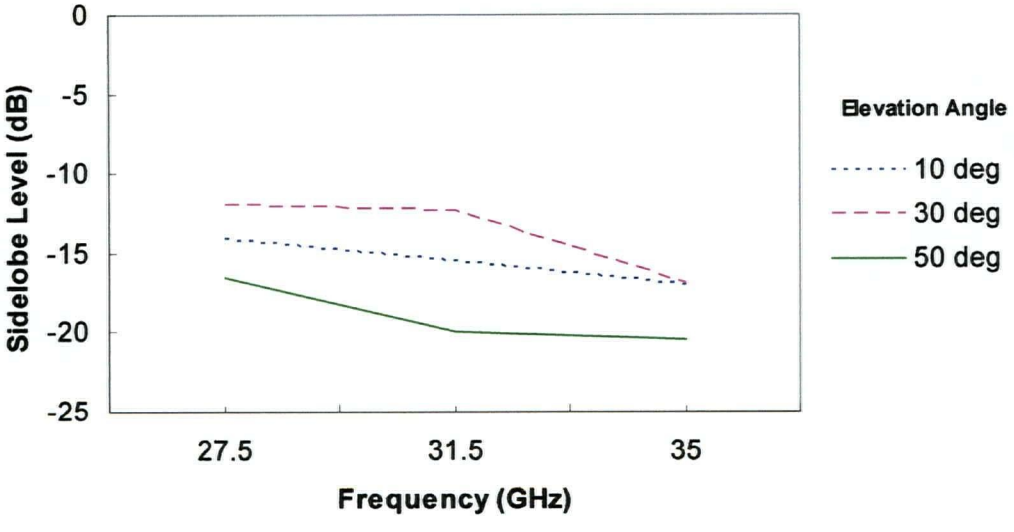

Figure 6.2-4 Sidelobe Level vs. Frequency, for Focal Length = 80 cm

The calculated results in Table 5.2-3, for a parabolic reflector at an elevation angle of 30°, are compared to the measured results of the antenna below in Figures 6.2-5 – 6.2-7.

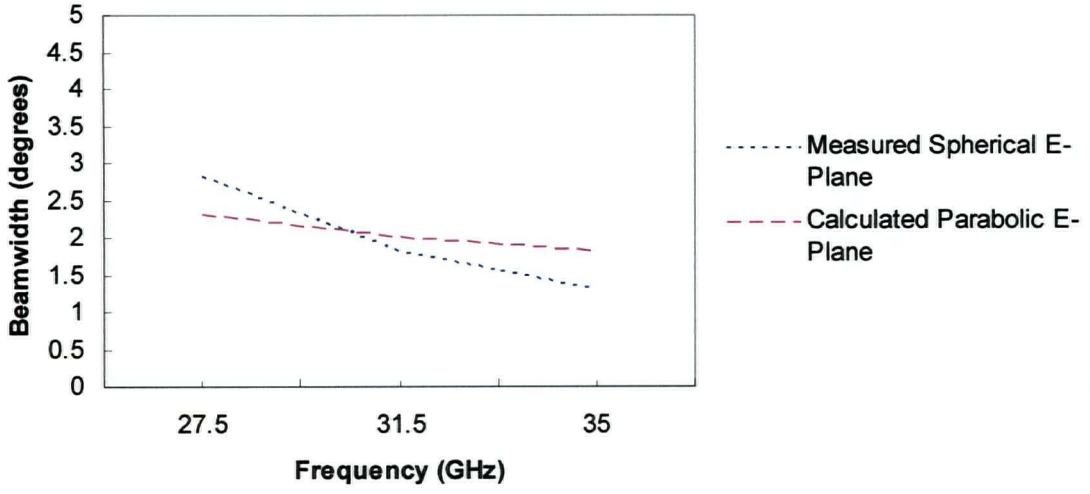

Figure 6.2-5 E-Plane Beamwidth vs. Frequency for Measured and Calculated Results, for Focal Length = 80 cm, and Elevation Angle ≈ 30°

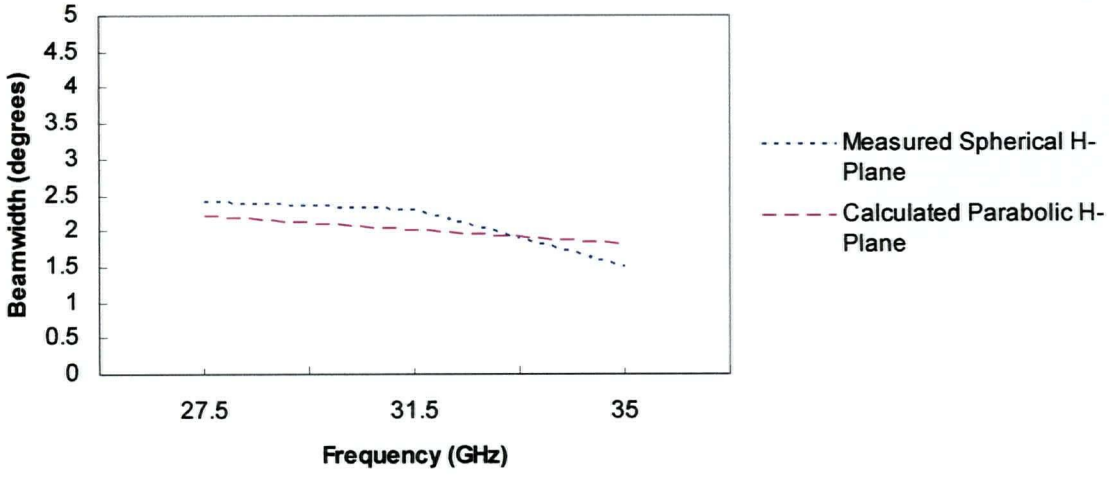

Figure 6.2-6 H-Plane Beamwidth vs. Frequency for Measured and Calculated Results, for Focal Length = 80 cm, and Elevation Angle ≈ 30°

From these plots one can see the calculated beamwidths for a parabolic reflector match very closely with the measured beamwidths of the spherical reflector. The comparison plots for elevation angles 30° and 50° are shown in Appendix F, Figures F-5 – F-8. At all elevation angles the beamwidths in the E-plane are slightly lower for the

measured spherical reflector than the calculated parabolic reflector by approximately 0.5° to 1°. However, the accuracy of the measured E-plane measurements is estimated to be within ±1°. Therefore, it can only be generally said that both the calculated and measured beamwidth results are quite similar. The spherical reflector actually closely resembles a parabolic reflector due to its very large *f/D* ratio. For this reason, the spherical aberration experienced by the spherical reflector is less, and the benefits of a spherical reflector such as lower costs and a wider beam scanning area are still realized.

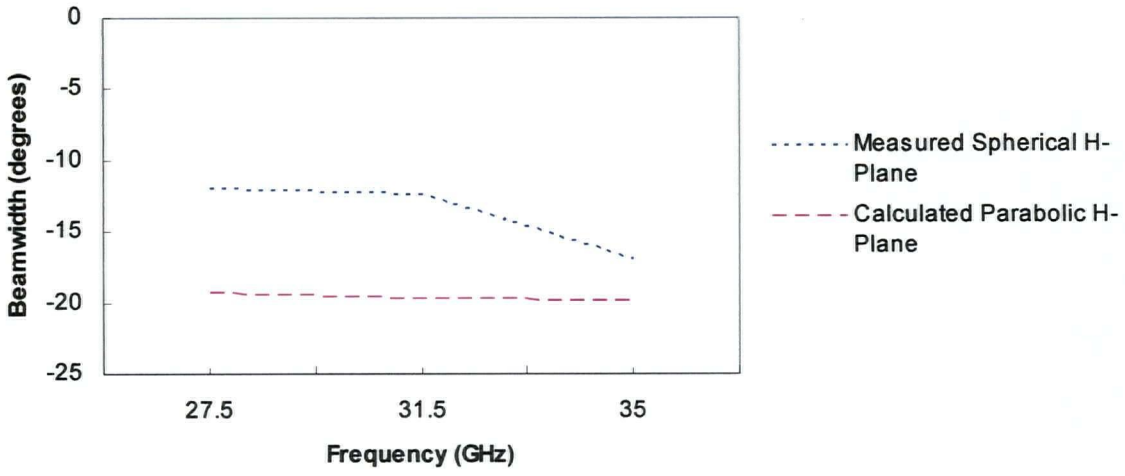

Figure 6.2-7 H-Plane Sidelobe Level vs. Frequency for Measured and Calculated Results, for Focal Length = 80 cm, and Elevation Angle ≈ 30°

In Figure 6.2-7 above, the sidelobe levels calculated for the parabolic reflector are lower than the measured values for the spherical reflector. At 27.5 GHz the sidelobe level was 7.4 dB lower, and at 35 GHz the sidelobe level was only 2.0 dB lower. As expected, this trend was the same for all focal lengths and elevation angles; these can be seen in Appendix F, Figures F-9 and F-10. This can most likely be attributed to two main sources. Firstly, the feed horn allows for large amounts of spillover due to its low edge taper. Excess spillover causes a loss of power in the main beam, which then manifests

itself in higher sidelobe levels and reduced gain [20, pg 343]. As discussed previously, as frequency increases the edge taper increases also, this explains why the sidelobe levels are dropping at 35 GHz. This was most likely the main source of the sidelobes being higher than the calculated results. Two methods of correcting for the excess spillover are either using a feed horn with a narrower beamwidth, or using a reflector with a larger diameter. The second possible cause for the measured sidelobes being larger than the calculated sidelobes is, on the side of the antenna range, there were a number of metal objects that could not be easily removed. When performing the radiation pattern measurements, scattering from both the ground and these objects could have occurred such that the sidelobe levels would be slightly increased. However, absorbing foam was used directly in front of the reflector in an attempt to reduce ground reflection.

In Table 5.2-4, directivities for both the measured and calculated results are shown. In Figure 6.2-8 below, the directivities are compared.

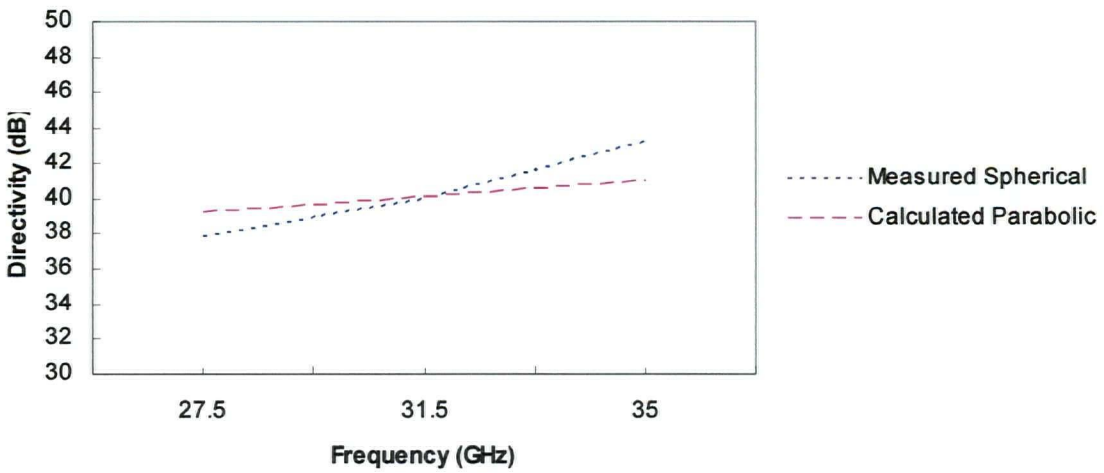

Figure 6.2-8 Directivity vs. Frequency for Measured and Calculated Results, for Focal Length = 80 cm, and Elevation Angle ≈ 30°

One can see the directivities for the measured and calculated results are comparable. At the lower frequencies where the edge taper was at its lowest, the measured directivities are slightly lower than the calculated. At 35 GHz the edge taper is at 9.574, roughly the optimum value, the measured directivity becomes larger than the calculated. One reason for this is the increase in gain from the reflector capturing a larger portion of the radiated power at the higher frequencies.

6.3 The Antenna Under Wet Conditions

In Chapter 5, Table 5.3-1, the results for the wet-antenna attenuation measurements are shown. From this table it is apparent that the average signal attenuation was less than 1 dB in almost all cases. There were fluctuations of a fraction of a decibel. These were due to the build-up and run-off of water on the reflector surface [9]. As expected, at higher frequencies there were higher levels of attenuation. At each elevation angle the increase in frequency corresponded to an increase in average signal attenuation. This is seen in Figure 6.3-1 below.

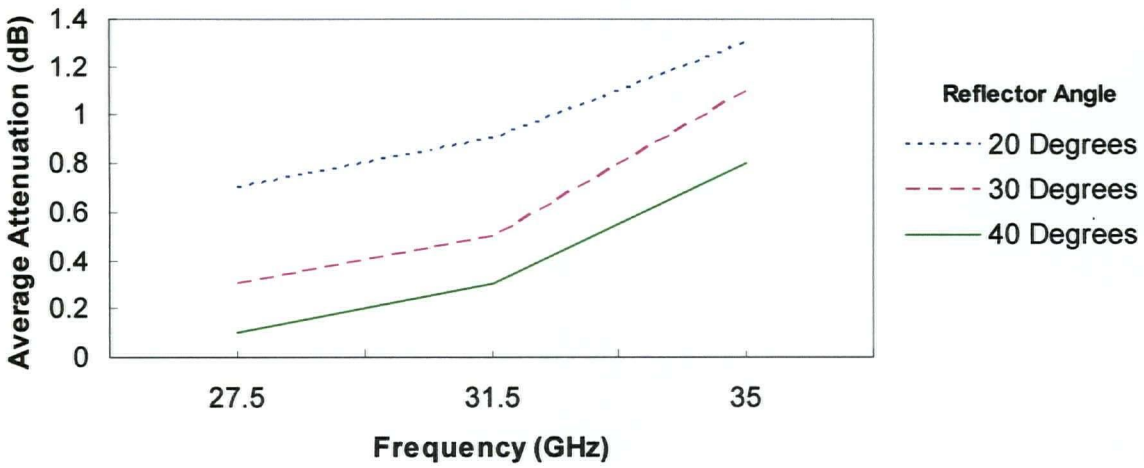

Figure 6.3-1 Average Attenuation vs. Frequency, for all Reflector Angles

Also apparent in Figure 6.3-1, is the increase in signal attenuation with decreasing elevation angle. It is important to note that this observation was made using the method of simulating the elevation angles described in Section 4.2.1.2 and shown in Figures 4.2-1 and 4.2-2. Using this method, the angle of the reflector became steeper with increasing elevation angle. If this simulated method had not been used, and the elevation angle had truly been changed by rotating the transmitter, the angle of the reflector would have moved in the opposite direction. This was shown in Figures 4.2-3 and 4.2-4 for an elevation angle of 10°. For this reason the attenuation was plotted versus the reflector angle.

The important observation that can be made by both scenarios is that the signal attenuation level increases with decreasing reflector angle (with respect to the ground). This can be attributed to water running off the reflector at a lower rate, and therefore causing higher attenuation levels. No conclusions can be drawn with regard to the effect of elevation angle on attenuation level. This is due to not truly changing the elevation

angle, but using the simulated method described above; therefore these measurements did not reflect a real situation.

It should also be noted, that when performing the measurements at reflector angles of 20° and 40°, the tilting of the antenna stand caused the horn to be offset from the vertical position by 20°. This did not seem to affect the attenuation levels of the antenna, as the lowest levels were recorded at an elevation angle of 40°.

6.4 CONCLUSIONS

The objective of this work was to measure the properties of a new antenna that was developed as a solution to the problem of wet-antenna attenuation at mm-wavelengths. It has been shown that this antenna, which is inherently of simple design and low cost, provides a performance level which would make it suitable for many applications.

Previous wet-antenna studies of conventional reflector antennas operating at mm-wavelengths in the Ka-band displayed losses of up 10 dB. The spherical reflector antenna investigated showed losses of an absolute maximum to be 1.6 dB at the highest considered frequency of 35 GHz, with average losses shown to be less than 1 dB. Radiation patterns and wet-antenna attenuation plots were obtained at three frequencies spanning the ka-band, and at three elevation angles including 10°, 30°, and 50°. At all frequencies and elevation angles the antennas performance was shown to be suitable for satellite and commercial applications. The demand for antennas that are capable of

meeting the stringent requirements of the Ka-band, while still providing a high level of performance is ever increasing. The antenna tested achieved the goals of this investigation and provides a solution to a current problem found in communications at mm-wavelengths.

6.5 Recommendations For Further Work

Possible future work includes optimization of the investigated antenna with regard to the feed horn's taper and reflector dimensions. Different feed horns could also be considered to provide different antenna polarizations, as well as wet-antenna attenuation measurements done using the true method of changing the elevation angle could also be considered.

References

[1] M. Kharadly, R. Ross, and B. Dow, "Analysis of the ACTS-Vancouver path propagation data," in *Proc. NAPEX XX and ACTS Prop. Studies Mini Workshop*, Fairbanks, AK, June 1996, pp. 67-83.

[2] V.N. Bringi and J. Beaver, "Ka-Band propagation studies using ACTS propagation terminal and the CSU-CHILL multiparameter radar," in *Proc. Ninth ACTS Propagation Studies Workshop, (APSW IX)*, Herndon, VA, Nov. 1996, pp. 61-82.

[3] S. Horan, F. Paulic, and B. Atle, "New Mexico ACTS propagation terminal status," in *Proc. NAPEX XXI and ACTS Prop. Studies Mini Workshop*, El Segundo, CA, June 1997, pp. 1-103-1-125.

[4] R. J. Acosta, R. Reinhart, D. X. Kifer, and C. Emrich, "Wet antenna studies at LeRC," in *Proc. NAPEX XXI and ACTS Prop. Studies Mini Workshop*, El Segundo, CA, June 1997, pp. 2-41-2-56.

[5] M. Kharadly and B. Dow, "The UBC/ACTS experiment – Status report," in *Proc. Ninth ACTS Propagation Studies Workshop (APSW IX)*, Herndon, VA, Nov. 1996, pp. 45-59.

[6] M. M. Z. Kharadly and R. Ross, "Effect of Wet Antenna Attenuation on Propagation Data Statistics," *IEEE Trans. Comm.*, vol. 49, no. 8, pp. 1183-1191, August, 2001.

[7] R. K. Crane, "Analysis of the Effects of Water on the ACTS Propagation Terminal Antenna," *IEEE Trans. Comm.*, vol. 50, no. 7, pp. 954-965, July, 2002.

[8] M. M. Z. Kharadly and R. Ross, "Performance of some conventional ka-band antennas in (simulated) rain." Millennium Conference on Antennas and Propagation (AP2000), Davos, Switzerland, Abstract # 472, April 2000.

[9] M. M. Z. Kharadly and R. Ross, "Evaluation of some conventional terminal antennas' performance in rain at ka-band frequencies." Proc 7th Ka-Band Utilization Conference , Santa Margherita Ligure, Genoa, Italy, pp. 303-308, September, 2001.

[10] J.Y.C. Cheah, "Wet antenna effect on VSAT rain margin," *IEEE Trans. Comm.*, vol. 41, no. 7, pp. 1238-1244, August, 1993.

[11] M. M. Z. Kharadly and A. Chan, "New antenna concept for efficient ka-band terminal operation in rain," *Proc 4th Ka-Band Utilization Conference*, Venice, Italy, pp. 223-230, November, 1998.

[12] M. M. Z. Kharadly and A. Chan., U.S. Patent 6,052,094, issued April 18, 2000.

[13] T. S. Chu, "A Multibeam Spherical Reflector Antenna," *Antenna and Propagations Society International Symposium*, vol. 7, pp. 94-101, December, 1969.

[14] K. K. Chan, R. Blasing, and B. Wallace, "Multiple Beam Lens Antenna for LEO Communication Satellite," *Antenna and Propagations Society International Symposium AP-S. Digest*, vol. 3, pp. 1684-1687, July, 1996.

[15] T. Vu, Quoc Vu, and Dinh Doan, "High-Efficiency Spherical Reflector Antenna – A Case Study," *IEEE Trans. on Antennas and Propagation*, vol. 25, no. 3, pp. 351-356, May, 1976.

[16] Collin, Robert E. and Zucker, Francis J. Antenna Theory Part 2. New York: McGraw-Hill Book Company, pp. 669, 1969.

[17] Blake, Lamont V. Antennas. New York: John Wiley & Sons, Inc., pp. 133-135, 1966.

[18] Ulaby, Fawwaz T. Fundementals of Applied Electromagnetics. New Jersey: Prentice Hall, pp. 351-353, 1999.

[19] Schelkunoff, Sergei A. and Friis, Harald T. Antennas Theory and Practice. New York: John Wiley & Sons, Inc., 1952.

[20] Stutzman, Warren L. and Thiele, Gary A. Antenna Theory and Design Second Edition. New York: John Wiley & Sons, Inc., 1998.

APPENDIX A

Pyramidal Feed Horn Radiation Patterns for the H-plane

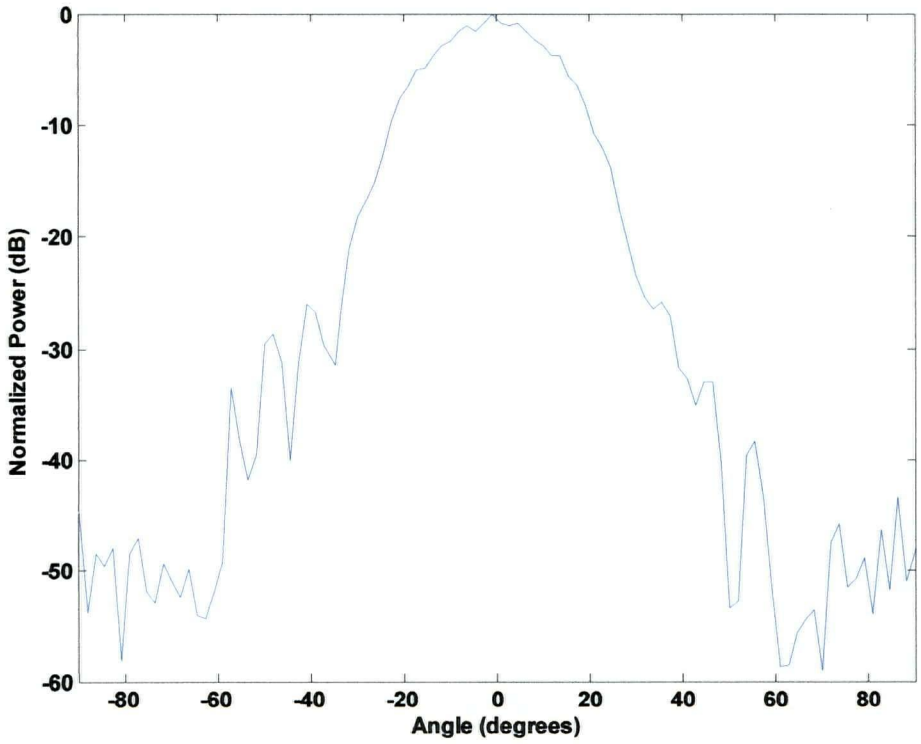

Figure A-1 H-plane Radiation Pattern for the Feed Horn with f = 27.5 GHz

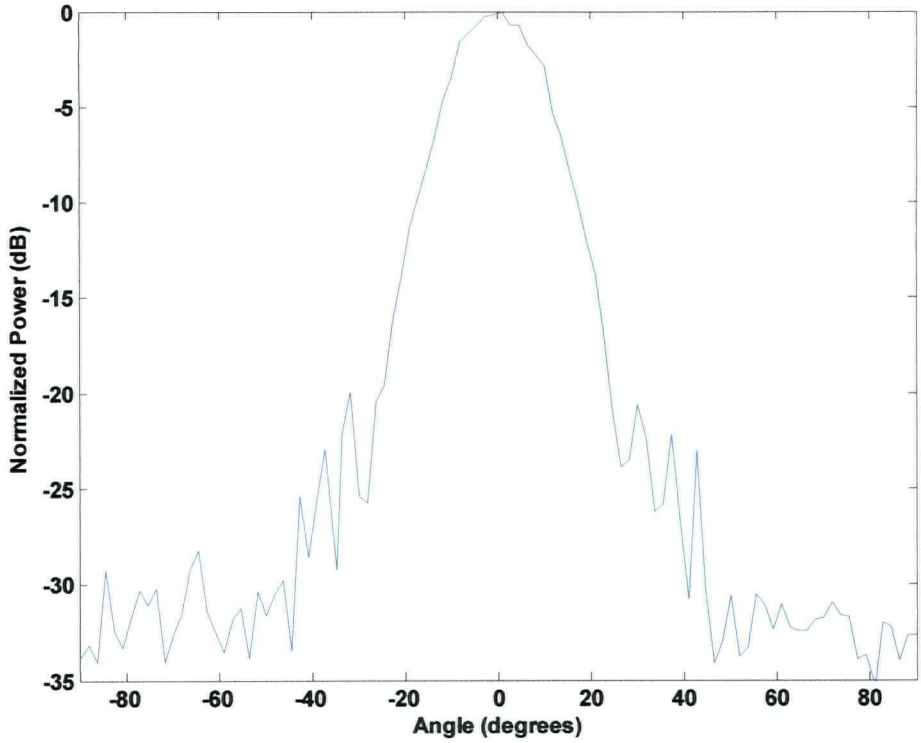

Figure A-2 H-plane Radiation Pattern for the Feed Horn with f = 31.5 GHz

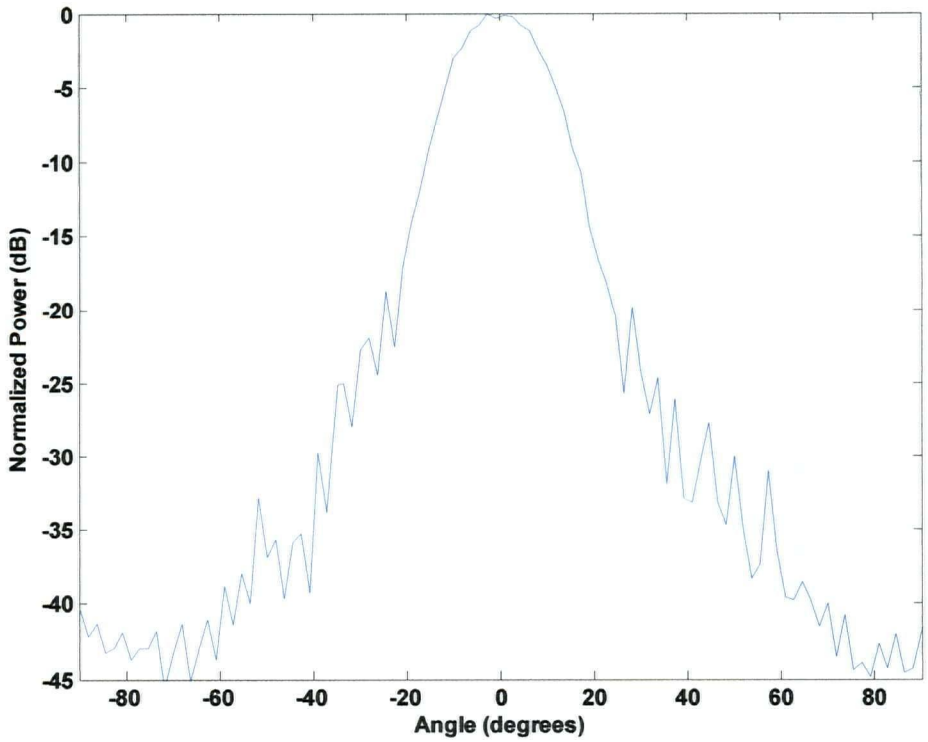

Figure A-3 H-plane Radiation Pattern for the Feed Horn with f = 35 GHz

APPENDIX B

Pyramidal Feed Horn Radiation Patterns for the E-plane

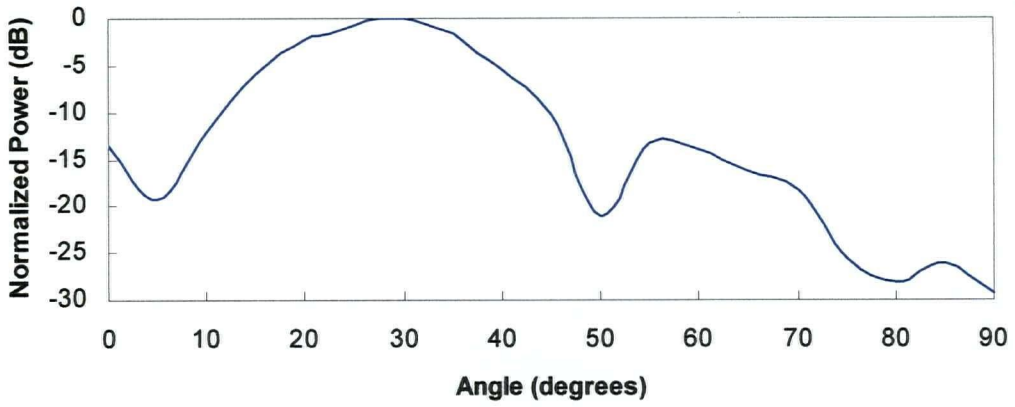

Figure B-1 E-plane Radiation Pattern for the Feed Horn with f = 27.5 GHz

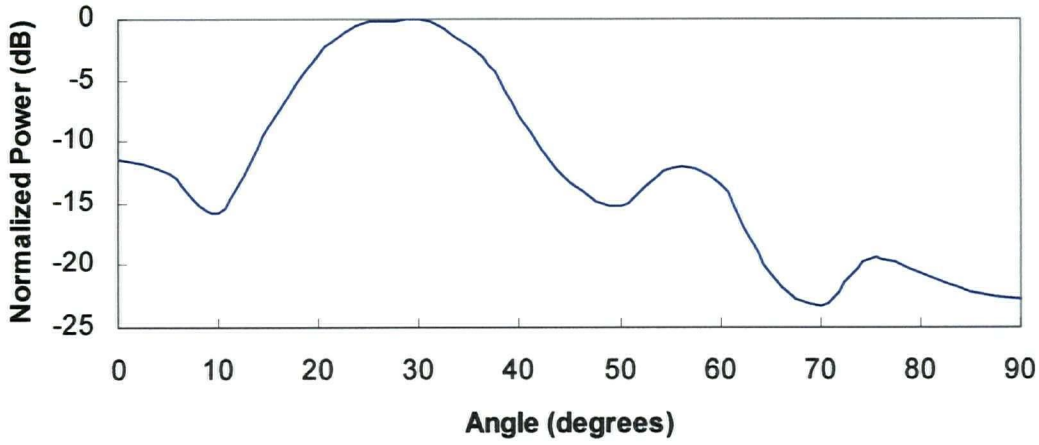

Figure B-2 E-plane Radiation Pattern for the Feed Horn with f = 31.5 GHz

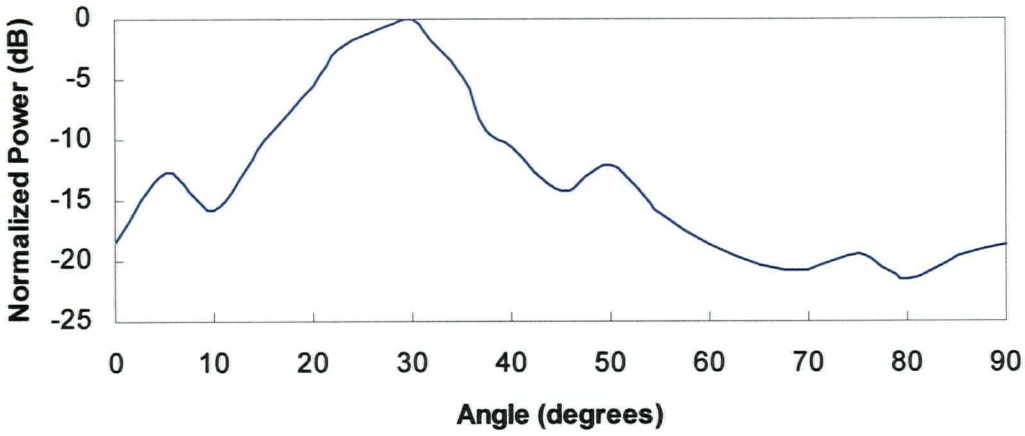

Figure B-3 E-plane Radiation Pattern for the Feed Horn with f = 35 GHz

APPENDIX C

Spherical Reflector Radiation Patterns for the H-plane

C-1 FOCAL LENGTH OF 70 CM

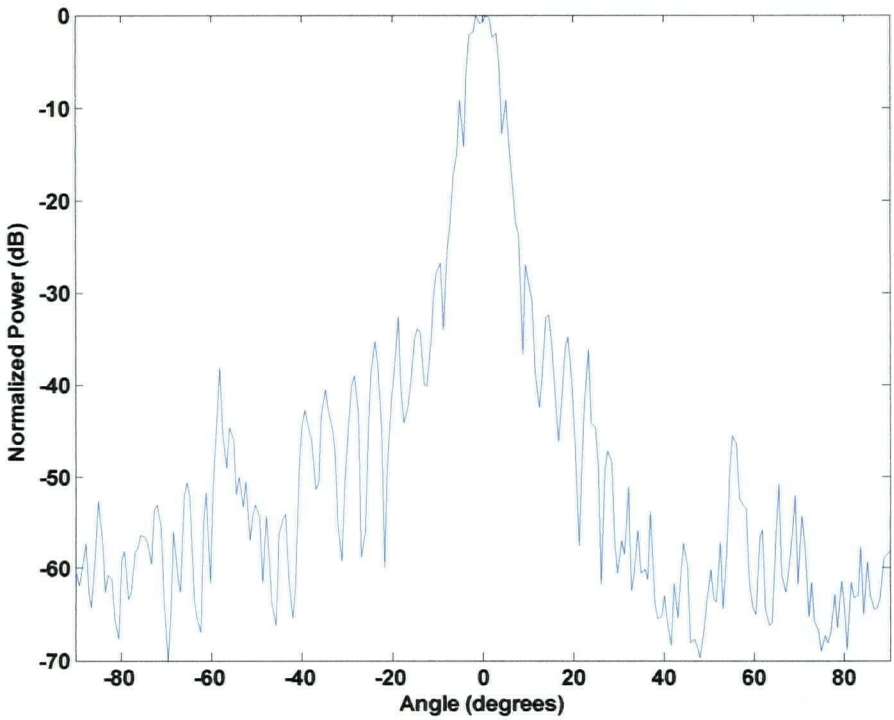

Figure C-1 H-plane Radiation Pattern for the Spherical Reflector Antenna with Focal Length = 70 cm, f = 27.5 GHz, and Elevation Angle ≈ 10°

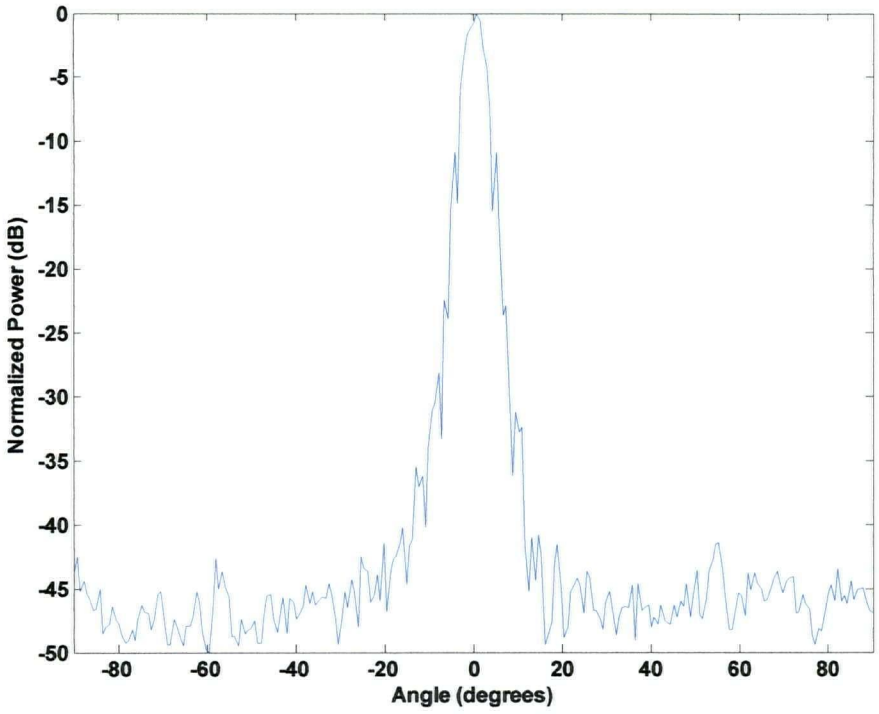

Figure C-2 H-plane Radiation Pattern for the Spherical Reflector Antenna with Focal Length = 70 cm, f = 31.5 GHz, and Elevation Angle ≈ 10°

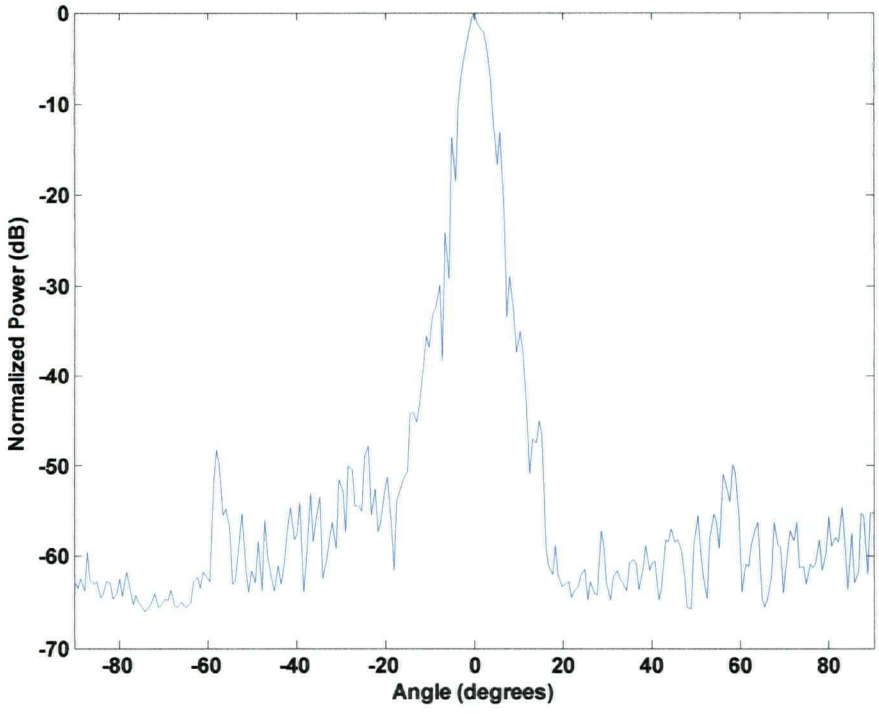

Figure C-3 H-plane Radiation Pattern for the Spherical Reflector Antenna with Focal Length = 70 cm, f = 35 GHz, and Elevation Angle ≈ 10°

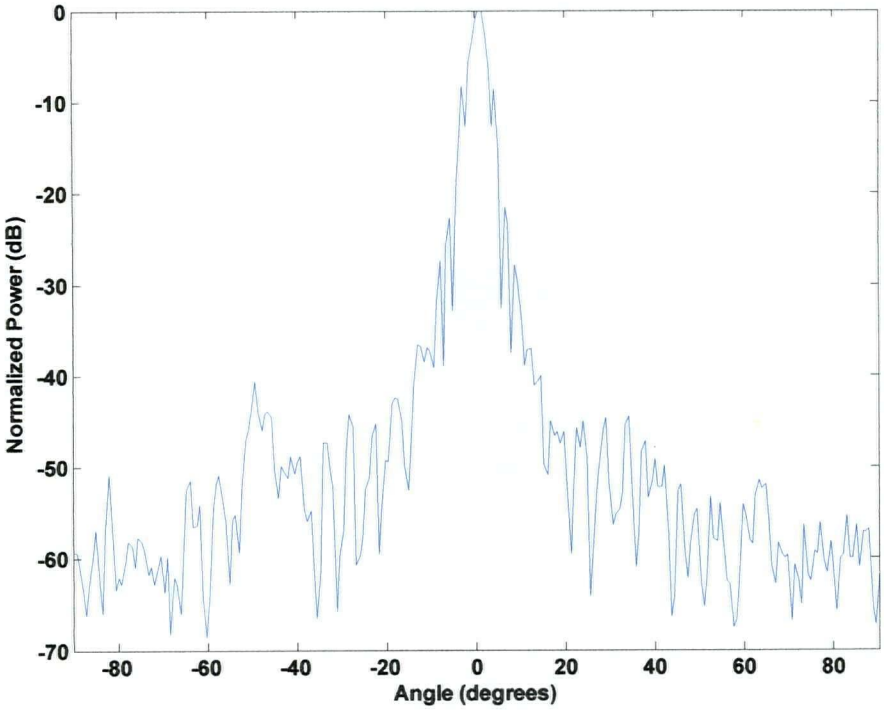

Figure C-4 H-plane Radiation Pattern for the Spherical Reflector Antenna with Focal Length = 70 cm, f = 27.5 GHz, and Elevation Angle ≈ 30°

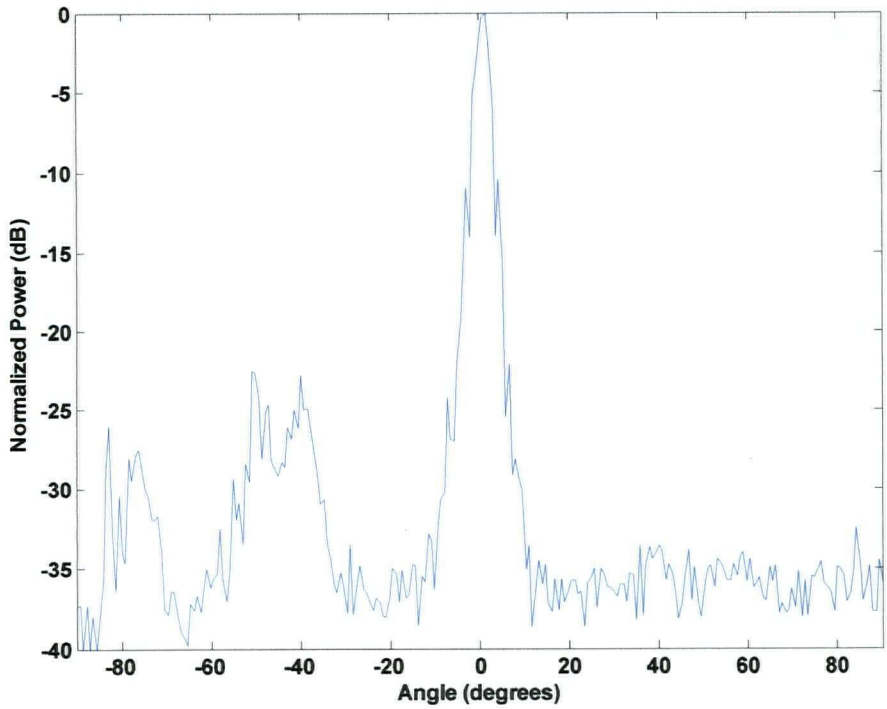

Figure C-5 H-plane Radiation Pattern for the Spherical Reflector Antenna with Focal Length = 70 cm, f = 31.5 GHz, and Elevation Angle ≈ 30°

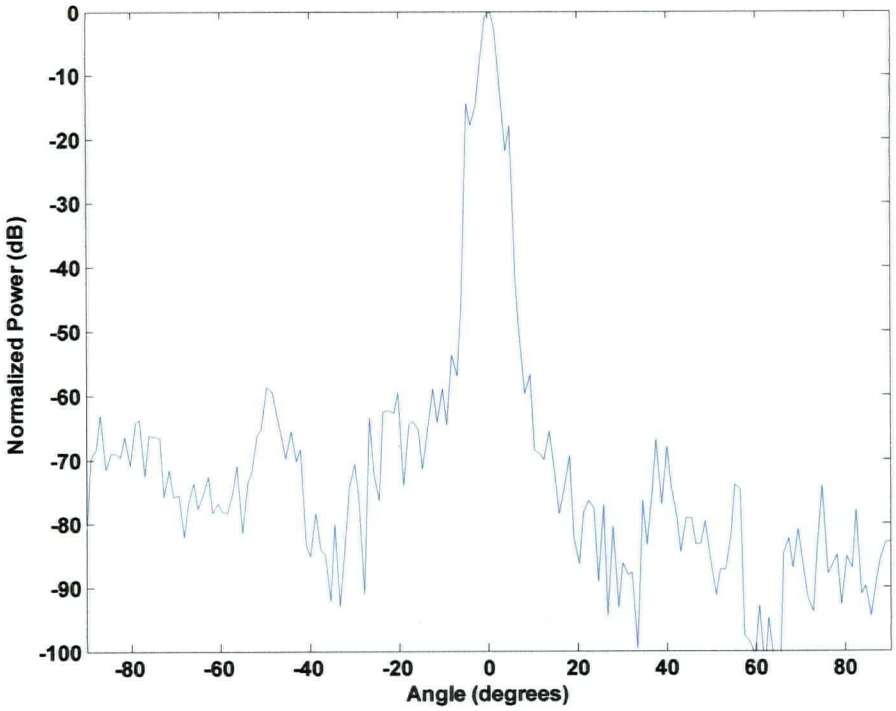

Figure C-6 H-plane Radiation Pattern for the Spherical Reflector Antenna with Focal Length = 70 cm, f = 35 GHz, and Elevation Angle ≈ 30°

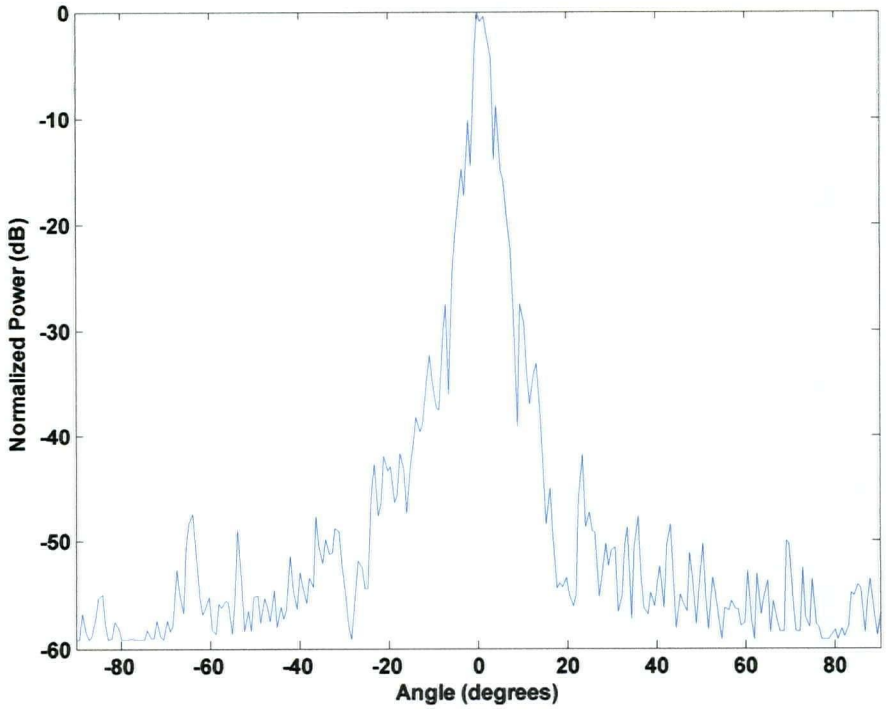

Figure C-7 H-plane Radiation Pattern for the Spherical Reflector Antenna with Focal Length = 70 cm, f = 27.5 GHz, and Elevation Angle ≈ 50°

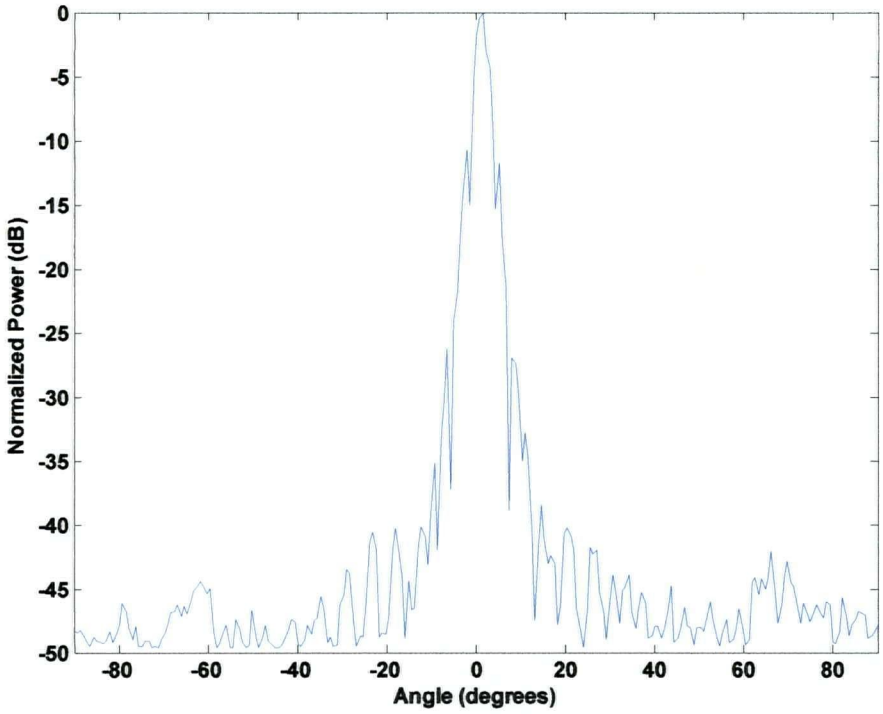

Figure C-8 H-plane Radiation Pattern for the Spherical Reflector Antenna with Focal Length = 70 cm, f = 31.5 GHz, and Elevation Angle ≈ 50°

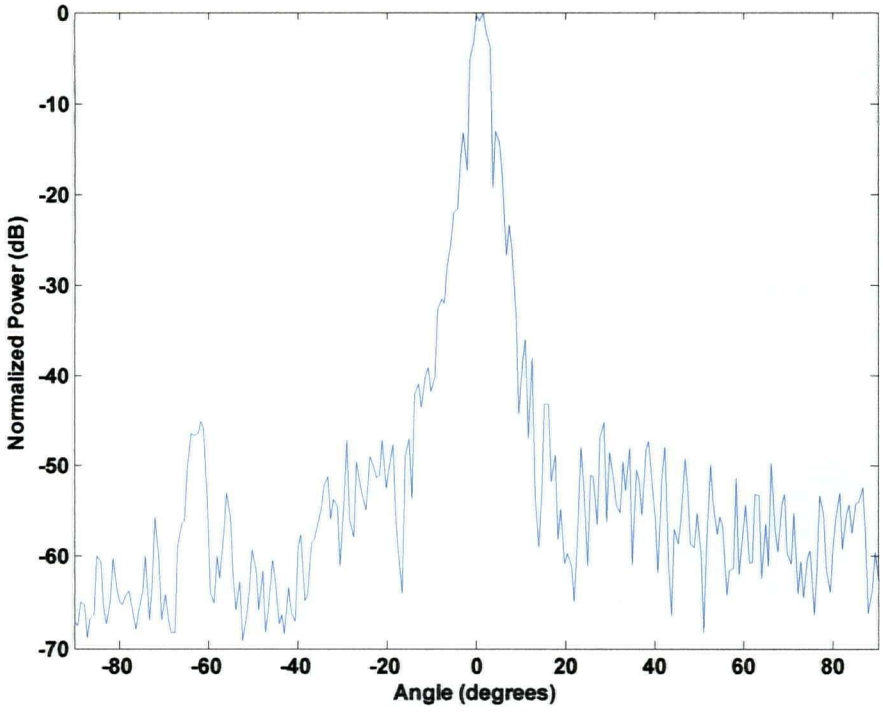

Figure C-9 H-plane Radiation Pattern for the Spherical Reflector Antenna with Focal Length = 70 cm, f = 35 GHz, and Elevation Angle ≈ 50°

C-2 Focal Length of 75 cm

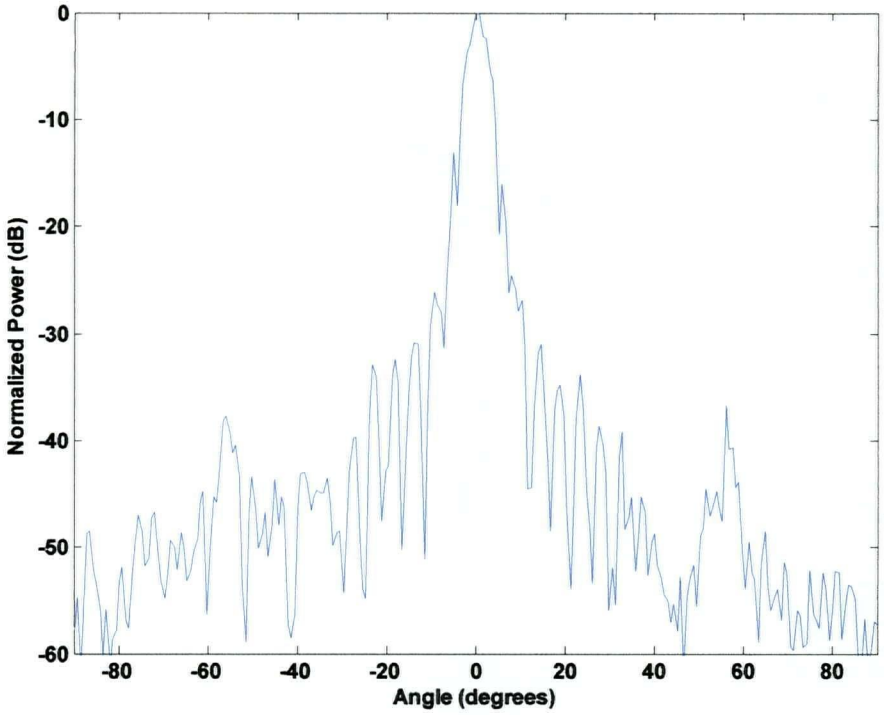

Figure C-10 H-plane Radiation Pattern for the Spherical Reflector Antenna with Focal Length = 75 cm, f = 27.5 GHz, and Elevation Angle ≈ 10°

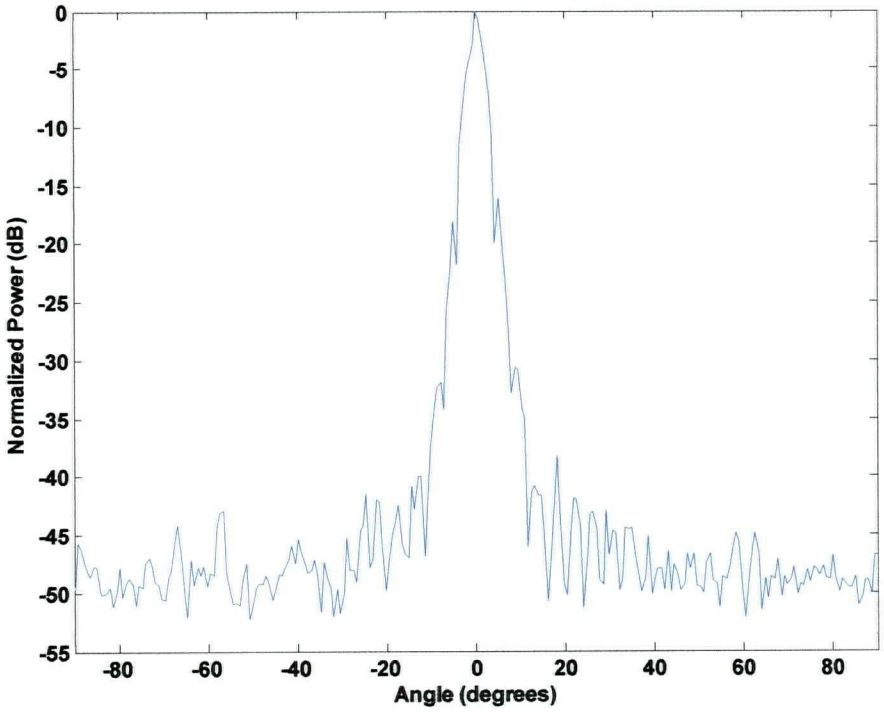

Figure C-11 H-plane Radiation Pattern for the Spherical Reflector Antenna with Focal Length = 75 cm, f = 31.5 GHz, and Elevation Angle ≈ 10°

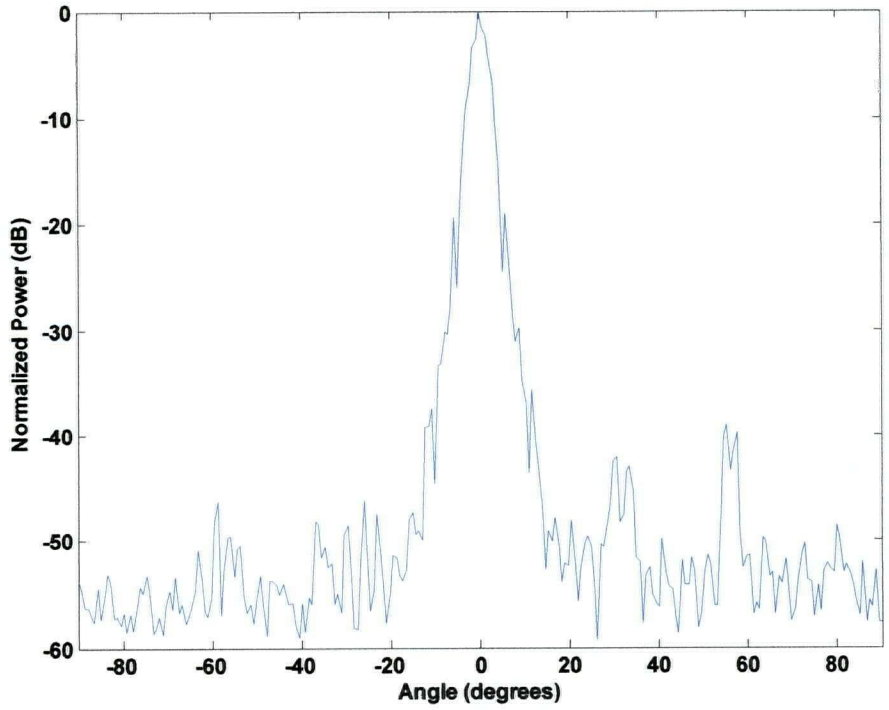

Figure C-12 H-plane Radiation Pattern for the Spherical Reflector Antenna with Focal Length = 75 cm, f = 35 GHz, and Elevation Angle ≈ 10°

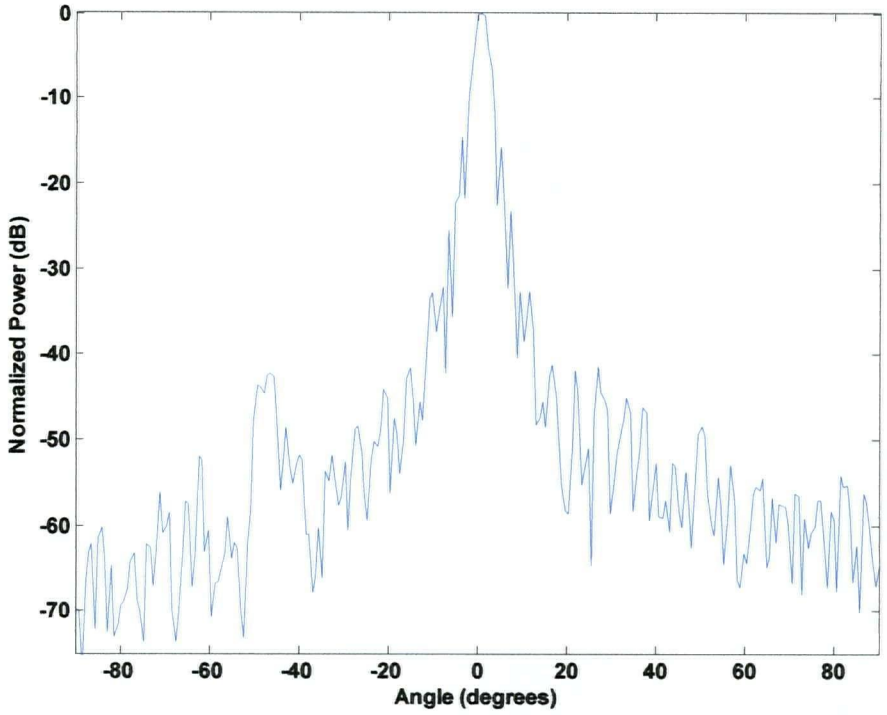

Figure C-13 H-plane Radiation Pattern for the Spherical Reflector Antenna with Focal Length = 75 cm, f = 27.5 GHz, and Elevation Angle ≈ 30°

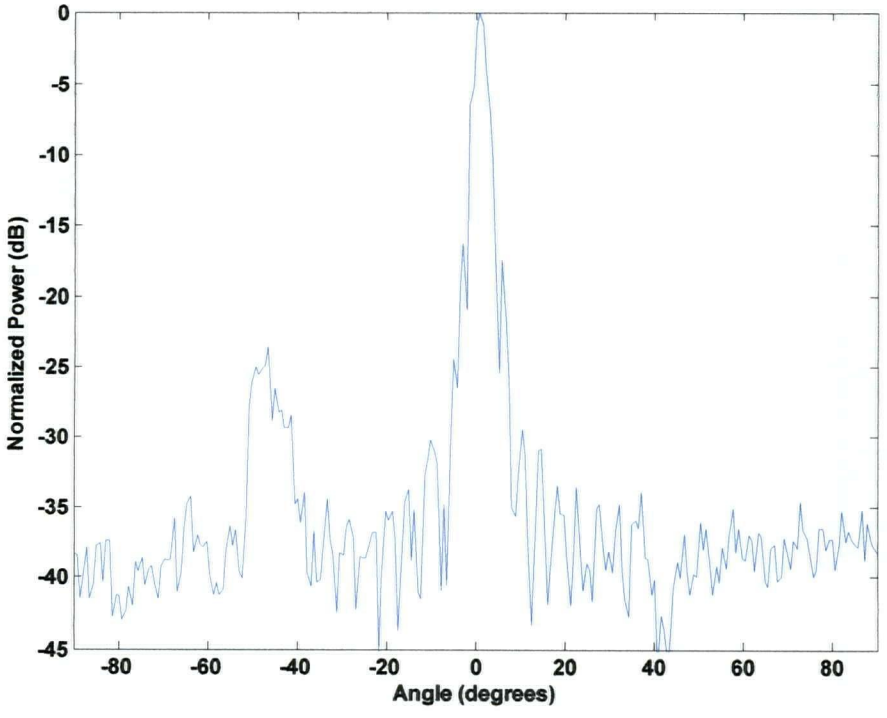

Figure C-14 H-plane Radiation Pattern for the Spherical Reflector Antenna with Focal Length = 75 cm, f = 31.5 GHz, and Elevation Angle ≈ 30°

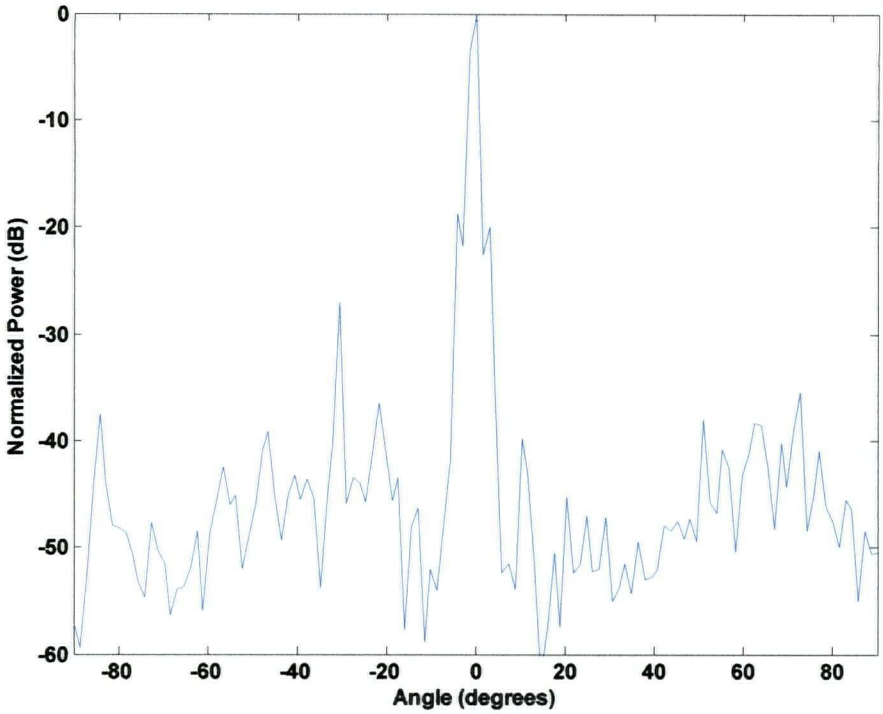

Figure C-15 H-plane Radiation Pattern for the Spherical Reflector Antenna with Focal Length = 75 cm, f = 35 GHz, and Elevation Angle ≈ 30°

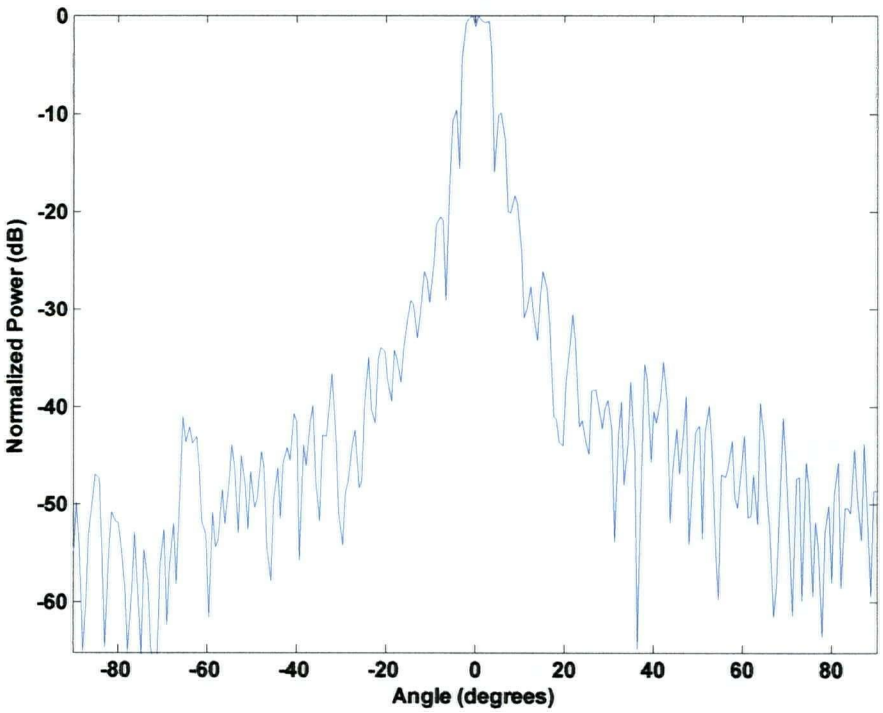

Figure C-16 H-plane Radiation Pattern for the Spherical Reflector Antenna with Focal Length = 75 cm, f = 27.5 GHz, and Elevation Angle ≈ 50°

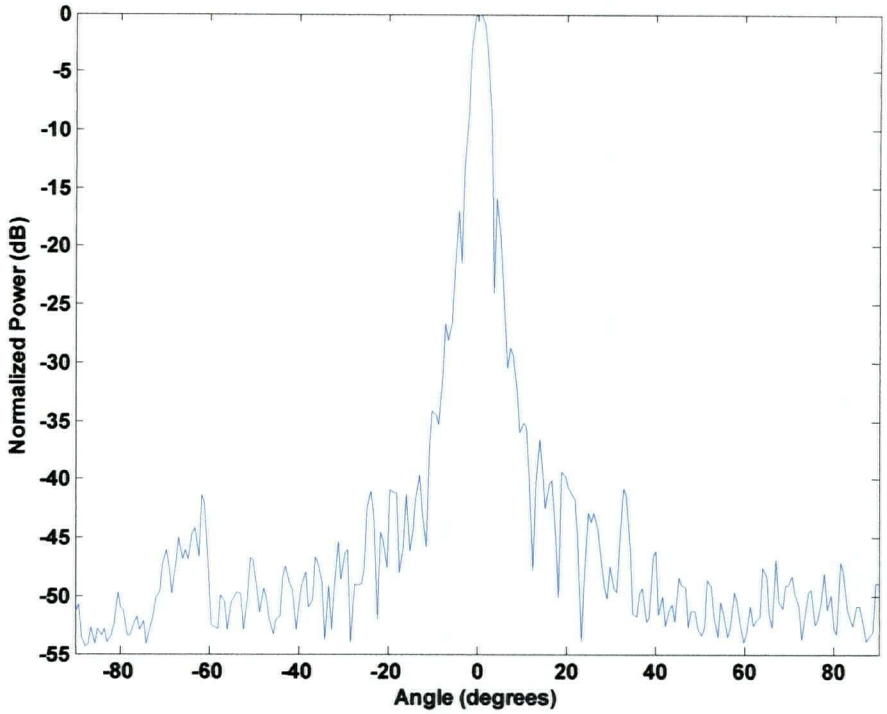

Figure C-17 H-plane Radiation Pattern for the Spherical Reflector Antenna with Focal Length = 75 cm, f = 31.5 GHz, and Elevation Angle ≈ 50°

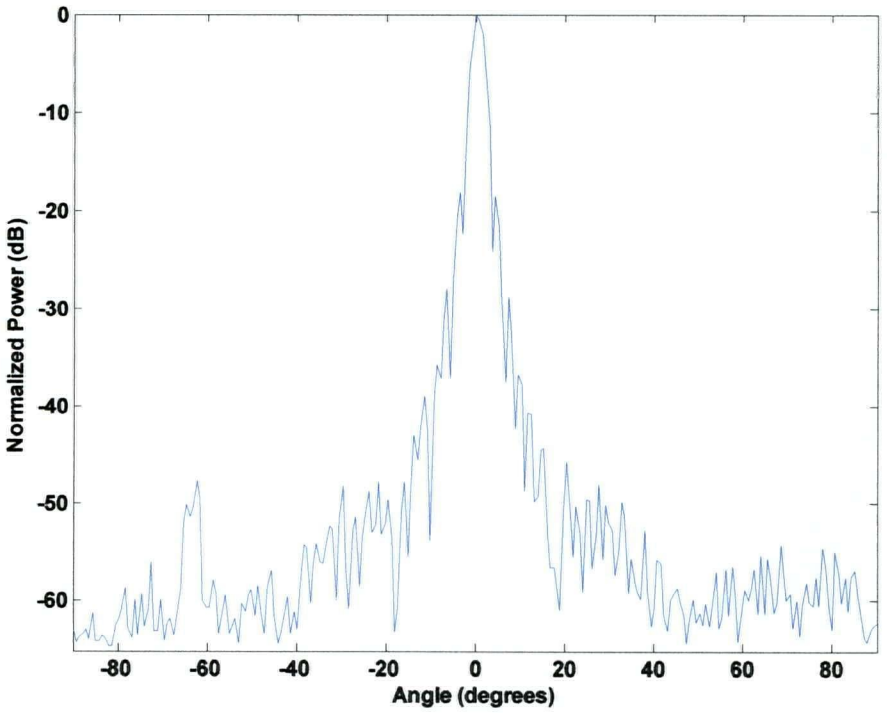

Figure C-18 H-plane Radiation Pattern for the Spherical Reflector Antenna with Focal Length = 75 cm, f = 35 GHz, and Elevation Angle ≈ 50°

C-3 Focal Length of 80 cm

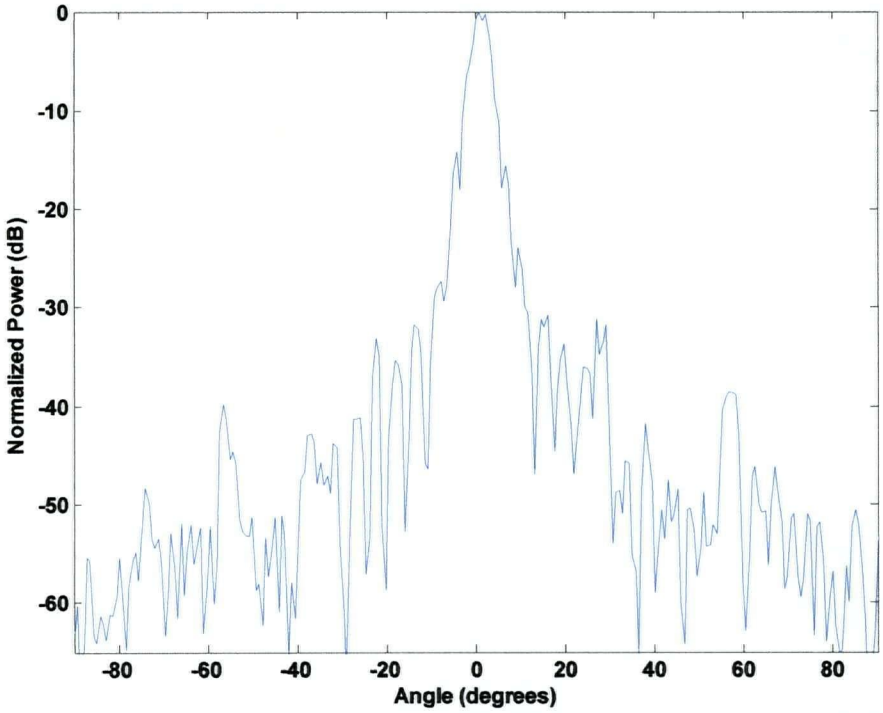

Figure C-19 H-plane Radiation Pattern for the Spherical Reflector Antenna with Focal Length = 80 cm, f = 27.5 GHz, and Elevation Angle ≈ 10°

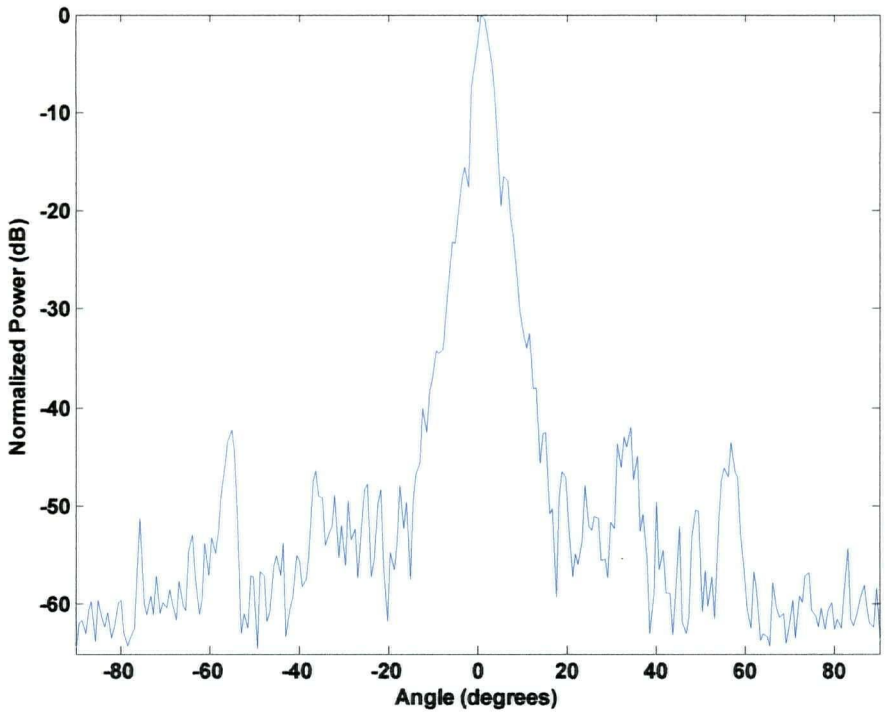

Figure C-20 H-plane Radiation Pattern for the Spherical Reflector Antenna with Focal Length = 80 cm, f = 31.5 GHz, and Elevation Angle ≈ 10°

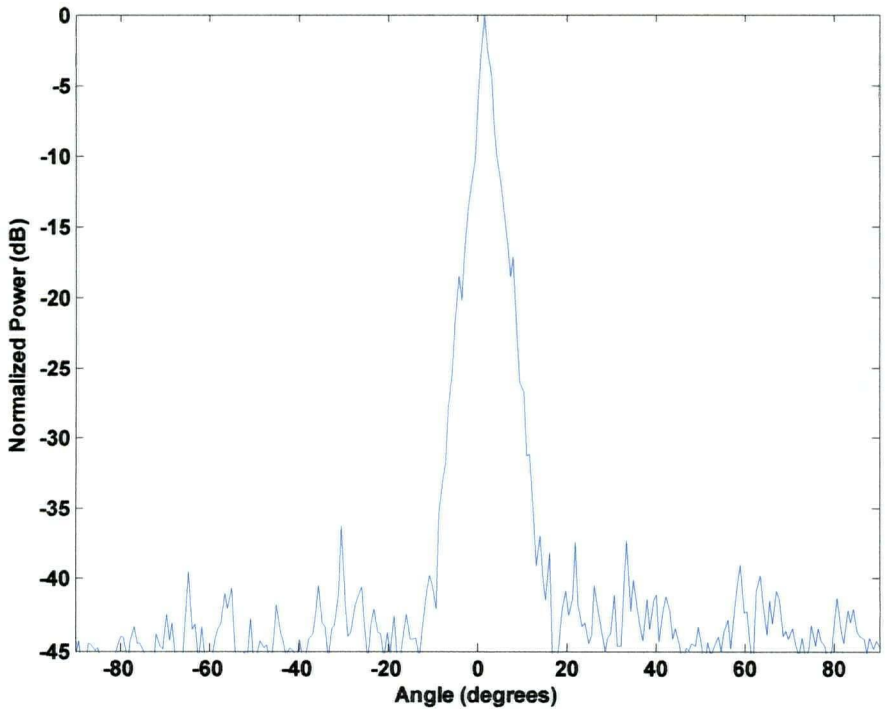

Figure C-21 H-plane Radiation Pattern for the Spherical Reflector Antenna with Focal Length = 80 cm, f = 35 GHz, and Elevation Angle ≈ 10°

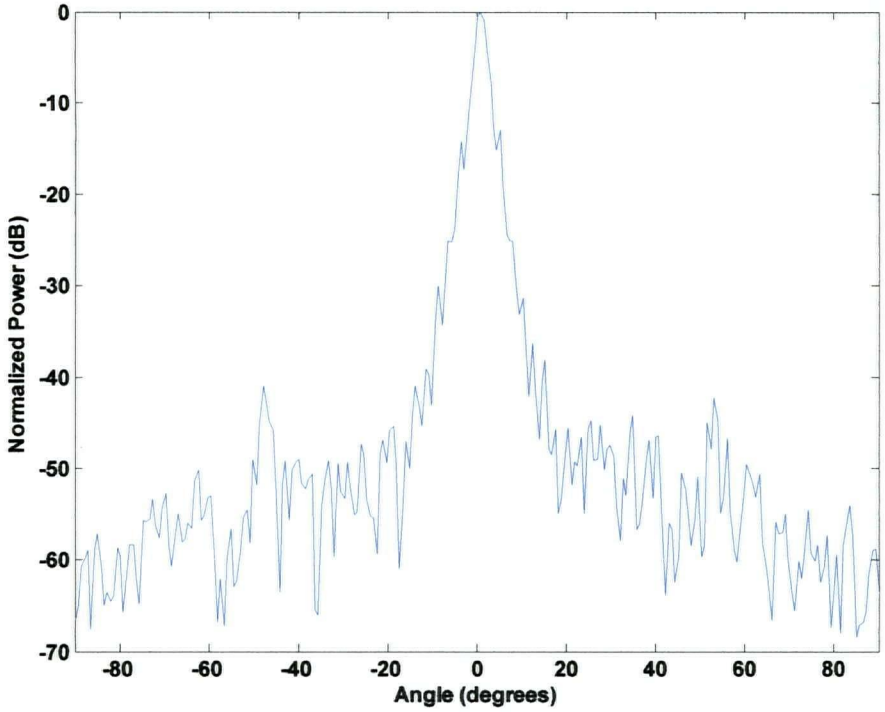

Figure C-22 H-plane Radiation Pattern for the Spherical Reflector Antenna with Focal Length = 80 cm, f = 27.5 GHz, and Elevation Angle ≈ 30°

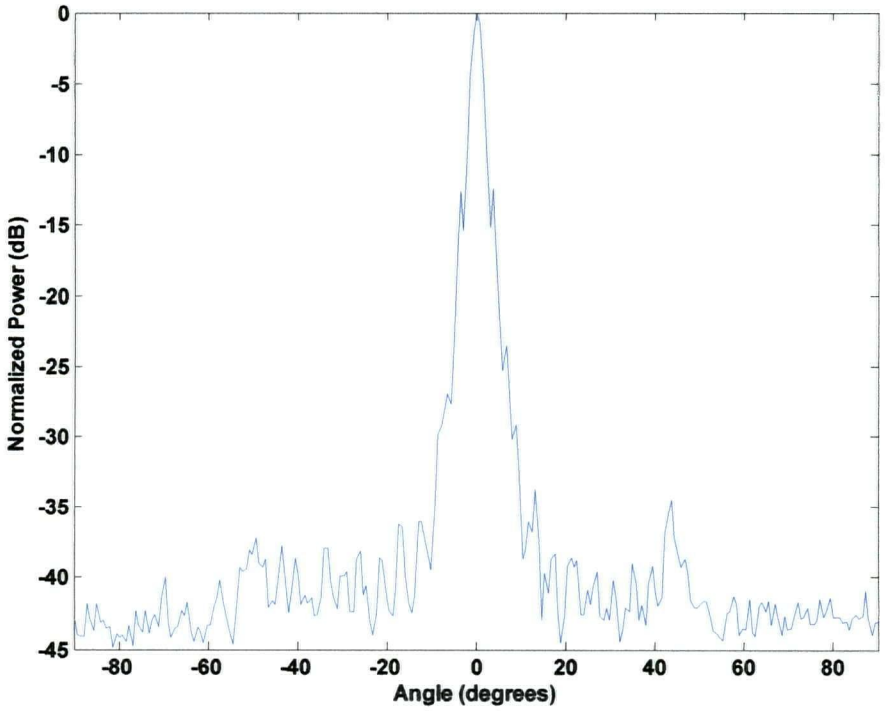

Figure C-23 H-plane Radiation Pattern for the Spherical Reflector Antenna with Focal Length = 80 cm, f = 31.5 GHz, and Elevation Angle ≈ 30°

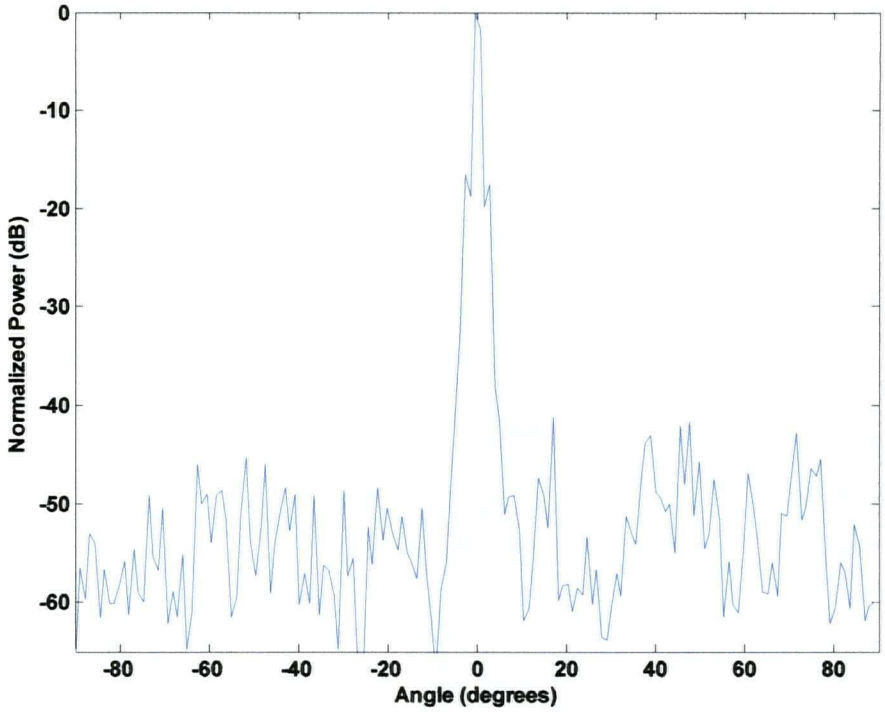

Figure C-24 H-plane Radiation Pattern for the Spherical Reflector Antenna with Focal Length = 80 cm, f = 35 GHz, and Elevation Angle ≈ 30°

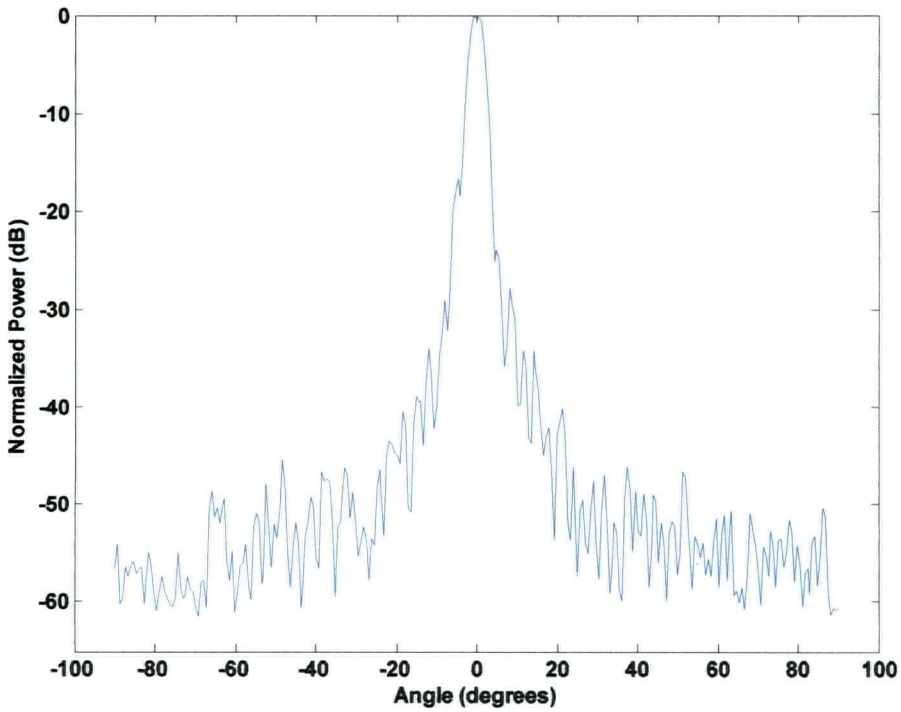

Figure C-25 H-plane Radiation Pattern for the Spherical Reflector Antenna with Focal Length = 80 cm, f = 27.5 GHz, and Elevation Angle ≈ 50°

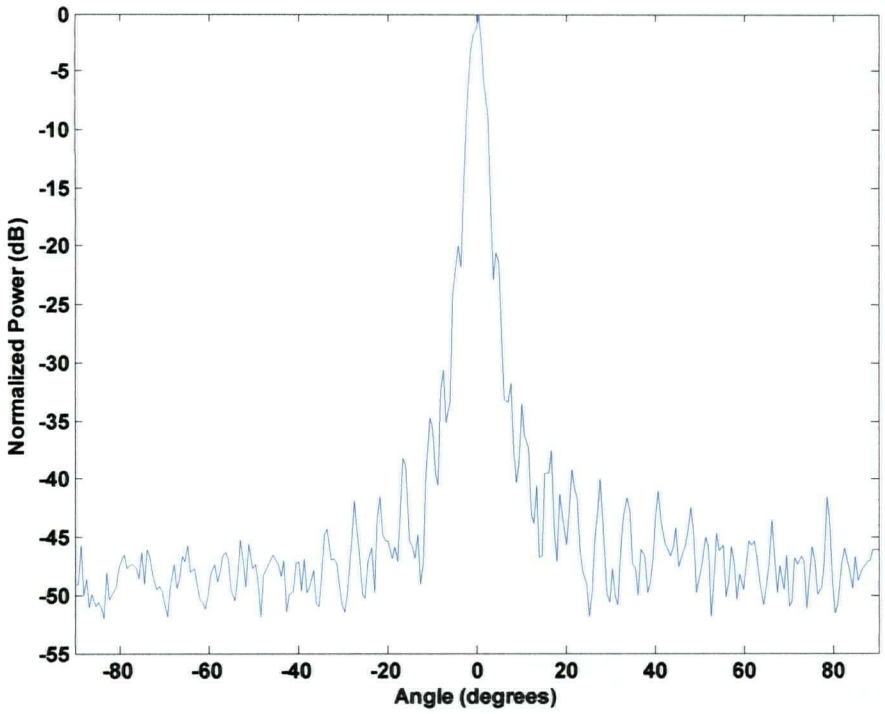

Figure C-26 H-plane Radiation Pattern for the Spherical Reflector Antenna with Focal Length = 80 cm, f = 31.5 GHz, and Elevation Angle ≈ 50°

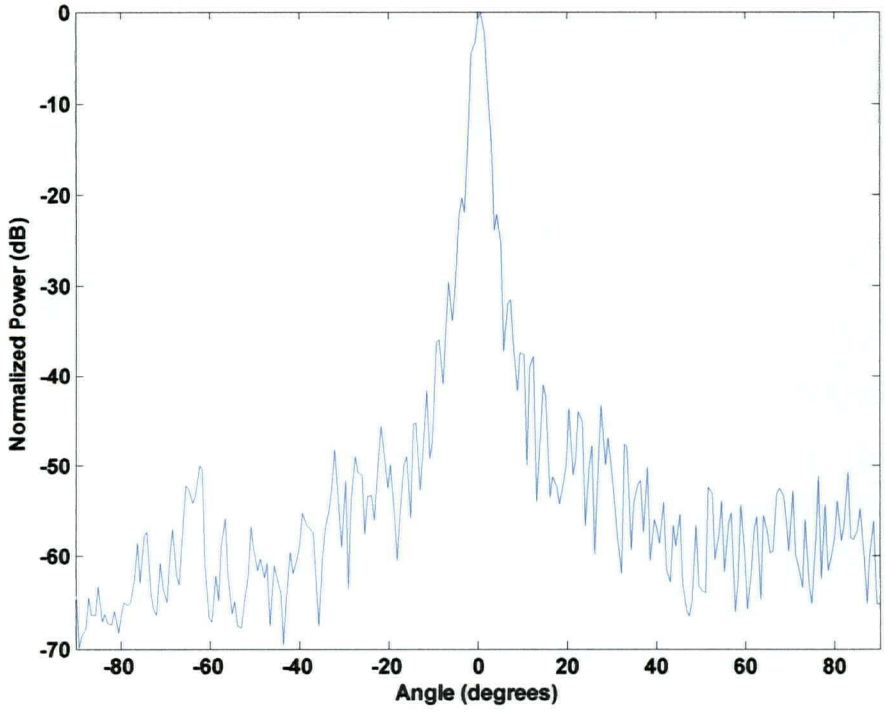

Figure C-27 H-plane Radiation Pattern for the Spherical Reflector Antenna with Focal Length = 80 cm, f = 35 GHz, and Elevation Angle ≈ 50°

C-4 Focal Length of 85 cm

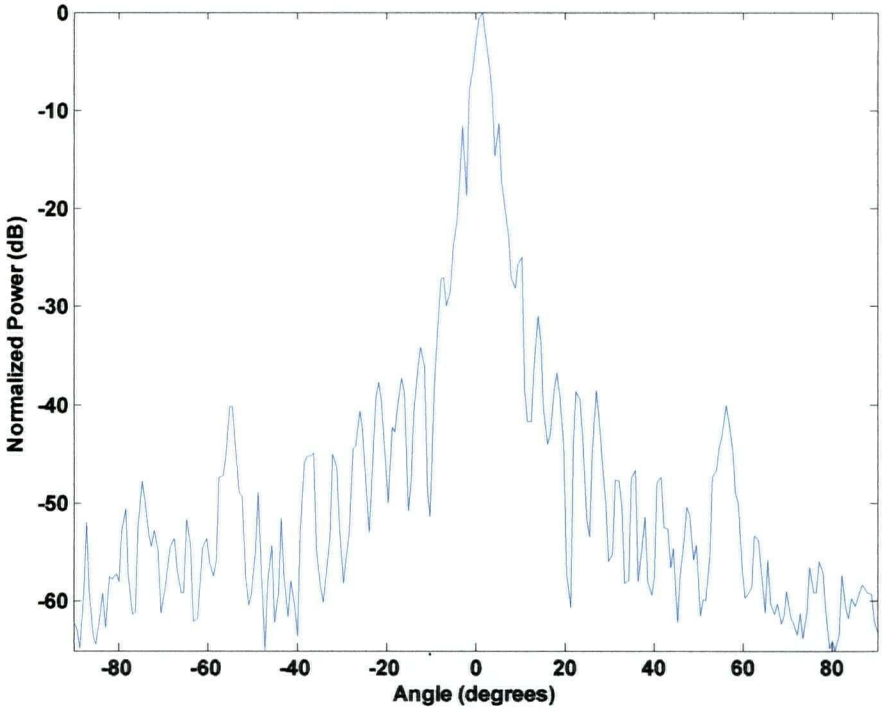

Figure C-28 H-plane Radiation Pattern for the Spherical Reflector Antenna with Focal Length = 85 cm, f = 27.5 GHz, and Elevation Angle ≈ 10°

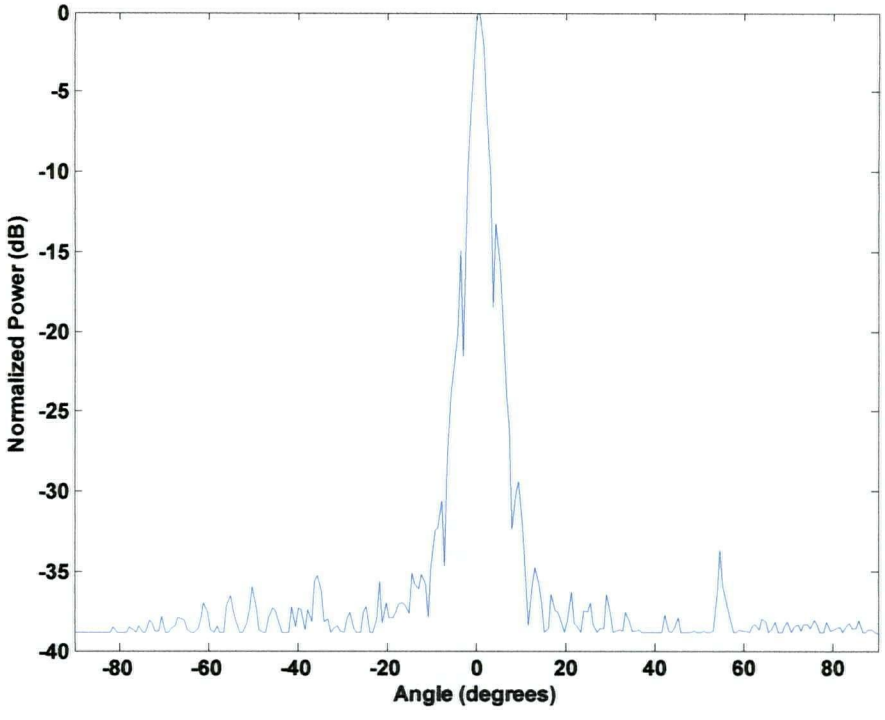

Figure C-29 H-plane Radiation Pattern for the Spherical Reflector Antenna with Focal Length = 85 cm, f = 31.5 GHz, and Elevation Angle ≈ 10°

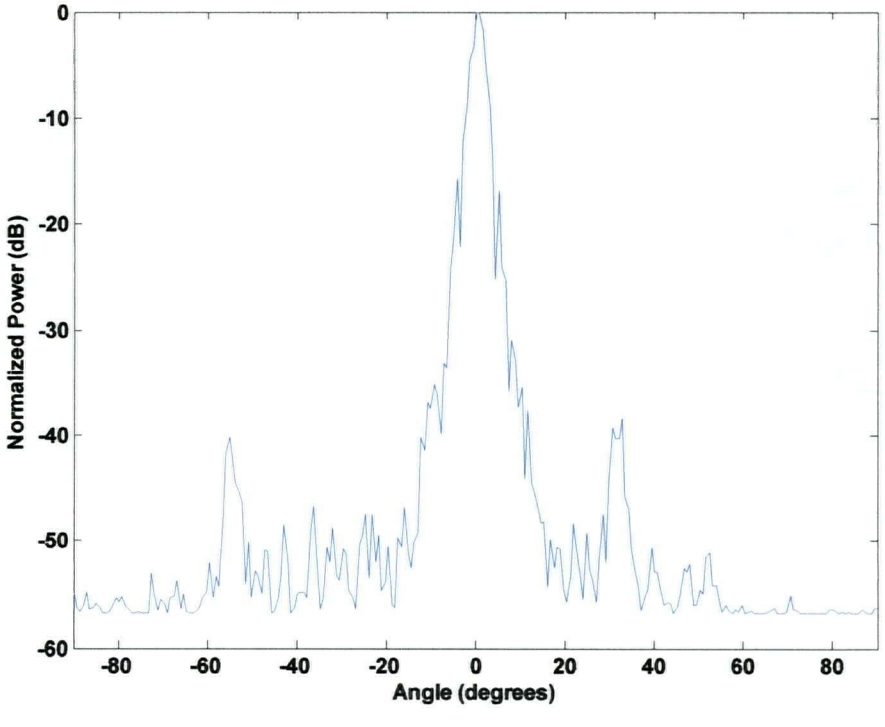

Figure C-30 H-plane Radiation Pattern for the Spherical Reflector Antenna with Focal Length = 85 cm, f = 35 GHz, and Elevation Angle ≈ 10°

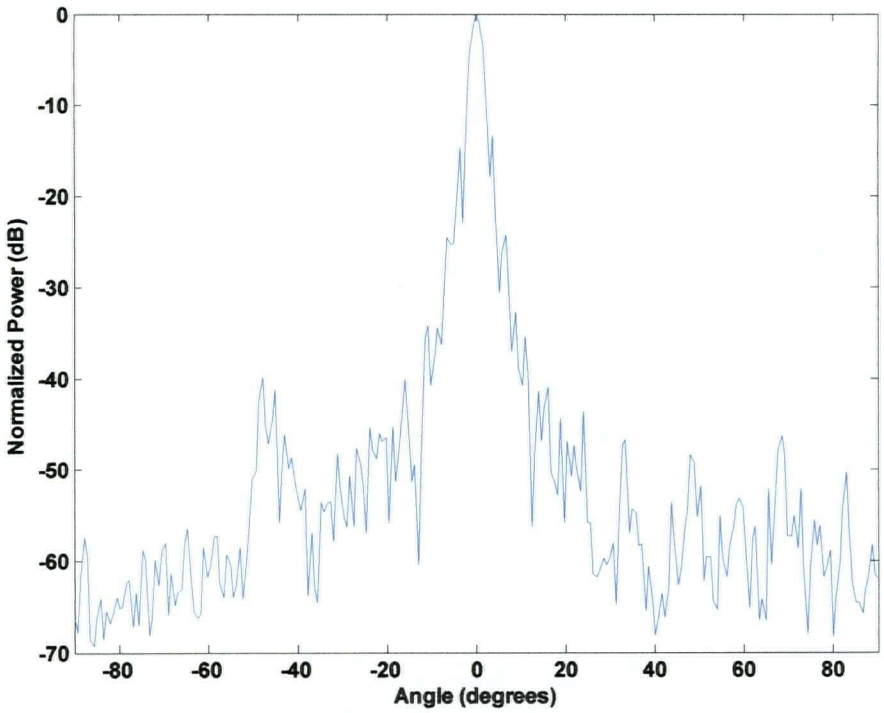

Figure C-31 H-plane Radiation Pattern for the Spherical Reflector Antenna with Focal Length = 85 cm, f = 27.5 GHz, and Elevation Angle ≈ 30°

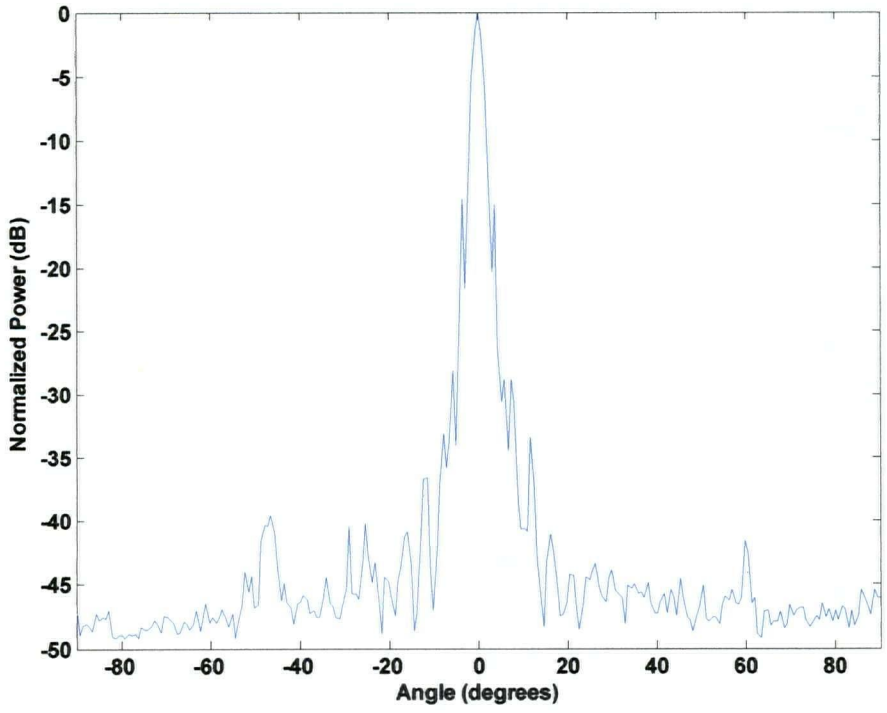

Figure C-32 H-plane Radiation Pattern for the Spherical Reflector Antenna with Focal Length = 85 cm, f = 31.5 GHz, and Elevation Angle ≈ 30°

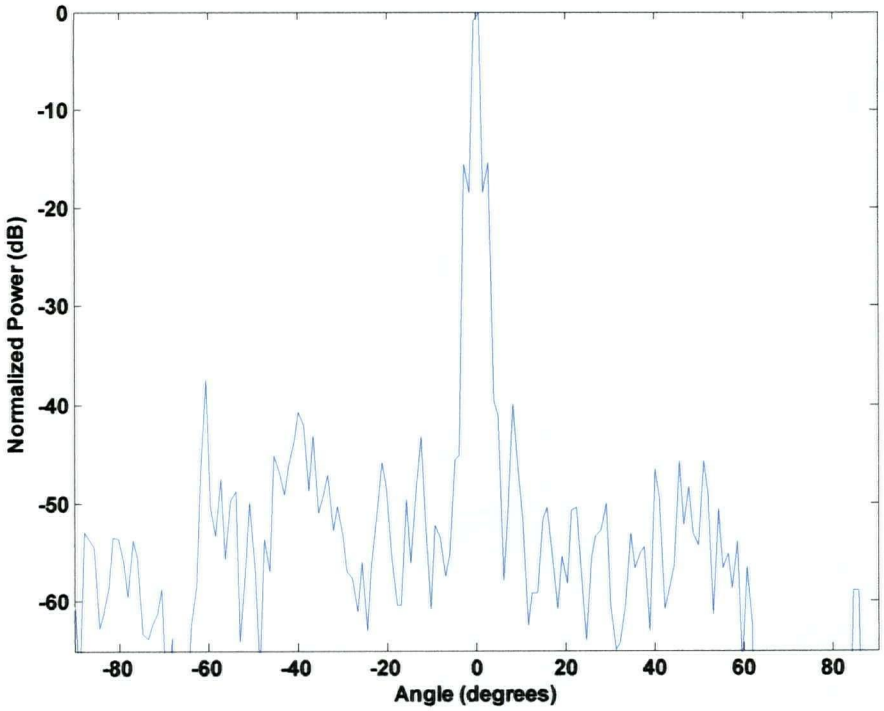

Figure C-33 H-plane Radiation Pattern for the Spherical Reflector Antenna with Focal Length = 85 cm, f = 35 GHz, and Elevation Angle ≈ 30°

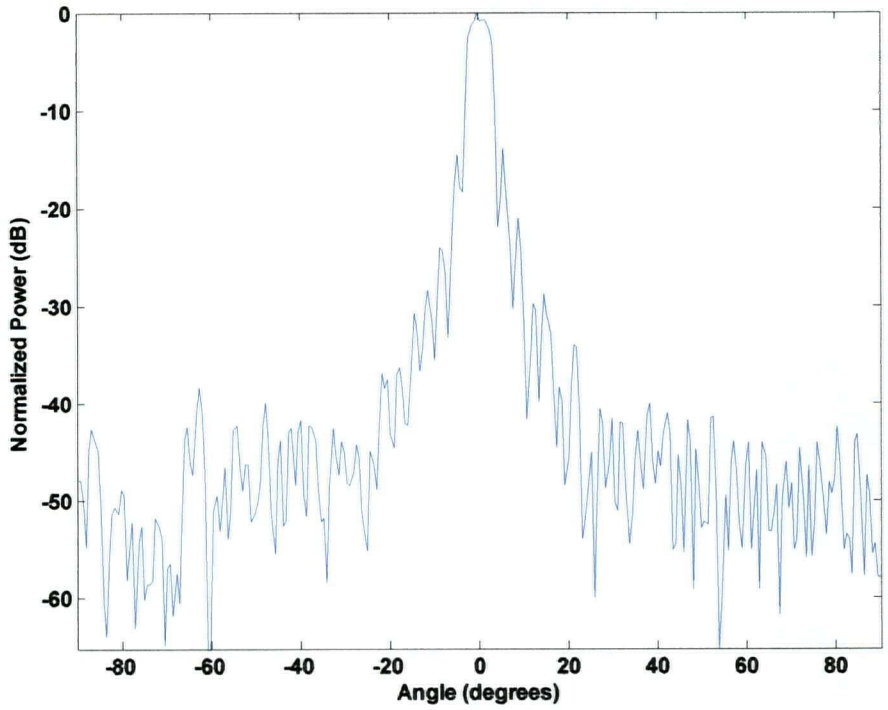

Figure C-34 H-plane Radiation Pattern for the Spherical Reflector Antenna with Focal Length = 85 cm, f = 27.5 GHz, and Elevation Angle ≈ 50°

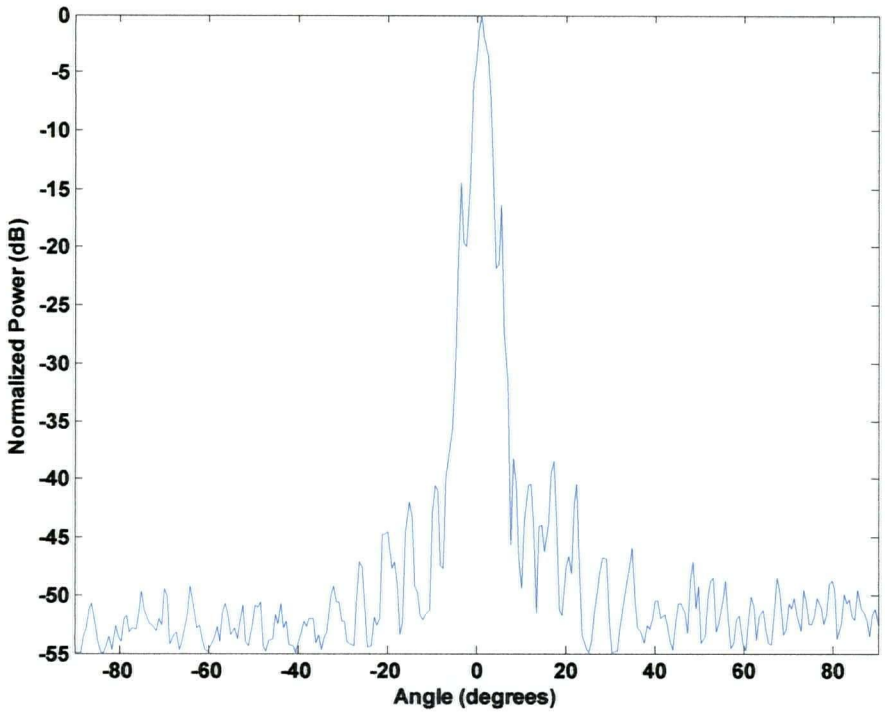

Figure C-35 H-plane Radiation Pattern for the Spherical Reflector Antenna with Focal Length = 85 cm, f = 31.5 GHz, and Elevation Angle ≈ 50°

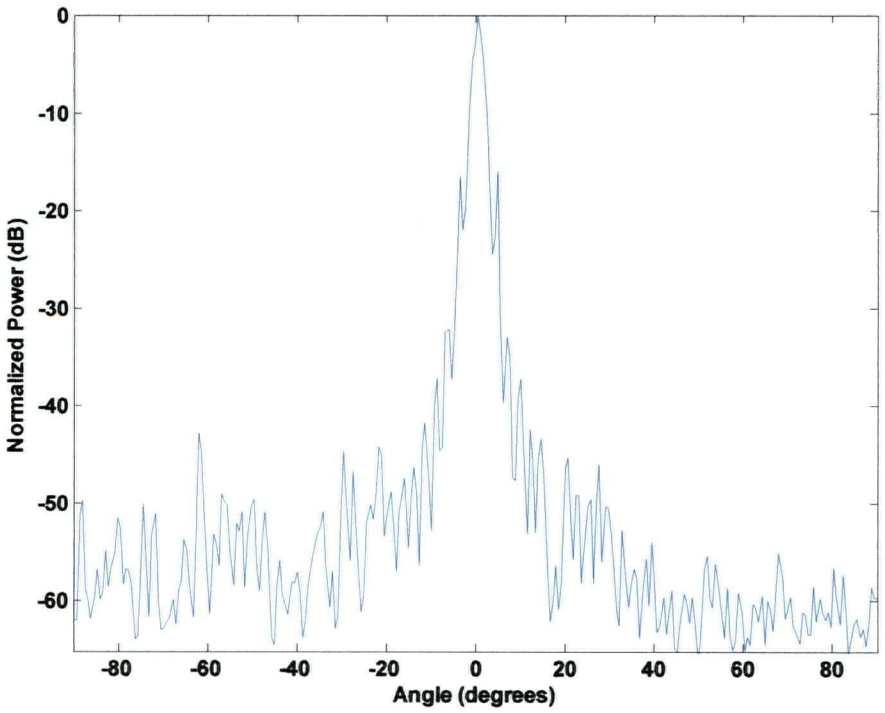

Figure C-36 H-plane Radiation Pattern for the Spherical Reflector Antenna with Focal Length = 85 cm, f = 35 GHz, and Elevation Angle ≈ 50°

APPENDIX D

Spherical Reflector Radiation Patterns for the E-plane

D-1 FOCAL LENGTH OF 70 CM

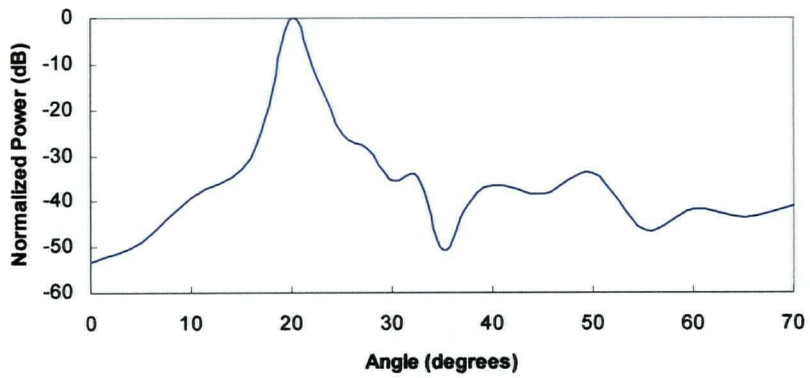

Figure D-1 E-plane Radiation Pattern for the Spherical Reflector Antenna with Focal Length = 70 cm, f = 27.5 GHz, and Elevation Angle ≈ 10°

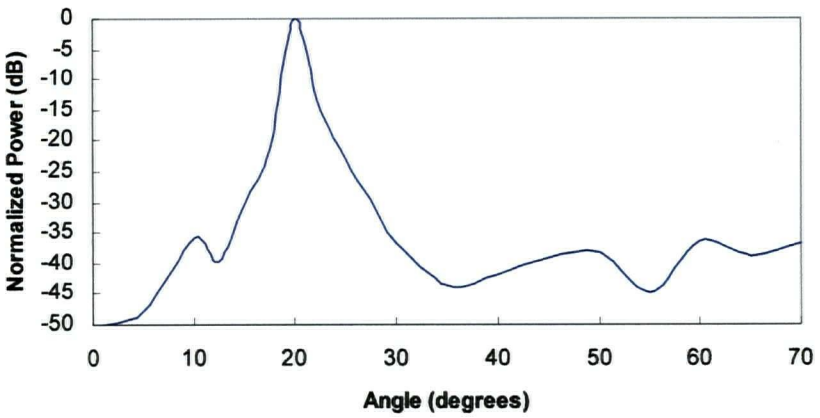

Figure D-2 E-plane Radiation Pattern for the Spherical Reflector Antenna with Focal Length = 70 cm, f = 31.5 GHz, and Elevation Angle ≈ 10°

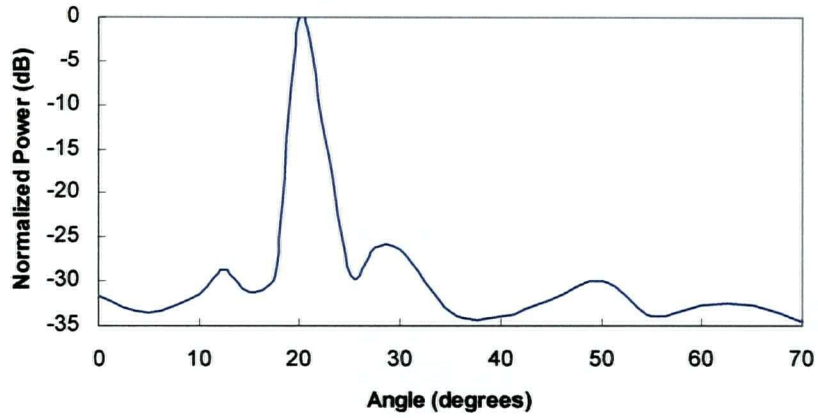

Figure D-3 E-plane Radiation Pattern for the Spherical Reflector Antenna with Focal Length = 70 cm, f = 35 GHz, and Elevation Angle ≈ 10°

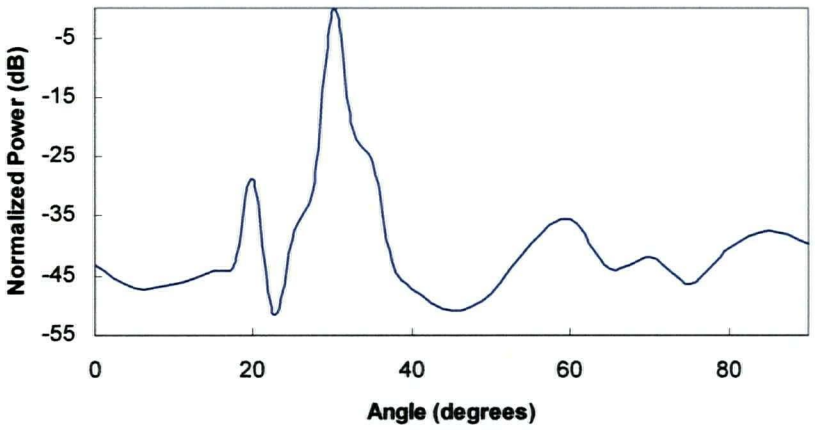

Figure D-4 E-plane Radiation Pattern for the Spherical Reflector Antenna with Focal Length = 70 cm, f = 27.5 GHz, and Elevation Angle ≈ 30°

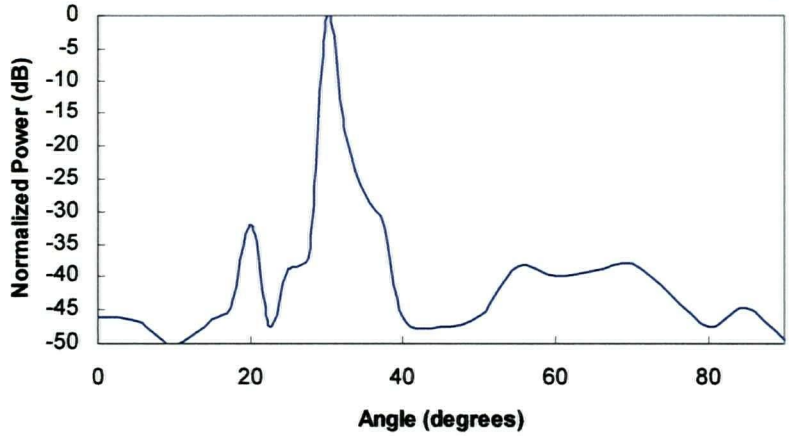

Figure D-5 E-plane Radiation Pattern for the Spherical Reflector Antenna with Focal Length = 70 cm, f = 31.5 GHz, and Elevation Angle ≈ 30°

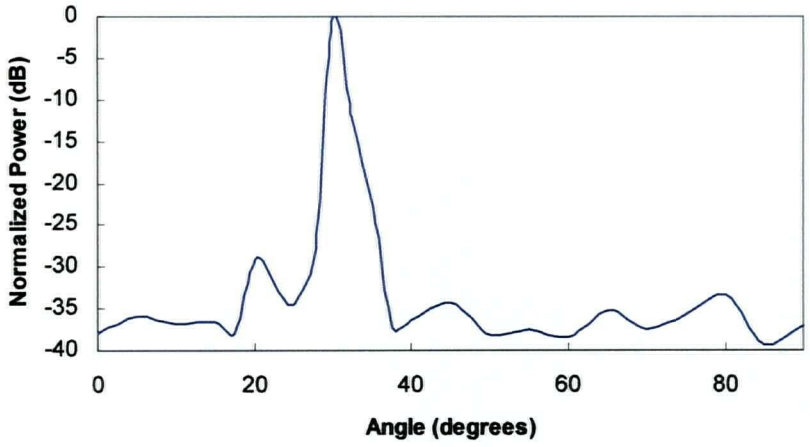

Figure D-6 E-plane Radiation Pattern for the Spherical Reflector Antenna with Focal Length = 70 cm, f = 35 GHz, and Elevation Angle ≈ 30°

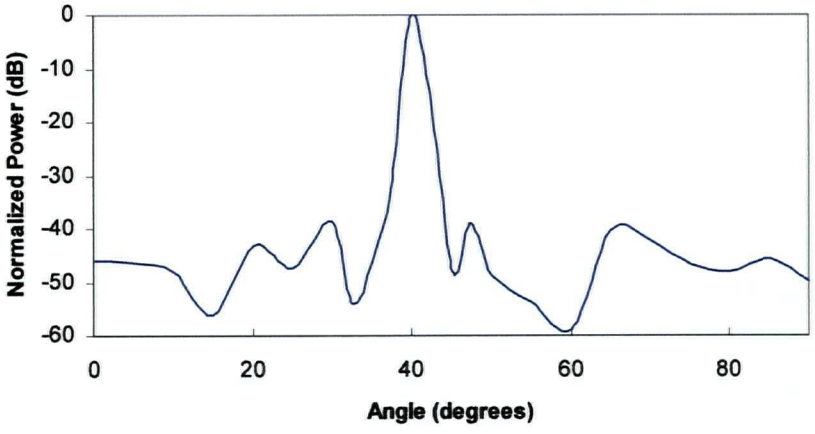

Figure D-7 E-plane Radiation Pattern for the Spherical Reflector Antenna with Focal Length = 70 cm, f = 27.5 GHz, and Elevation Angle ≈ 50°

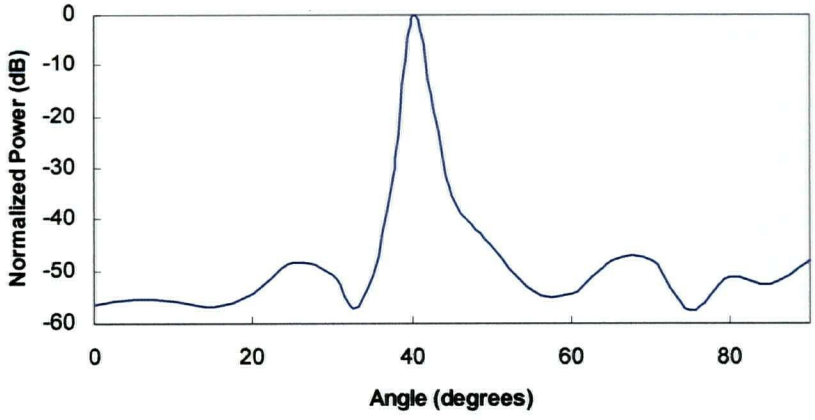

Figure D-8 E-plane Radiation Pattern for the Spherical Reflector Antenna with Focal Length = 70 cm, f = 31.5 GHz, and Elevation Angle ≈ 50°

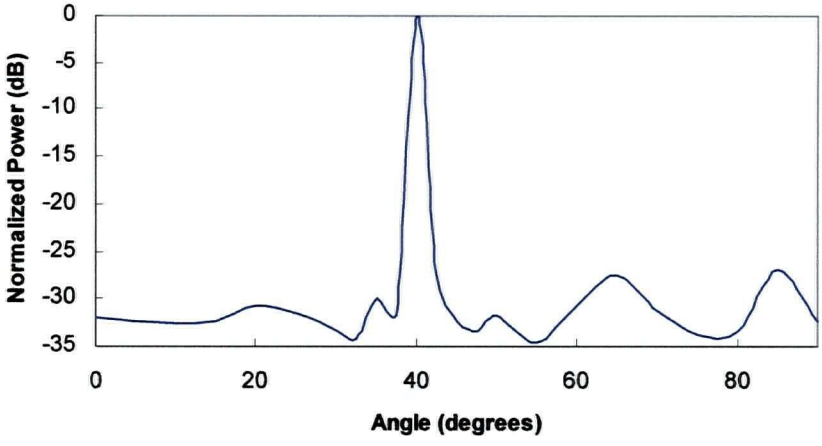

Figure D-9 E-plane Radiation Pattern for the Spherical Reflector Antenna with Focal Length = 70 cm, f = 35 GHz, and Elevation Angle ≈ 50°

D-2 Focal Length of 75 cm

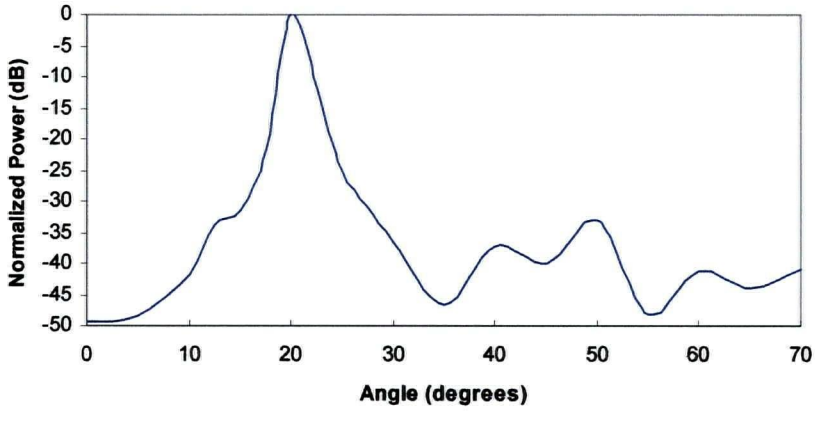

Figure D-10 E-plane Radiation Pattern for the Spherical Reflector Antenna with Focal Length = 75 cm, f = 27.5 GHz, and Elevation Angle ≈ 10°

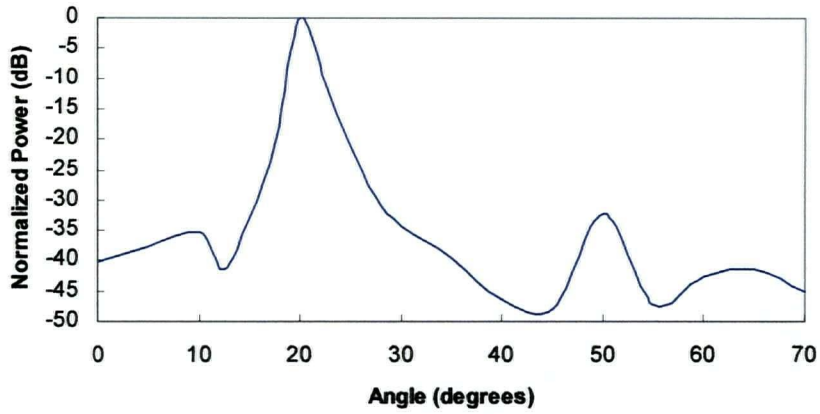

Figure D-11 E-plane Radiation Pattern for the Spherical Reflector Antenna with Focal Length = 75 cm, f = 31.5 GHz, and Elevation Angle ≈ 10°

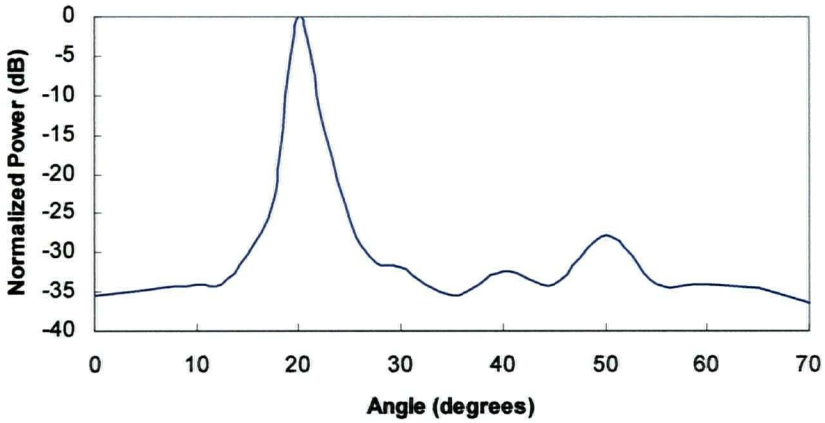

Figure D-12 E-plane Radiation Pattern for the Spherical Reflector Antenna with Focal Length = 75 cm, f = 35 GHz, and Elevation Angle ≈ 10°

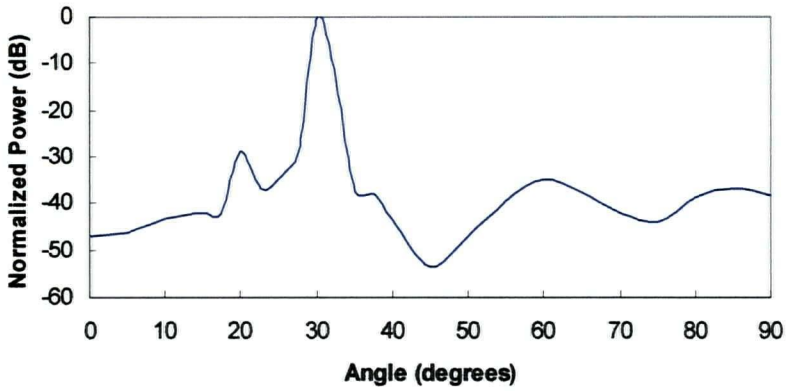

Figure D-13 E-plane Radiation Pattern for the Spherical Reflector Antenna with Focal Length = 75 cm, f = 27.5 GHz, and Elevation Angle ≈ 30°

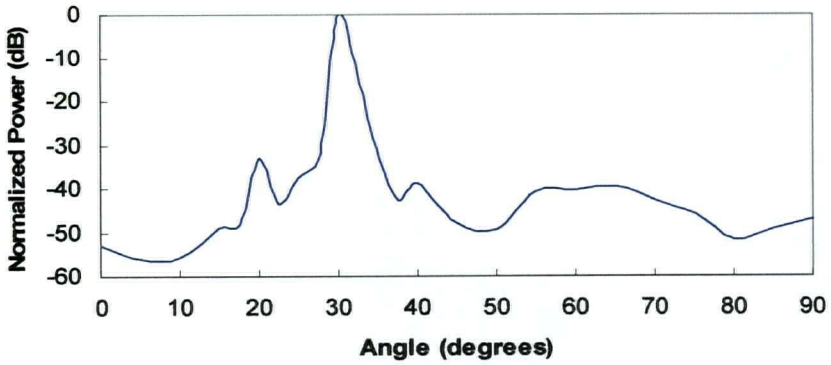

Figure D-14 E-plane Radiation Pattern for the Spherical Reflector Antenna with Focal Length = 75 cm, f = 31.5 GHz, and Elevation Angle ≈ 30°

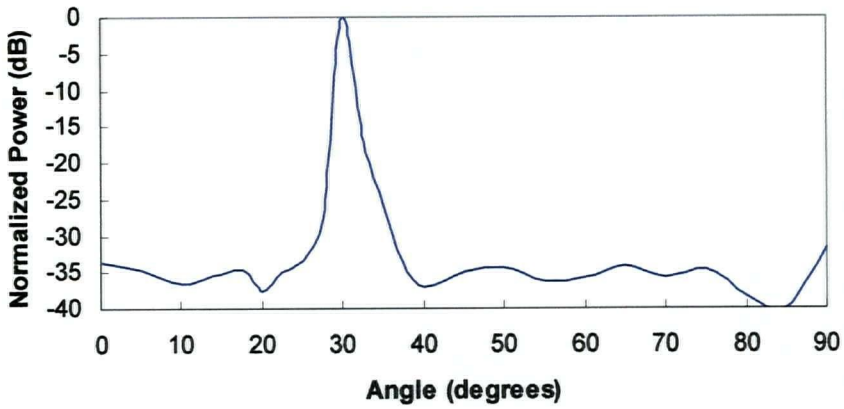

Figure D-15 E-plane Radiation Pattern for the Spherical Reflector Antenna with Focal Length = 75 cm, f = 35 GHz, and Elevation Angle ≈ 30°

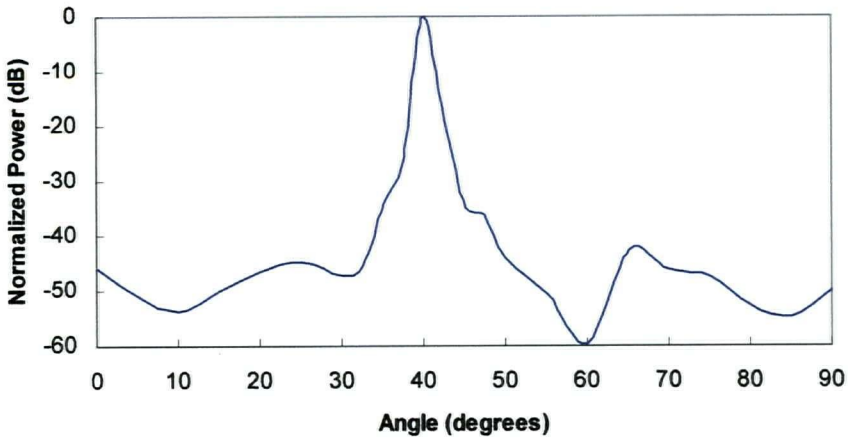

Figure D-16 E-plane Radiation Pattern for the Spherical Reflector Antenna with Focal Length = 75 cm, f = 27.5 GHz, and Elevation Angle ≈ 50°

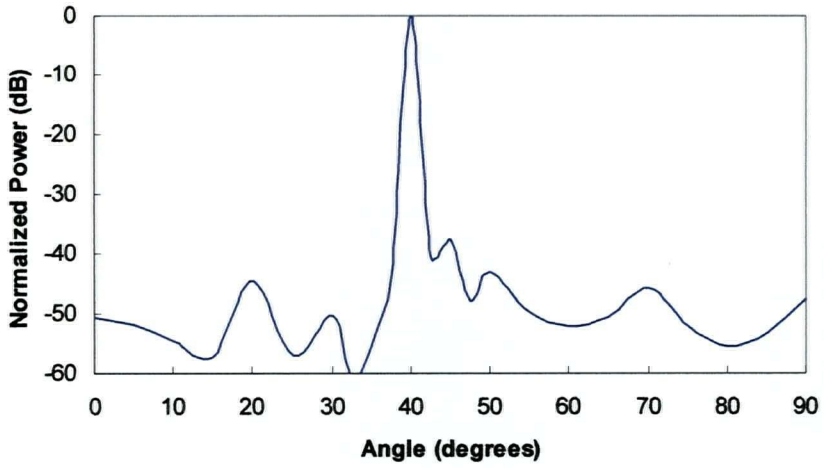

Figure D-17 E-plane Radiation Pattern for the Spherical Reflector Antenna with Focal Length = 75 cm, f = 31.5 GHz, and Elevation Angle ≈ 50°

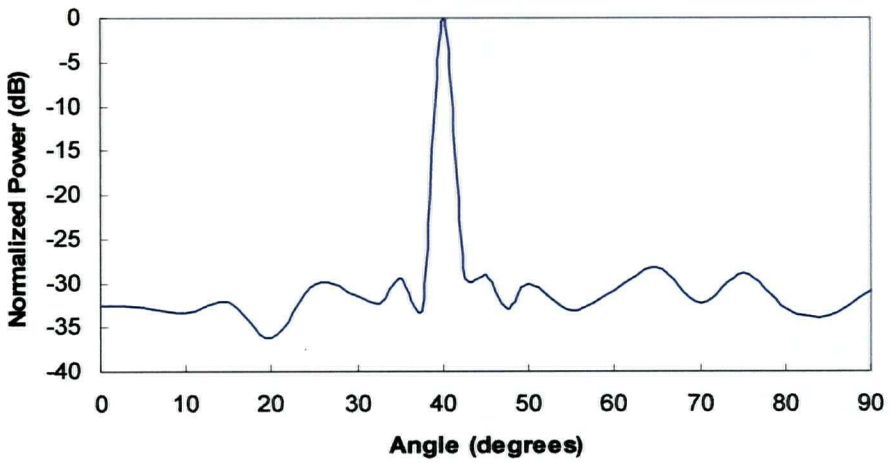

Figure D-18 E-plane Radiation Pattern for the Spherical Reflector Antenna with Focal Length = 75 cm, f = 35 GHz, and Elevation Angle ≈ 50°

D-3 Focal Length of 80 cm

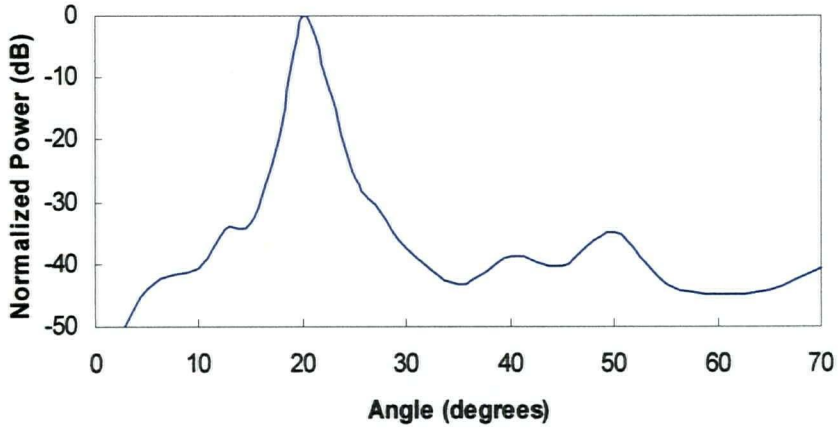

Figure D-19 E-plane Radiation Pattern for the Spherical Reflector Antenna with Focal Length = 80 cm, f = 27.5 GHz, and Elevation Angle ≈ 10°

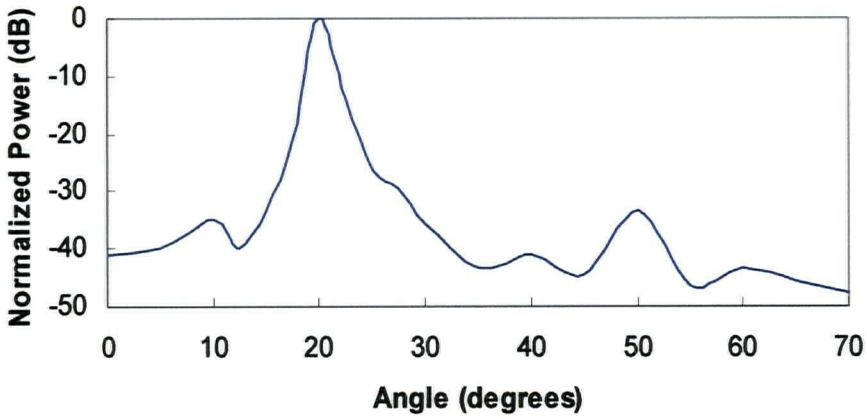

Figure D-20 E-plane Radiation Pattern for the Spherical Reflector Antenna with Focal Length = 80 cm, f = 31.5 GHz, and Elevation Angle ≈ 10°

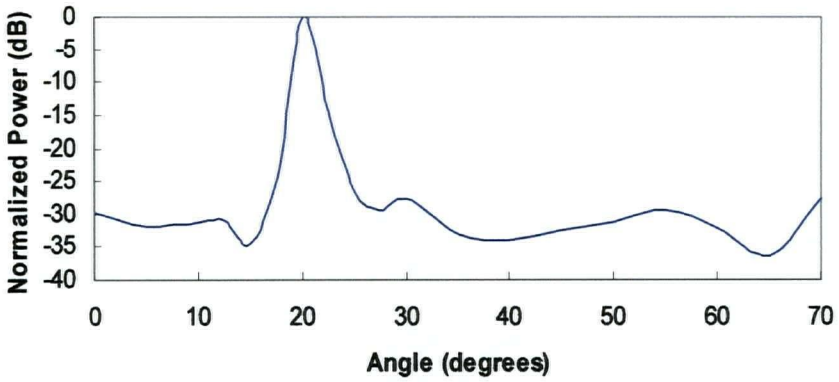

Figure D-21 E-plane Radiation Pattern for the Spherical Reflector Antenna with Focal Length = 80 cm, f = 35 GHz, and Elevation Angle ≈ 10°

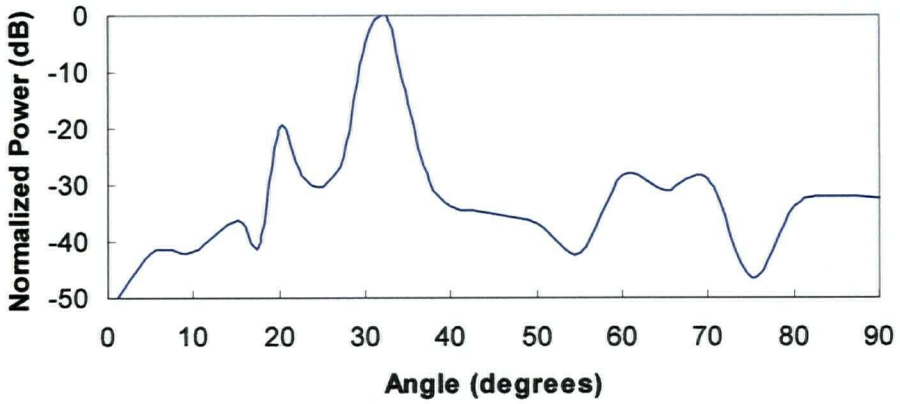

Figure D-22 E-plane Radiation Pattern for the Spherical Reflector Antenna with Focal Length = 80 cm, f = 27.5 GHz, and Elevation Angle ≈ 30°

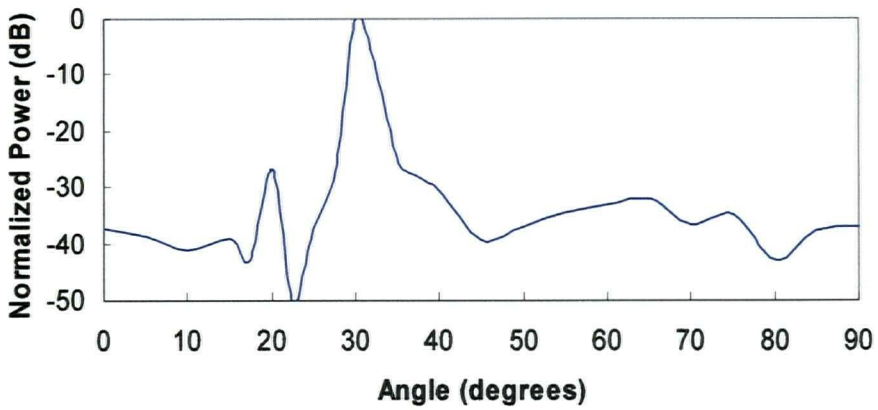

Figure D-23 E-plane Radiation Pattern for the Spherical Reflector Antenna with Focal Length = 80 cm, f = 31.5 GHz, and Elevation Angle ≈ 30°

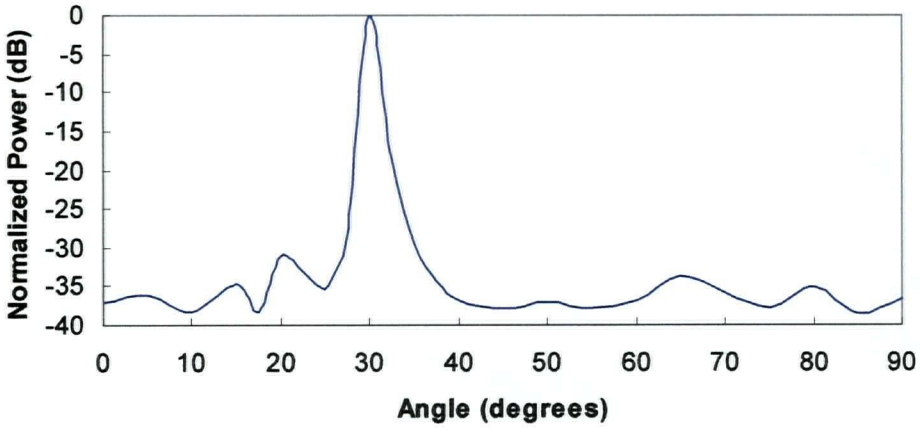

Figure D-24 E-plane Radiation Pattern for the Spherical Reflector Antenna with Focal Length = 80 cm, f = 35 GHz, and Elevation Angle ≈ 30°

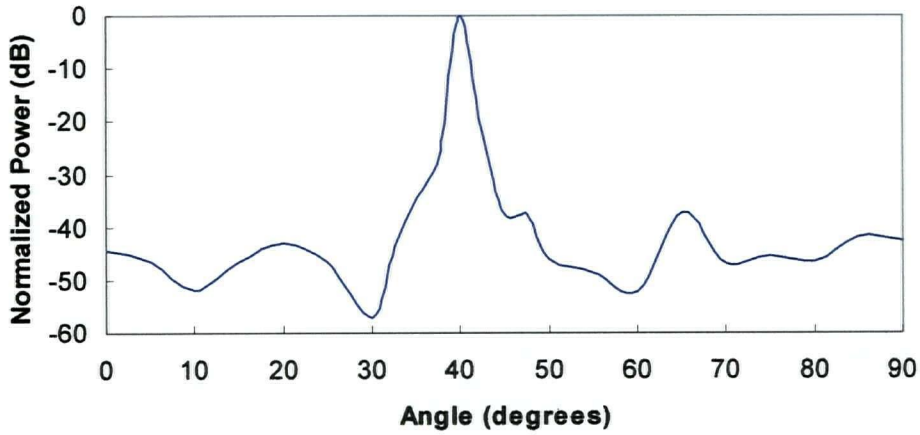

Figure D-25 E-plane Radiation Pattern for the Spherical Reflector Antenna with Focal Length = 80 cm, f = 27.5 GHz, and Elevation Angle ≈ 50°

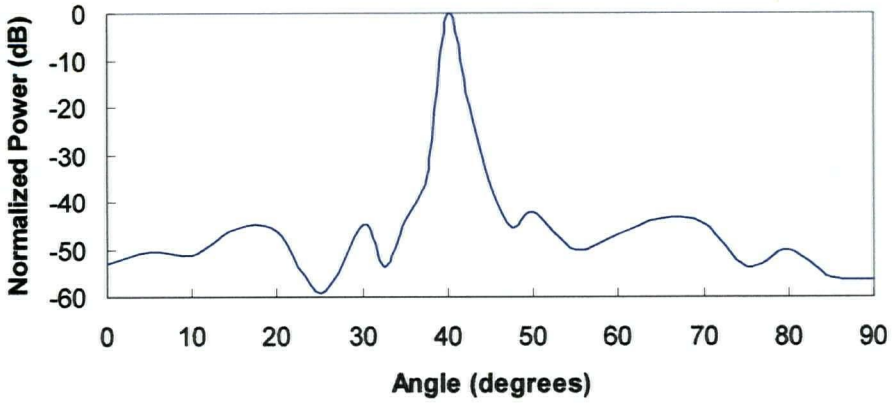

Figure D-26 E-plane Radiation Pattern for the Spherical Reflector Antenna with Focal Length = 80 cm, f = 31.5 GHz, and Elevation Angle ≈ 50°

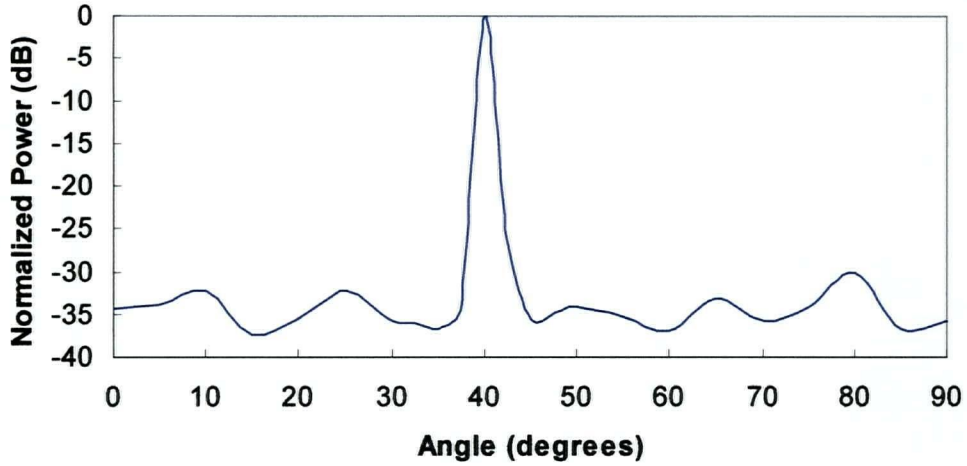

Figure D-27 E-plane Radiation Pattern for the Spherical Reflector Antenna with Focal Length = 80 cm, f = 35 GHz, and Elevation Angle ≈ 50°

D-4 Focal Length of 85 cm

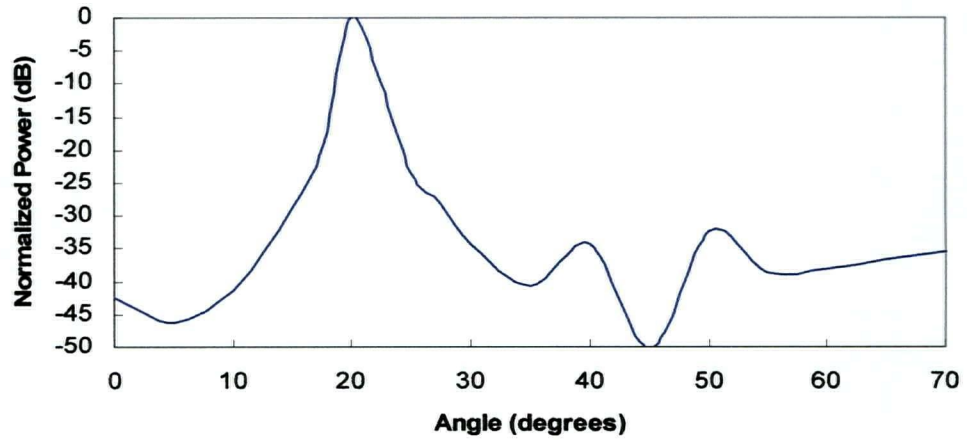

Figure D-28 E-plane Radiation Pattern for the Spherical Reflector Antenna with Focal Length = 85 cm, f = 27.5 GHz, and Elevation Angle ≈ 10°

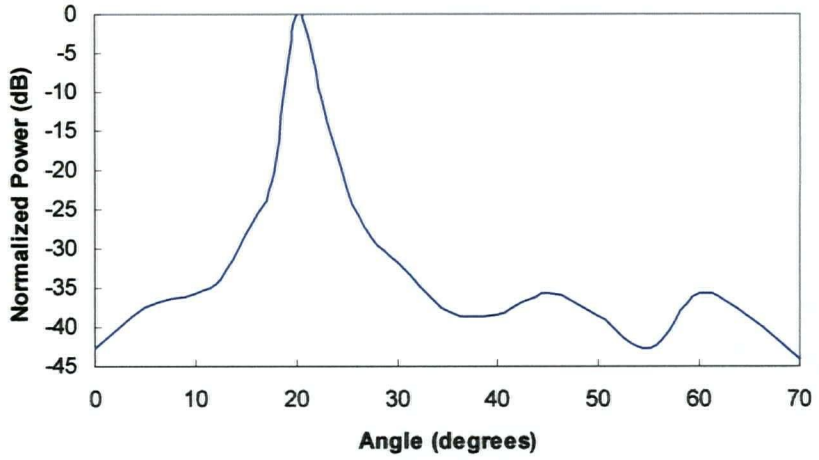

Figure D-29 E-plane Radiation Pattern for the Spherical Reflector Antenna with Focal Length = 85 cm, f = 31.5 GHz, and Elevation Angle ≈ 10°

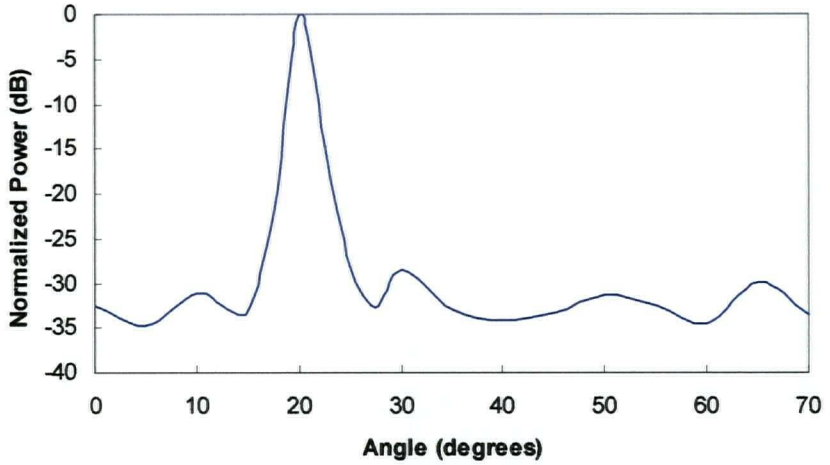

Figure D-30 E-plane Radiation Pattern for the Spherical Reflector Antenna with Focal Length = 85 cm, f = 35 GHz, and Elevation Angle ≈ 10°

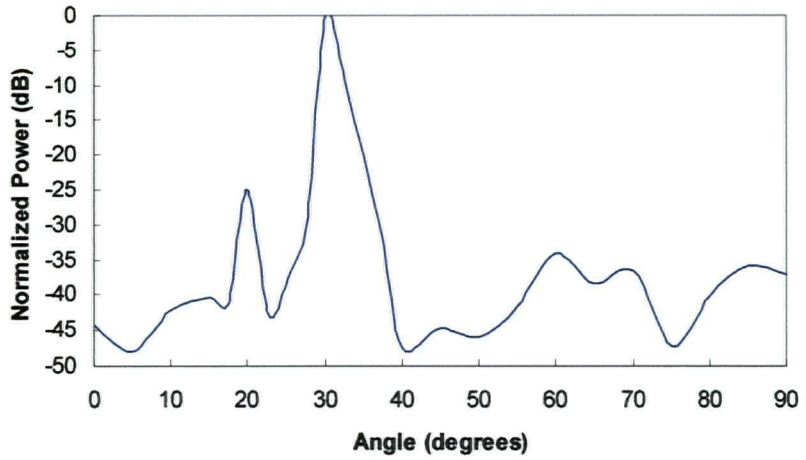

Figure D-31 E-plane Radiation Pattern for the Spherical Reflector Antenna with Focal Length = 85 cm, f = 27.5 GHz, and Elevation Angle ≈ 30°

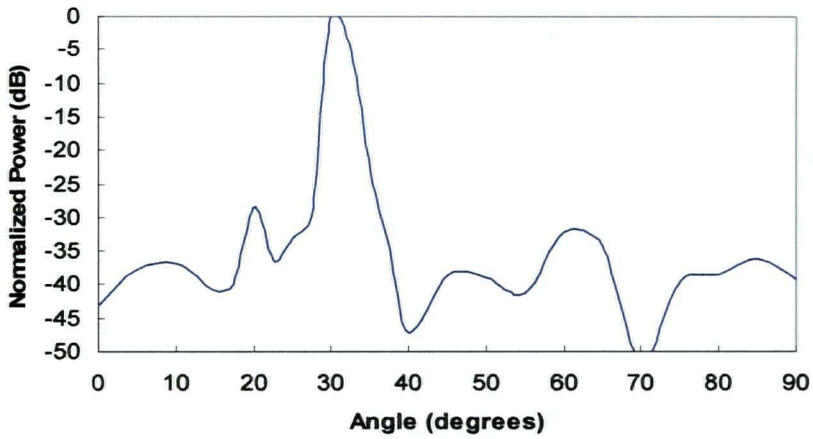

Figure D-32 E-plane Radiation Pattern for the Spherical Reflector Antenna with Focal Length = 85 cm, f = 31.5 GHz, and Elevation Angle ≈ 30°

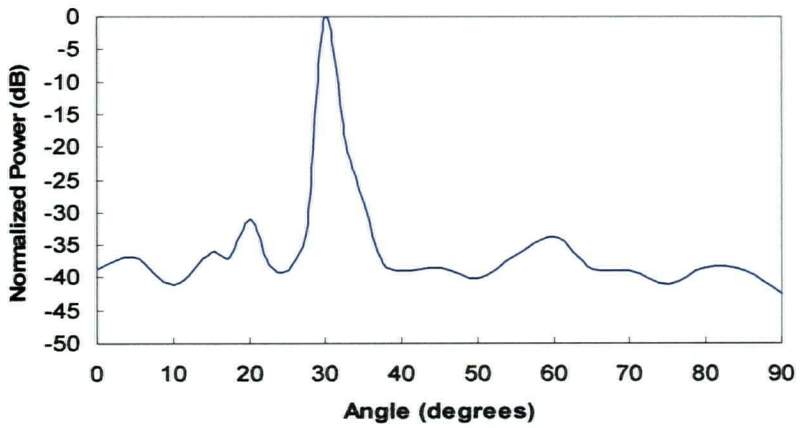

Figure D-33 E-plane Radiation Pattern for the Spherical Reflector Antenna with Focal Length = 85 cm, f = 35 GHz, and Elevation Angle ≈ 30°

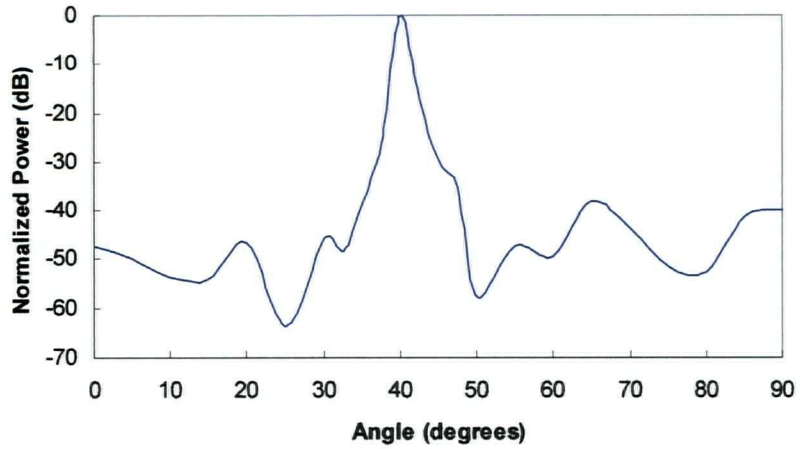

Figure D-34 E-plane Radiation Pattern for the Spherical Reflector Antenna with Focal Length = 85 cm, f = 27.5 GHz, and Elevation Angle ≈ 50°

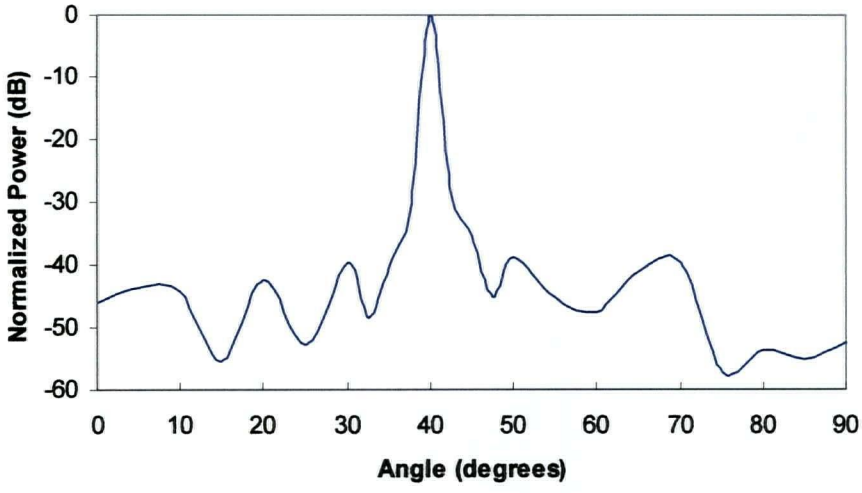

Figure D-35 E-plane Radiation Pattern for the Spherical Reflector Antenna with Focal Length = 85 cm, f = 31.5 GHz, and Elevation Angle ≈ 50°

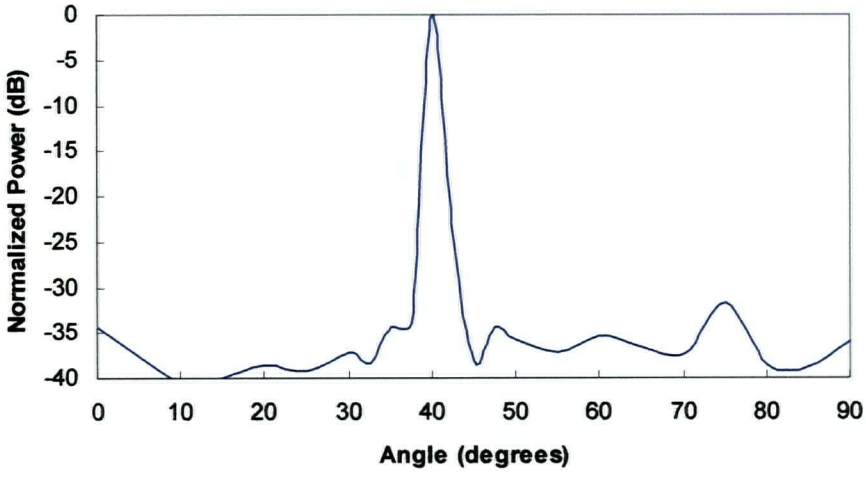

Figure D-36 E-plane Radiation Pattern for the Spherical Reflector Antenna with Focal Length = 85 cm, f = 35 GHz, and Elevation Angle ≈ 50°

APPENDIX E

Rain Attenuation Plots

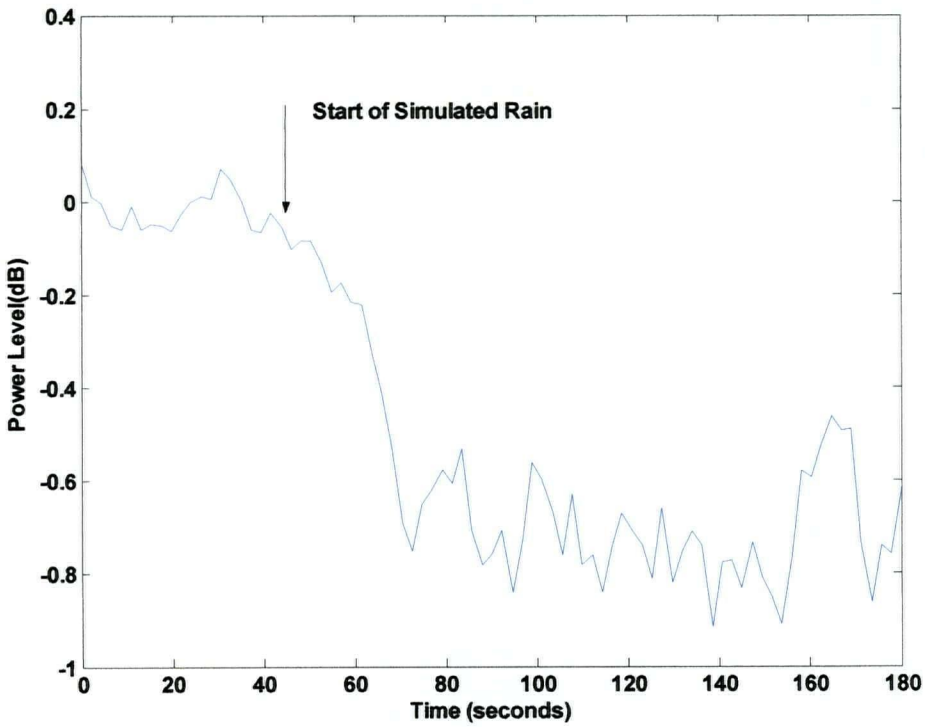

Figure E-1 Rain-Attenuation Plot for Reflector Angle ≈ 20° and f = 27.5 GHz

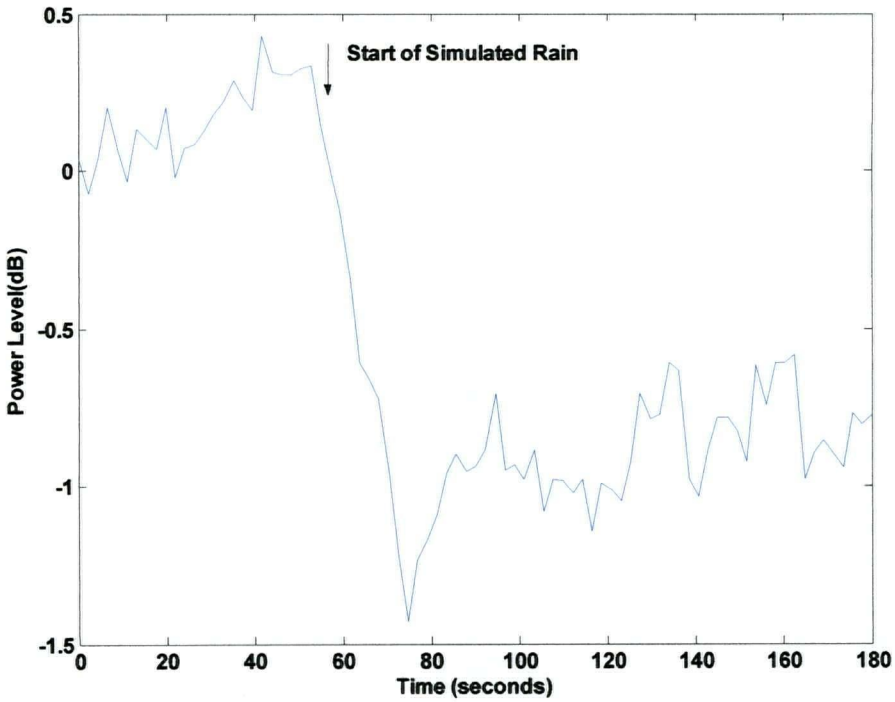

Figure E-2 Rain-Attenuation Plot for Reflector Angle ≈ 20° and f = 31.5 GHz

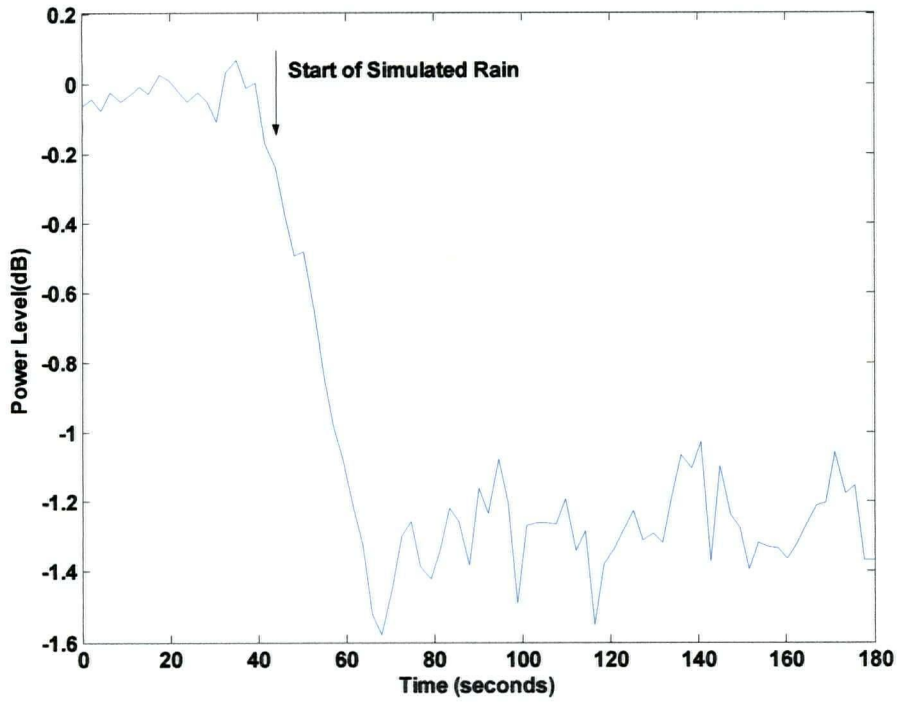

Figure E-3 Rain-Attenuation Plot for Reflector Angle ≈ 20° and f = 35 GHz

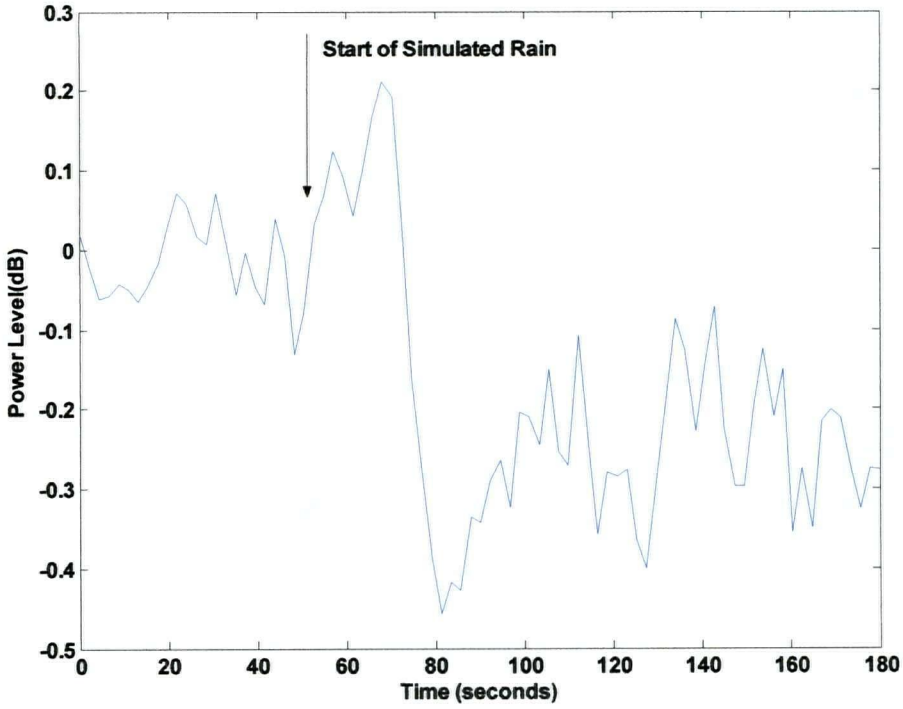

Figure E-4 Rain-Attenuation Plot for Reflector Angle ≈ 30° and f = 27.5 GHz

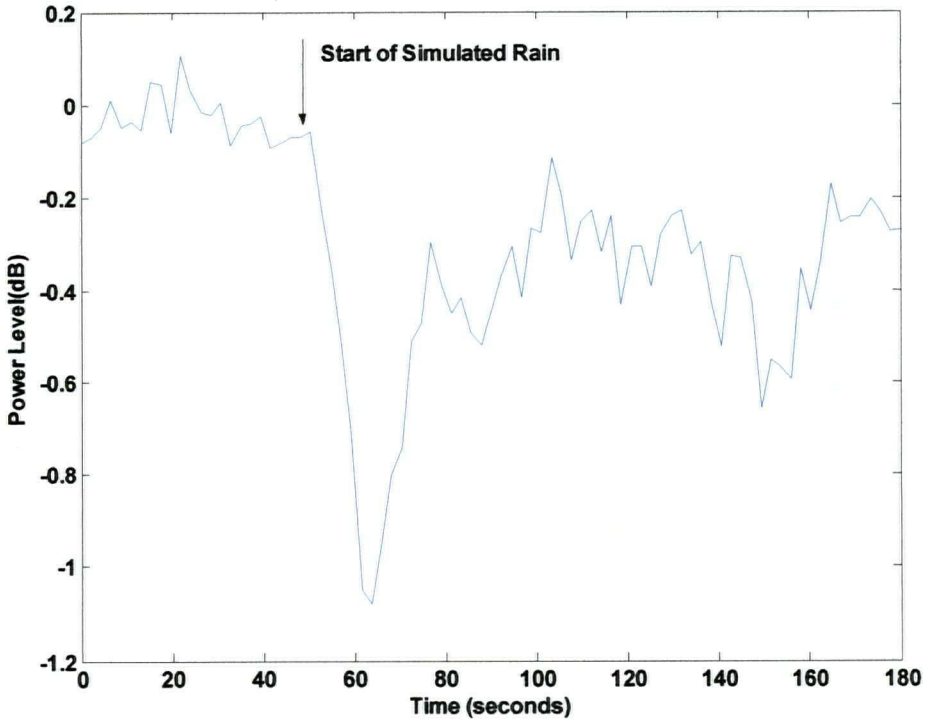

Figure E-5 Rain-Attenuation Plot for Reflector Angle ≈ 30° and f = 31.5 GHz

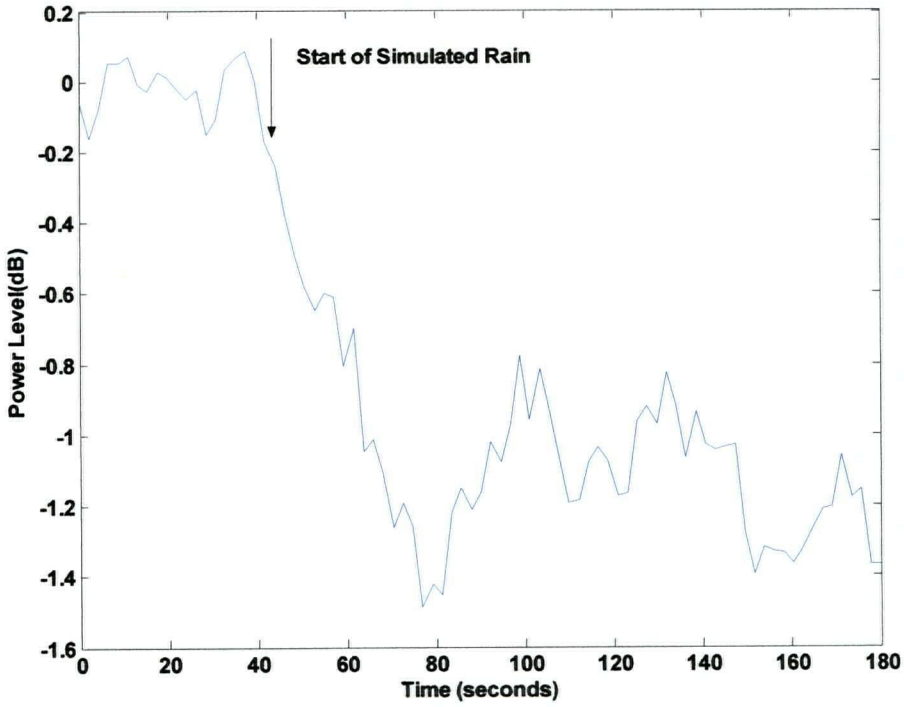

Figure E-6 Rain-Attenuation Plot for Reflector Angle ≈ 30° and f = 35 GHz

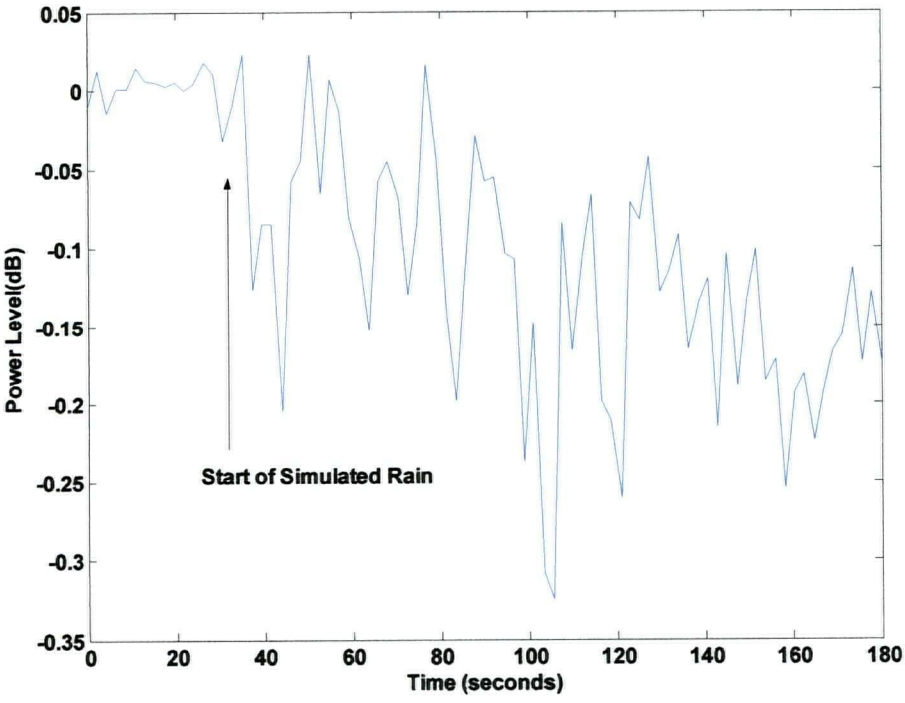

Figure E-7 Rain-Attenuation Plot for Reflector Angle ≈ 40° and f = 27.5 GHz

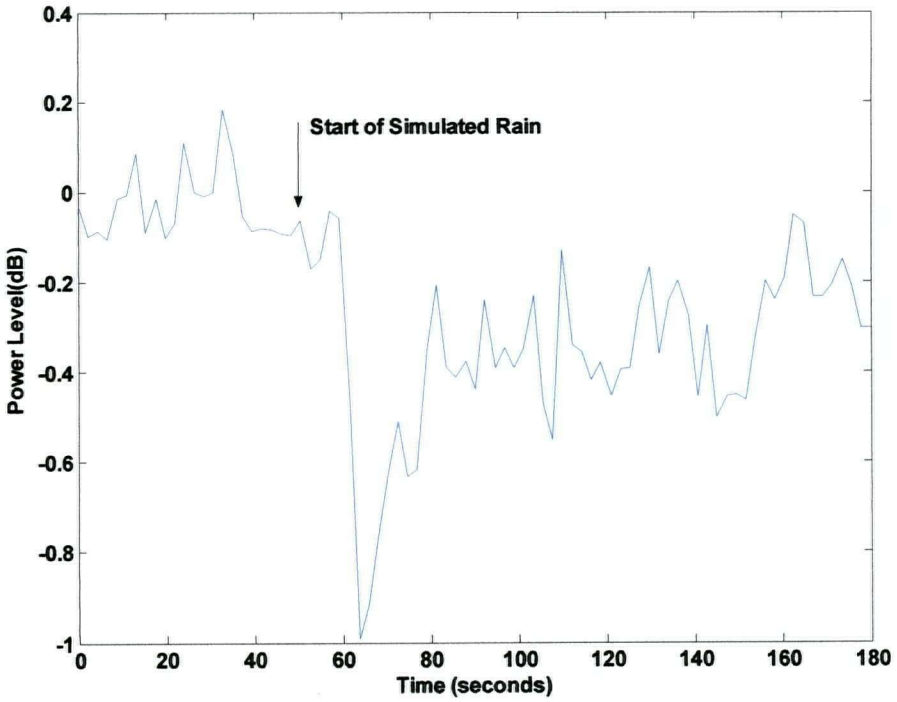

Figure E-8 Rain-Attenuation Plot for Reflector Angle ≈ 40° and f = 31.5 GHz

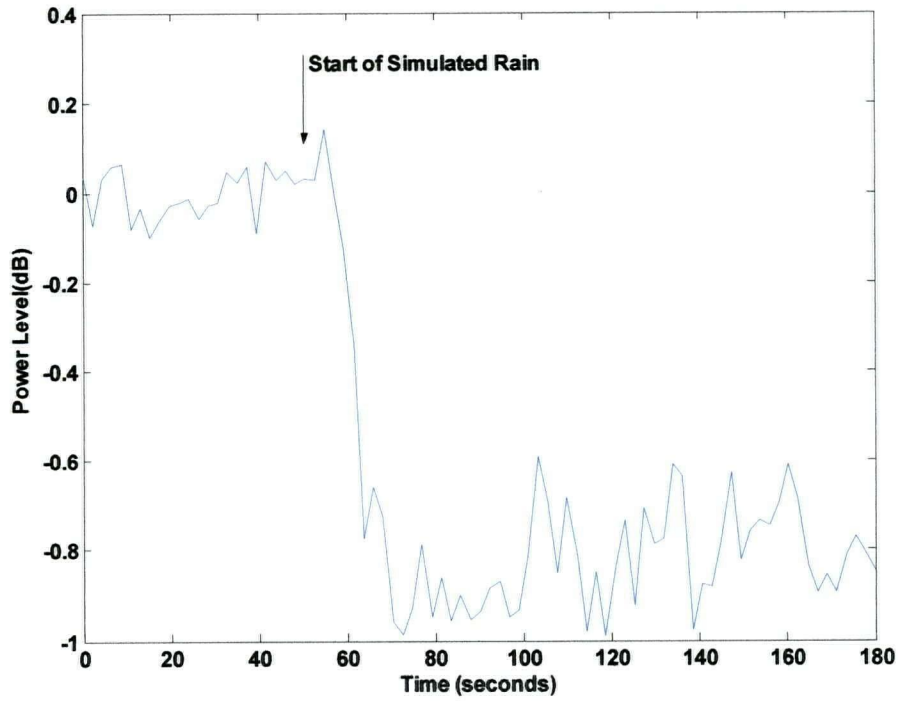

Figure E-9 Rain-Attenuation Plot for Reflector Angle ≈ 40° and f = 35 GHz

APPENDIX F

Comparison Plots

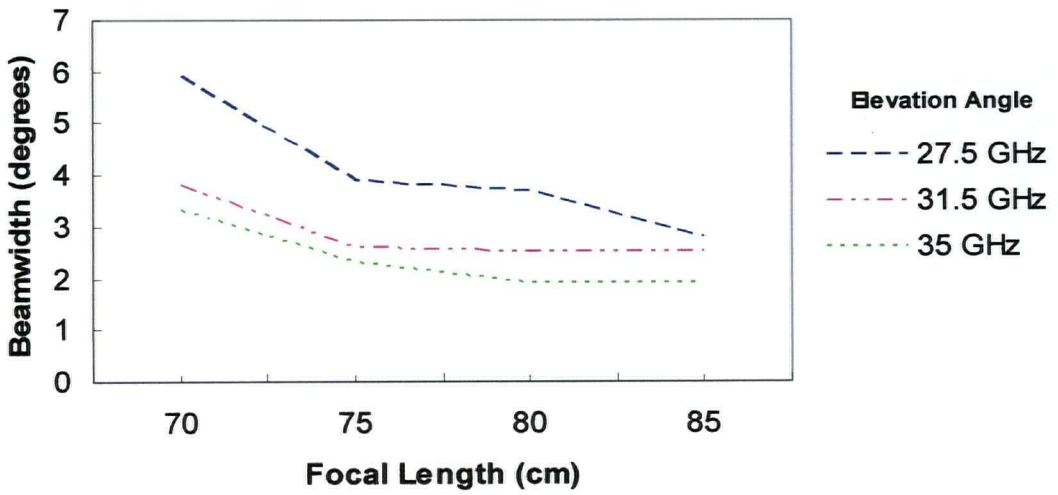

Figure F-1 Beamwidth vs. Focal Length, for Elevation Angle ≈ 10°

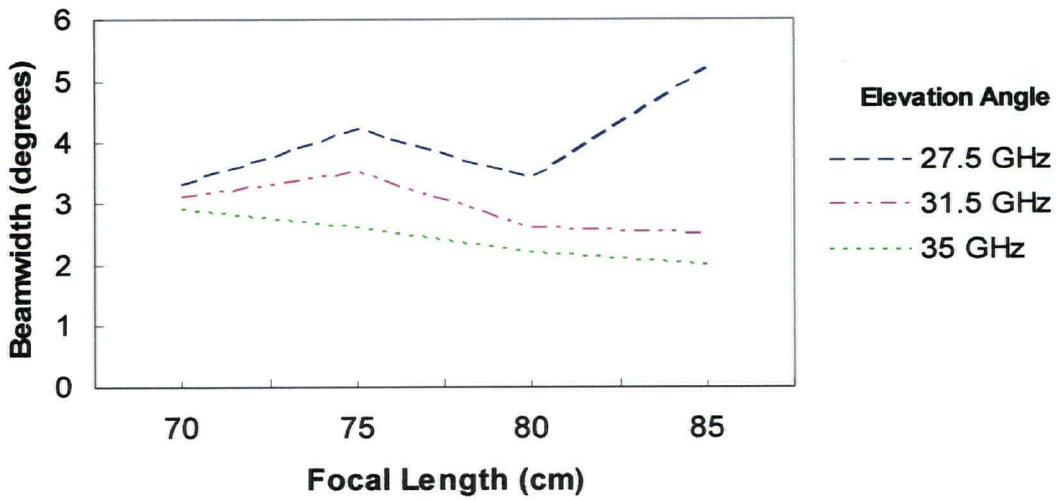

Figure F-2 Beamwidth vs. Focal Length, for Elevation Angle ≈ 50°

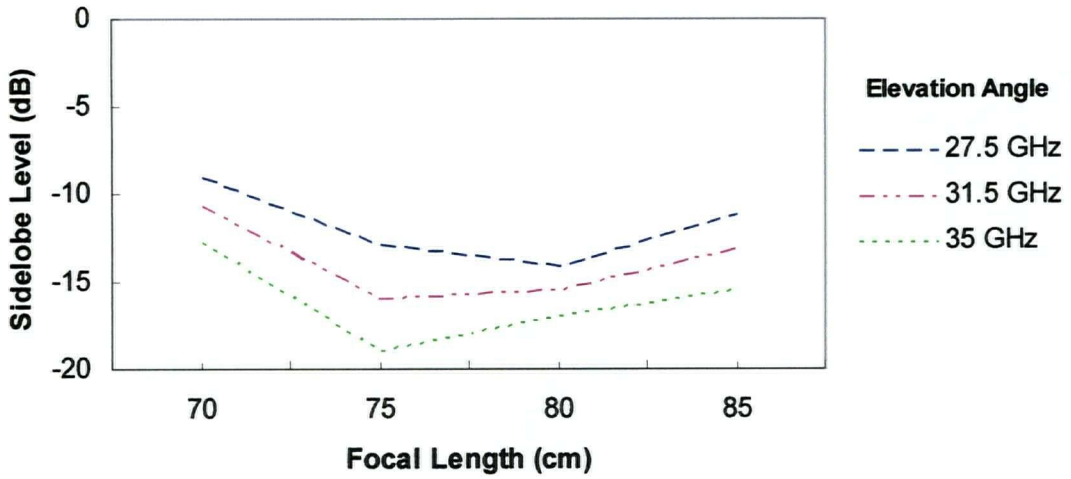

Figure F-3 Sidelobe Level vs. Focal Length, for Elevation Angle ≈ 10°

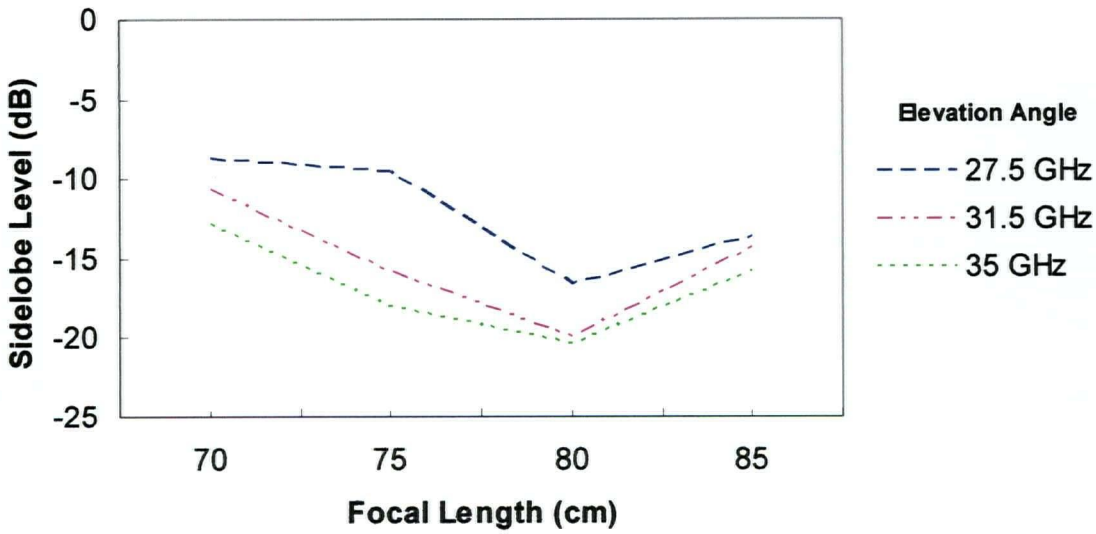

Figure F-4 Sidelobe Level vs. Focal Length, for Elevation Angle ≈ 50°

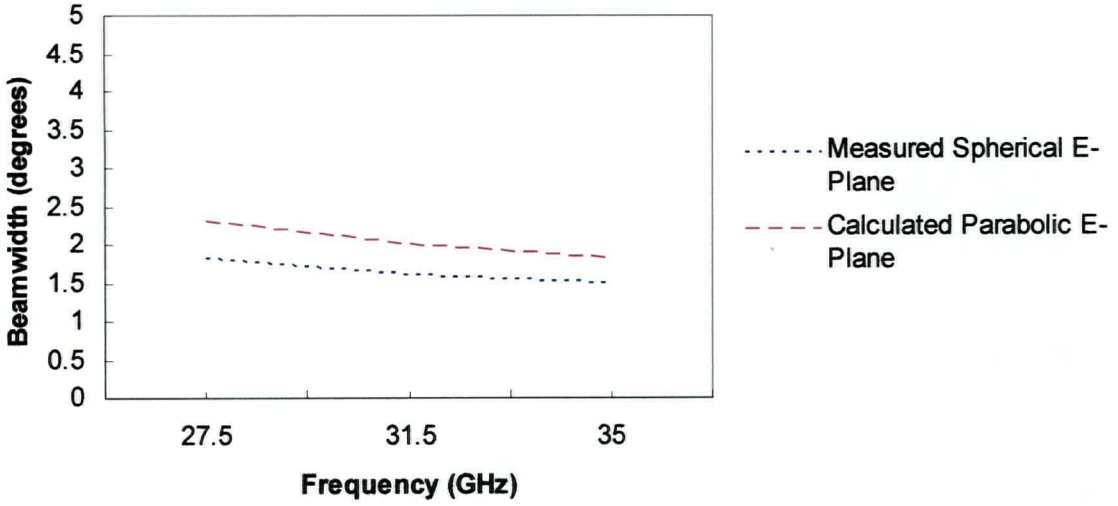

Figure F-5 E-Plane Beamwidth vs. Frequency for Measured and Calculated Results, for Focal Length = 80 cm, and Elevation Angle ≈ 10°

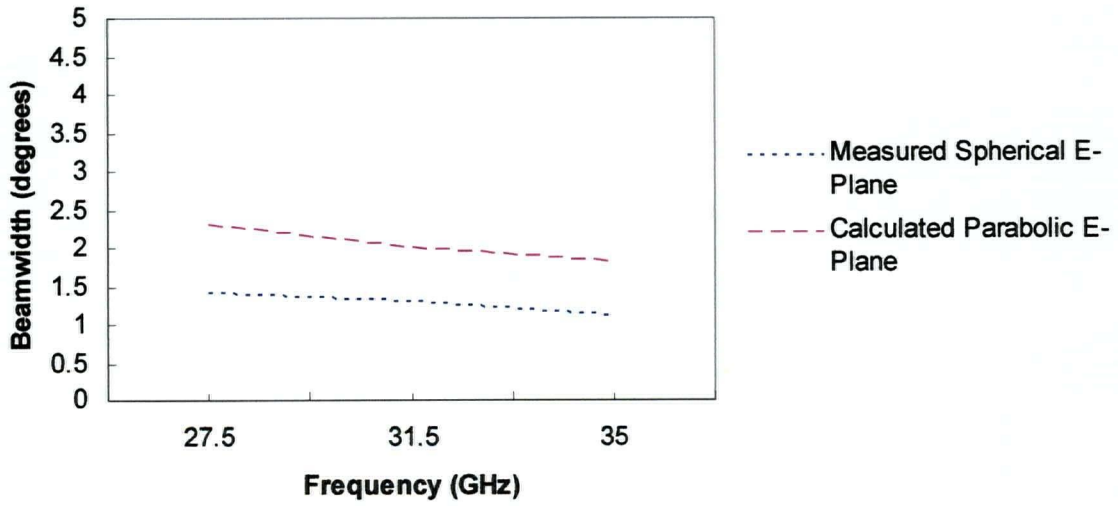

Figure F-6 E-Plane Beamwidth vs. Frequency for Measured and Calculated Results, for Focal Length = 80 cm, and Elevation Angle ≈ 50°

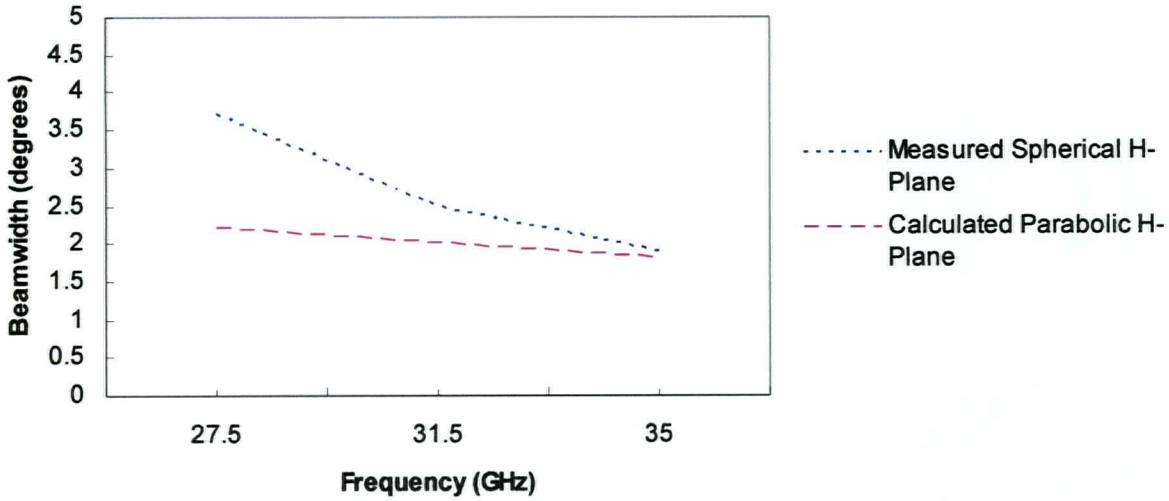

Figure F-7 H-Plane Beamwidth vs. Frequency for Measured and Calculated Results, for Focal Length = 80 cm, and Elevation Angle ≈ 10°

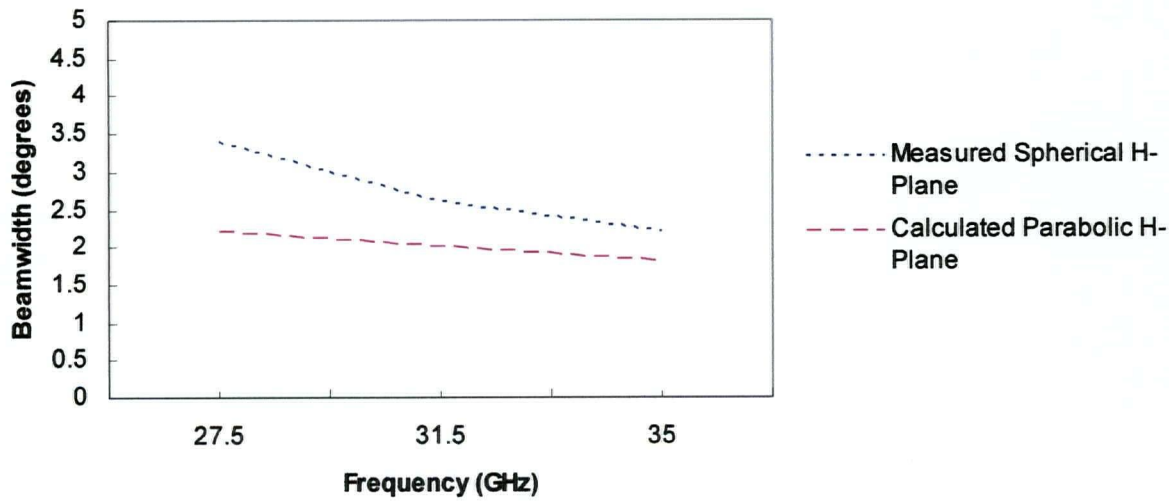

Figure F-8 H-Plane Beamwidth vs. Frequency for Measured and Calculated Results, for Focal Length = 80 cm, and Elevation Angle ≈ 50°

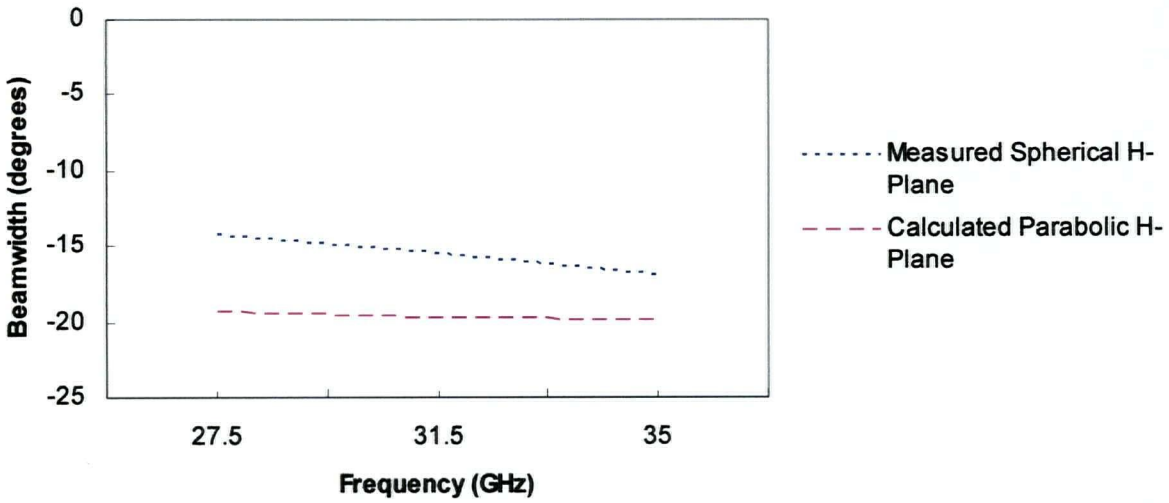

Figure F-9 H-Plane Sidelobe Level vs. Frequency for Measured and Calculated Results, for Focal Length = 80 cm, and Elevation Angle ≈ 10°

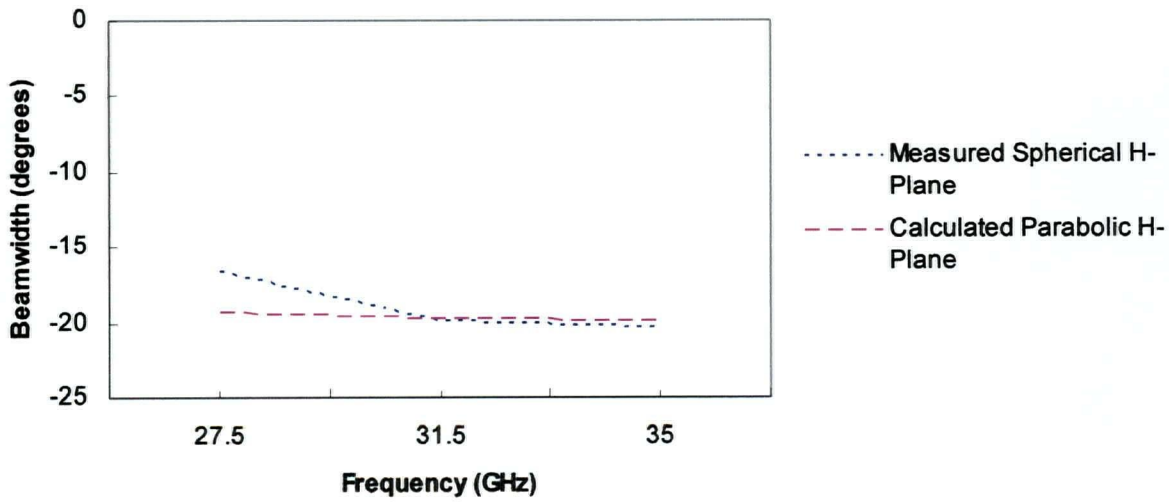

Figure F-10 H-Plane Sidelobe Level vs. Frequency for Measured and Calculated Results, for Focal Length = 80 cm, and Elevation Angle ≈ 50°

APPENDIX G

Software Programs Used

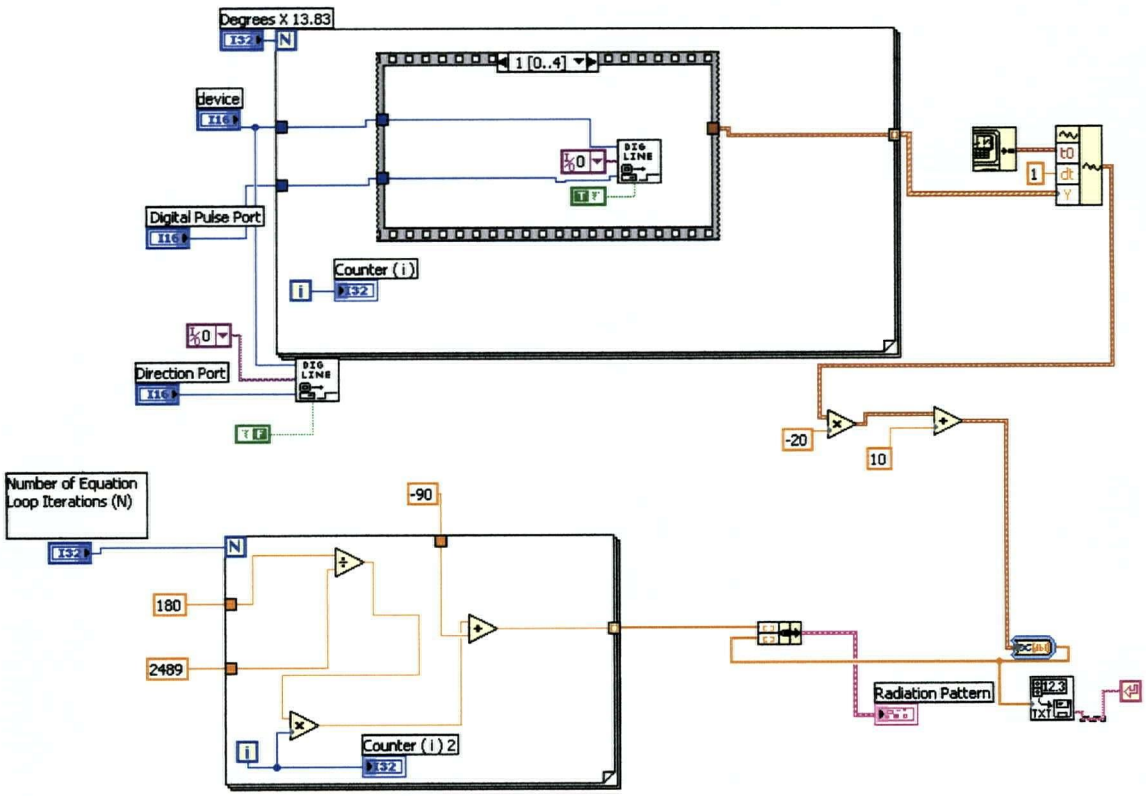

Figure G-1 LabVIEW Virtual Instrument used to Collect Radiation Pattern Measurements

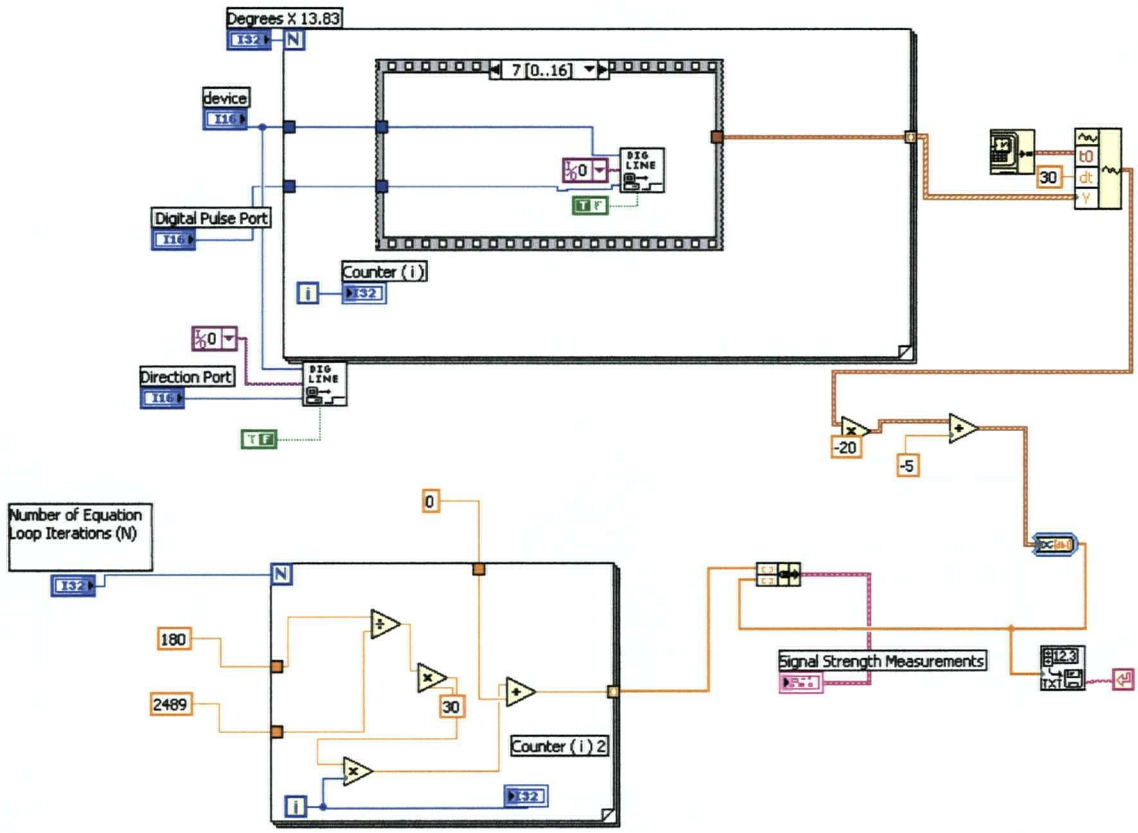

Figure G-2 LabVIEW Virtual Instrument used to Collect Signal Strength Measurements for Wet-Antenna Attenuation Tests